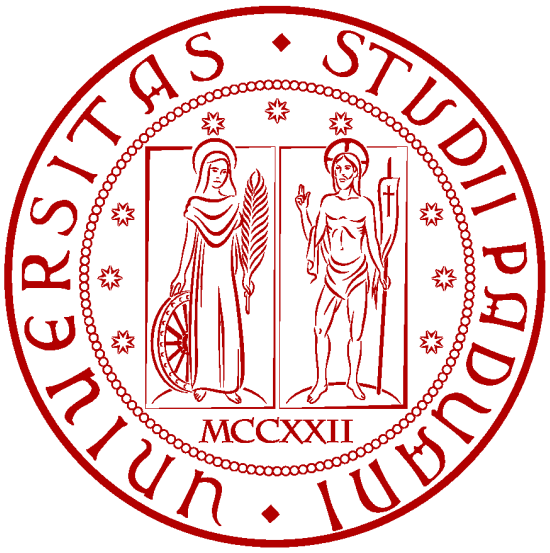

UNIVERSITÀ DEGLI STUDI DI PADOVA

DIPARTIMENTO DI FISICA E ASTRONOMIA "GALILEO GALILEI"
DIPARTIMENTO DI INGEGNERIA DELL'INFORMAZIONE
Corso di Laurea Magistrale in Fisica

TESI DI LAUREA MAGISTRALE

Violation of a tripartite Bell inequality by weak measurements

Relatore: **Dott. Giuseppe Vallone**
Controrelatore: **Dott. Michele Merano**

Laureando: **Mirko Pittaluga**
Matricola: **1104727**

Anno Accademico 2015 - 2016

Dedicato ai miei genitori
e a mia sorella
senza i quali questa avventura
non sarebbe stata possibile.

ABSTRACT

Non-locality is one of the most characteristic trait of Quantum Mechanics, and it is linked to the conceptually counter-intuitive ability of some objects (when adequately prepared) to instantaneously know about each other's state, no matter how much space-separated they are. At the development stage of Quantum Mechanics, non-locality had been an argument of intense debate among scientists [1] [2] due to its consequences that seemed to contradict physicist common sense. The scientific debate on the argument faced a turning point with the publication of the landmark paper by J. S. Bell in 1964 [3] which ended the discussion whether or not non-locality was a true aspect of physical reality, raising it to one of the fundamental aspect of our comprehension of the physical world.

The scientific interest for non-locality has recently substantially increased due to its striking applications in Quantum Information Theory [4] [5] [6]. The major innovative traits of Quantum Information Theory, compared to Classical Information Theory, arise in fact from the deployment of non-locality as a resource for information manipulation and transmission.

The aim of this thesis is to shed a new light on the argument from an experimental point of view, proving whether is possible or not to share non-local correlations among three observers sharing an entangled two photon pair. This work is one of the first to address this issue, and aims to prove experimentally what has been hypothesized theoretically by Silva, et al. in their 2015 article [7].

ACKNOWLEDGEMENT

I would like to express my deepest gratitude to Matteo Schiavon e Luca Calderaro, the two Ph.D. students of Quantum Future research group I have joined in this project. From the experiment design to the data analysis, their assistance and suggestions have accompanied me through all the learning process of this master thesis.

I would also like to thank my supervisor Dr. Giuseppe Vallone for his guidance, supervision and example. It is probably due to his support and his advices that this project could end up successfully.

Finally I would like to thank all the members of Quantum Future research group in Padua, who made my the time spent on this thesis such an enjoyable, stimulating and productive experience.

CONTENTS

LIST OF FIGURES

1

INTRODUCTION

At the end of the 19^{th} century physics, intended as the scientific method applied to natural sciences, had achieved remarkable results in the comprehension and explanation of the reality (classical mechanics, classical electromagnetism, classical thermodynamics). At that time the common feeling in the scientific community was a general satisfaction and the belief that almost every aspect of the physical world had already been discovered, and that the explanation of the phenomena still to understand would have been given by a finest and more accurate study of the physical laws already discovered.

The scientific community thought that the still open issues of the theory developed back then were just limited "problems", whose solution wouldn't have affected much of the physical theoretic framework already developed. Two open issues seeking for an explanation were the black-body radiation and the photoelectric effect. The first one was pointed out by Rayleigh–Jeans, whom realised that classical statistical mechanics and classical electromagnetism predicted that a black body in thermal equilibrium would have emitted a radiation with infinite amount of energy, a clearly non-physical result. The second one was an experimental fact first noticed by H. Hertz in 1887 whom wasn't able to explain the frequency-threshold-effect observed in the emission of charged particles by a metal illuminated by an electromagnetic wave with the classical electromagnetic theory.

The two problems were solved independently at the beginning of the 20^{th} century respectively by M. Plank (who was able to correctly predict the black-body radiation spectra introducing a quantization in the interaction between the black-body and the EM field) and by A. Eninstein (who was able to explain the photoelectric effect introducing a quantization of the EM field and assuming the atomic nature of matter).

These two discoveries opened a completely new research field for physicist, and revealed to the scientific community that the theoretical tools developed until that moment to understand reality were completely inadequate to explain a vast class of phenomena that involved small-scale systems. Since these two pioneering discoveries, some of the greatest physicist of that time (N. Bohr, L. de Broglie, A. H. Compton, P. A. M. Dirac, E. Schrödinger, M. Born, W. Pauli, W. Heisenberg to name a few) worked on the development of new tools to explain physical reality, placing the building blocks of a new physical theory, Quantum Mechanics, that would change forever our conception of the world and our idea of how the mechanisms that rule nature work. The initial development of the theory concluded in 1930 with the publication of *"The principles of Quantum Mechanics"* by P. A. M. Dirac [8], a book where all the new discoveries about Quantum Mechanics were fixed and formalized. Quantum Mechanics, with all its successive developments, had an enormous impact in physics, and lays at the basis of all the most modern and sophisticated physical theories

(Quantum Field Theory (QFT), Quantum Electrodynamic (QED) and the Standard Model).

One of the most recent developments of Quantum Mechanics has been its application to Information Theory. Information theory is the subject that studies the quantification, storage, and communication of information; its foundation dates back to 1948, with the publication of the landmark paper by C. E. Shannon *"A Mathematical Theory of Communication"* [9]. Its application to the development of new technologies is deeply affecting our everyday life, and it is the biggest responsible for all those innovations that are shifting us towards a new model of "communication society".

Quantum Information is the study of the information processing tasks that can be accomplished using quantum mechanical systems. The use of quantum systems as information carriers introduces a completely new paradigm for information theory, leading to the development of new protocols for both computing and cryptography. It is worth noting that, since its initial development in the 80s, quantum information has given a great quantity of remarkable theoretical results, whose experimental implementation is still at its infancy, due to the difficulties in the implementation an control of quantum systems. Nevertheless, in the recent years, a big technological improvement has pushed for unprecedented experimental results [10] [11] [12] [13] [14] [15] [16] that make it reasonable to believe that a future where quantum technology will have an impact on every day life is not that far away.

The aim of this thesis fits perfectly with the scenario just described, since we wish to investigate experimentally a fundamental characteristic of quantum systems, something that is sometimes considered the "the characteristic trait" [17] that distinguishes quantum mechanics from the classical theory: *non-locality*. In the following sections we will better define what non-locality is, for the moment we just point out that our work is one of first experimental implementations of a device capable of detecting non-local correlations between three observers sharing a two-photon entangled state.

The purpose of this work is double: in first place we want to shed some new light on non-local correlations, demonstrating a property until now just theoretically predicted. This is in fact one of the first works to obtain experimentally this result. Only at the final stage of this project a study with similar results has been published [18]. THe second intent of this thesis is to build a stable apparatus capable of measuring multiple consecutive non-local correlations; this result may have important applications for Quantum Random Number Generation or for Quantum Key Distribution.

In the following we will describe briefly the structure of this thesis.

In the first chapter we will focus on the concept of non-locality. Firstly we will introduce the qubit, the basic unit of quantum information. This will give us the opportunity to introduce some aspects of quantum mechanics of interest for the rest of the thesis. We will then explain the concepts of non-locality, entanglement and weak measurements.

In the second chapter we will focus on the theoretical framework of our work. We will discuss Bell inequalities and CHSH correlations, the most common tools used to prove the presence of non-local correlations between a multiple system. We will then present and characterize a scenario where non-local correlations are shared among a number of observers larger then two. We will finally discuss the possible applications of such multiple non-local correlations.

In the third chapter we will describe how a photonic entangled state can be experimentally produced, studying the physics of the process. We will then describe the setup actually employed in our experiment.

In the fourth chapter we will describe theoretically and practically our experiment.

In the fifth chapter we will show the obtained results, reporting both the characterization of theapparatus and the results of our experiment.

In the sixth chapter the conclusion of our work will be given.

Finally, in the appendixes, we will briefly review the fundamental tools needed to understand this work, discussing about: Quantum Mechanics, Classical Optics and Quantum Information.

2

NON-LOCALITY AND WEAK MEASUREMENT

In this chapter we will discuss some of the most fundamental aspects Quantum Mechanics we will be dealing with in our work. We will start introducing the qubit, the basic unit of quantum information. A deep comprehension of its properties is fundamental because we will often use a qubit to make examples in our our brief quantum mechanics explanation and because it is the physical state experimentally involved in our work. We will then introduce qubits composite systems and we will present the concepts of entangled states, non-locality and Weak Measurements.

In the following sections we will intensively make use of the concepts and tools presented in appendix A on page 75.

2.1 QUBIT

The basic unit of classical information theory is the *bit*, an object that can assume two values, 0 or 1. Similarly, quantum information theory has adopted its quantum counterpart, called *qubit* (*qu*antum *bit*) that is a two-level system described within the framework of quantum mechanics. Because of Quantum Mechanics Postulate 1, such a system corresponds to a two-dimensional Hilbert space $\mathscr{H} \approx \mathbb{C}^2$, with basis vectors $|0\rangle$ and $|1\rangle$. The great difference between bits and qubits is that a qubit can be in a state other than $|0\rangle$ or $|1\rangle$; indeed, any linear combination of these two states (called superposition) is allowed. The general qubit state $|\psi\rangle$ therefore is written as:

$$|\psi\rangle = \alpha\,|0\rangle + \beta\,|1\rangle \tag{2.1}$$

where α and β are complex numbers such that $|\alpha|^2 + |\beta|^2 = 1$. Postulate 1 states also that quantum states are defined up to a global phase factor (the vectors $|\psi\rangle$ and $e^{i\gamma}|\psi\rangle$ describe the same physical state). Therefore, it is possible to take as representative of the physical state the vector with $\alpha \in \mathbb{R}$. This, together with the requirement of normalization, allows us to write the state of a single qubit as

$$|\psi\rangle = \cos\frac{\theta}{2}\,|0\rangle + e^{i\phi}\sin\frac{\theta}{2}\,|1\rangle$$

with θ and ϕ real numbers. These numbers define a point on the surface of the unit three-dimensional sphere, the *Bloch sphere*, shown in figure 2.1. In this representation, the qubit $|\psi\rangle$ is associated with the point $(\sin\theta\cos\phi, \sin\theta\sin\phi, \cos\theta)$. The Z axis corresponds to the *computational basis* $\{|0\rangle, |1\rangle\}$, while the two other axes are associated to the *diagonal basis* $X \equiv \left\{|+\rangle = \frac{|0\rangle+|1\rangle}{\sqrt{2}}, |-\rangle = \frac{|0\rangle-|1\rangle}{\sqrt{2}}\right\}$ and the *circular basis* $Y \equiv \left\{|r\rangle = \frac{|0\rangle+i|1\rangle}{\sqrt{2}}, |l\rangle = \frac{|0\rangle-i|1\rangle}{\sqrt{2}}\right\}$ [4].

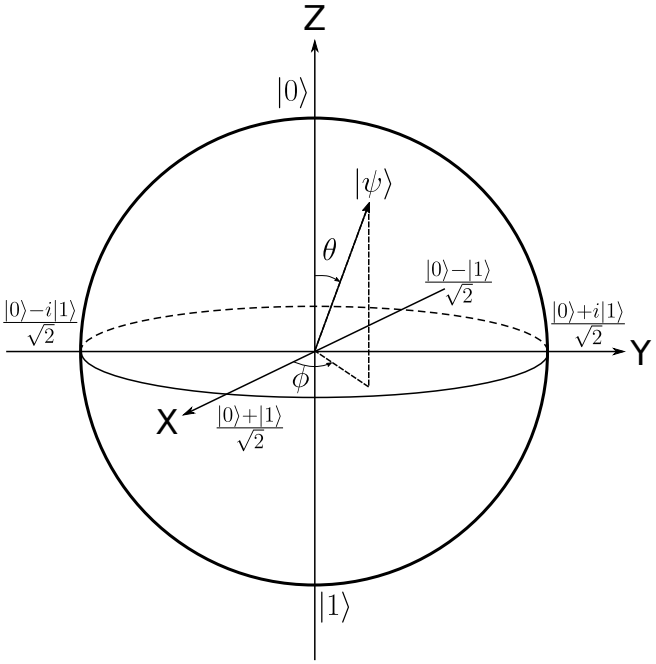

Figure 2.1.: Bloch sphere representation of a single qubit.

Another useful qubit representation is the matrix one, that associates the vectors of the computational basis with

$$|0\rangle = \begin{pmatrix} 1 \\ 0 \end{pmatrix} \qquad\qquad |1\rangle = \begin{pmatrix} 0 \\ 1 \end{pmatrix}$$

In equation 2.1 the qubit is in a pure state. A more general representation of the qubit can be given using the density matrix formalism; with this formalism a qubit (both in a pure or in a mixed state) can be written as:

$$\hat{\rho} = \frac{\mathbb{1}_2 + \mathbf{r} \cdot \boldsymbol{\sigma}}{2}$$

where $\mathbf{r}$ is a real three-dimensional vector such that $\|\mathbf{r}\| \leqslant 1$ and $\boldsymbol{\sigma}$ is the "vector" of the three Pauli matrices

$$\hat{\sigma}_1 = \hat{\sigma}_x = \begin{pmatrix} 0 & 1 \\ 1 & 0 \end{pmatrix} \qquad \hat{\sigma}_2 = \hat{\sigma}_y = \begin{pmatrix} 0 & -i \\ i & 0 \end{pmatrix} \qquad \hat{\sigma}_3 = \hat{\sigma}_z = \begin{pmatrix} 1 & 0 \\ 0 & -1 \end{pmatrix}$$

as components. The vector $\mathbf{r}$ corresponds a point in the Bloch sphere. It can be shown that a pure state is characterized by a vector $\mathbf{r}$ on the surface of the sphere ($\|\mathbf{r}\| = 1$), while a true mixed state is represented by a point inside the sphere.

It is possible to use any two-level quantum system in order to create a physical qubit. For example, the spin of an electron or two electronic levels of an atom are suitable for qubit realization. For our purpose, the most important physical system to realize a quantum bit is the photon, the the electromagnetic field quantum.

2.1.1 *Multiple qubit systems*

The difference between classical and quantum information is more marked when dealing with compound systems. Classically, the composition of n systems is described by an n-bit string of 0s and 1s (e.g. the composition of 8 bits is described by an 8-bit string called *byte*). In the quantum case, on the other hand, things are slightly more complicated. Quantum mechanics Postulate 2 says that the compound state of two systems lies in the tensor product of the two Hilbert spaces describing the single systems. Therefore, if the i-th qubit lies in $\mathscr{H}_i \approx \mathbb{C}^2$ space, the state describing the composition of n qubits is described by a vector in:

$$\mathscr{H} = \mathscr{H}_1 \otimes \cdots \otimes \mathscr{H}_n \approx \underbrace{\mathbb{C}^2 \otimes \cdots \otimes \mathbb{C}^2}_{n \text{ times}} \approx \mathbb{C}^{2^n}.$$

Like single-qubit systems, multiple-qubit systems can be represented using 2^n-component complex vectors.

2.2 ENTANGLED STATES AND EPR PARADOX

Postulate 2 enables us to introduce one of the most interesting and puzzling ideas associated with composite quantum systems and quantum mechanics in general: entanglement. If we consider the two qubit state

$$|\psi\rangle = \frac{|00\rangle + |11\rangle}{\sqrt{2}}$$

we can easily notice that there are no single qubit states $|a\rangle$ and $|b\rangle$ such that $|\psi\rangle = |a\rangle\,|b\rangle$. This example leads us to the definition of the simple and hard-to-understand concept of entanglement: a state of a composite system that can't be written as the product of states of its component systems is defined as an entangled state.

The properties of an entangled system are among the most challenging consequences of quantum mechanics. It was studying them that, for example, Einstein, Podolski and Rosen (ofter reffered as EPR) in their famous article published in 1935 *"Can Quantum-Mechanical Description of Physical Reality Be Considered Complete?"* [1] arose what they considered a leak in quantum mechanics theory. In their paper the authors criticised the Copenhagen interpretation of quantum mechanics, accusing quantum mechanics to be an incorrect (and at least incomplete) tool to describe physical reality. Their argument, as reformulated by Bhom [19] some years later, can be summarized as follows: let's consider a spin-zero particle decaying into two spin-half particles such that there is no interaction between them after decay. The quantum state of the two particles before to measurement can be written as:

$$|\psi_{AB}\rangle = \frac{|\uparrow\rangle_A\,|\downarrow\rangle_B - |\downarrow\rangle_A\,|\uparrow\rangle_B}{\sqrt{2}}$$

Here, subscripts A and B distinguish the two particles, which can be thought to be in the possession of two experimentalists called *Alice* and *Bob*[1]. The rules of quantum

1 The reformulation of quantum physics problems in terms of measurements on the system by some observers is a convention generally adopted in Quantum Information.

theory predict the outcomes of the measurements performed by the experimentalists. *Alice*, for example, will measure her particle to be spin-up in half of her measurements, *Alice*'s measurement causes the state of the two particles to collapse, so that if *Alice* measures spin-up in some direction $\mathbf{n}$, the quantum state after the measurement is the corresponding eigenstate:

$$|\psi_{AB}\rangle = |\uparrow_{\mathbf{n}}\rangle_A \, |\downarrow_{\mathbf{n}}\rangle_B$$

If *Bob* also measures spin in direction $\mathbf{n}$, he must get a spin-down result. Hence, spin measurements in the same direction are always anti-correlated, even if the particles are spatially separated, meaning that no signal can be exchanged among them. EPR saw this as evidence of the incompleteness of quantum theory: if there is no interaction between particles, then the only explanation for this anti-correlation between measurement outcomes is that each particle carries a pre-existing determinate value (appropriately anti-correlated with the value carried by the other particle) for that measurement. Such a property is unaccounted for by the quantum mechanical state description, and their paper concludes:

> *While we have thus shown that the wave function does not provide a complete description of the physical reality, we left open the question of whether or not such a description exists. We believe, however, that such a theory is possible.*

The goal of EPR was to show that quantum mechanics is incomplete, by demonstrating that quantum mechanics lacked some essential 'element of reality', according to their criterion. They hoped to return to a more classical view of the world, in which systems have properties which exist independently of the measurements performed on them.

Since the EPR paper the scientific community got really interested in the argument, and divided in two groups: one (those who agreed with EPR thesis) which tried to solve the paradox working on a new kind of theories (*hidden variables theories*) that could reconcile quantum mechanics results with a more classical vision of reality, the other one which worked on finding an acceptable interpretation of quantum mechanics that could justify its results to our "classical" eyes.

A fundamental advancement in this topic was given by the article *"On the Einstein-Podolsky-Rosen Paradox"* by J. S. Bell published in 1964 [3] which demonstrated that predictions of quantum theory are incompatible with those of any physical theory satisfying a natural notion of locality. Bell's argument will be exposed in the following sections.

2.3 NON-LOCALITY, BELL INEQUALITIES AND CHSH INEQUALITY

In his 1964 article, Bell proved that there is no Local Hidden Variable theory that can reproduce Quantum Mechanics results. Bell's theorem has deeply influenced our perception and understanding of physics, and arguably ranks among the most profound scientific discoveries ever made. In the following we will present the Bell theorem considering some properties of a thought experiment; we will take advantage of its explanation to introduce the concept of non-locality. The explanation closely follows the one given by Brunner, Cavalcanti, Pironio et al. in the review *"Bell nonlocality"* [20].

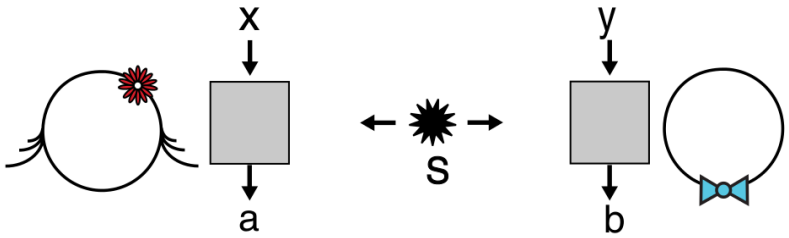

Figure 2.2.: Sketch of a Bell experiment. A source (**S**) distributes two physical systems to distant observers, *Alice* and *Bob*. Upon receiving their systems, each observer performs a measurement on it. The measurement chosen by *Alice* is labeled x and its outcome a. Similarly, *Bob* chooses measurement y and gets outcome b. The experiment is characterized by the joint probability distribution $P(ab|xy)$ of obtaining outcomes a and b when Alice and Bob choose measurements x and y. [20]

In a typical Bell experiment, two systems which may have previously interacted are spatially separated and are measured by two distant observers, *Alice* and *Bob* (see figure 2.2). *Alice* may choose to perform one of several possible measurements on her system. Let x denote her measurement choice. For instance, x may refer to the position of a knob on her measurement apparatus. Similarly, let y denote *Bob*'s measurement choice. Once the measurements are performed, they give outcomes a and b on the two systems. The actual values assigned to the measurement choices x, y and outcomes a, b are purely conventional; they are mere macroscopic labels distinguishing the different possibilities.

For each run of the experiment, the outcomes a and b may vary, even when the same choices of measurements x and y are made. These outcomes are thus in general governed by a probability distribution $P(ab|xy)$, which can of course depend on the particular experiment being performed. By repeating the experiment a sufficient number of times and collecting the observed data, one gets a fair estimate of such probabilities. When such an experiment is actually performed (for example by generating pairs of spin-1/2 particles and measuring the spin of each particle in different directions) it will in general be found that

$$P(ab|xy) \neq P(a|x)P(b|y)$$

implying that the outcomes on both sides are not statistically independent from each other. Even though the two systems may be separated by a large distance, and may even be spacelike separated, the existence of such correlations is nothing mysterious. In particular, it does not necessarily imply some kind of direct influence of one system on the other, for these correlations may simply reveal some dependence relation between the two systems which was established when they interacted in the past. This is at least what one would expect in a local theory. Being more precise, the assumption of locality implies that we should be able to identify a set of past factors, described by some variables λ, having a joint causal influence on both outcomes, and which fully account for the dependence between a and b. Once all such factors have been taken into account, the residual indeterminacies about the outcomes must now be decoupled; that is, the probabilities for a and b should factorize:

$$P(ab|xy,\lambda) = P(a|x,\lambda)P(b|y,\lambda)$$

This factorability condition simply expresses the fact that we have found an explanation according to which the probability for a depends only on the past variables λ and on the local measurement x, but not on the distant measurement and outcome, and analogously for the probability to obtain b. The variable λ will not necessarily be constant for all runs of the experiment, even if the procedure which prepares the particles to be measured is held fixed, because λ may involve physical quantities that are not fully controllable. The different values of λ across the runs should thus be characterized by a probability distribution $q(\lambda)$. Combined with the above factorability condition, we can thus write:

$$P(ab|xy) = \int_\Lambda q(\lambda) P(a|x,\lambda) P(b|y,\lambda) d\lambda \tag{2.2}$$

where we also implicitly assumed that the measurements x and y can be freely chosen in a way that is independent of λ, i.e., that $q(\lambda|x,y) = q(\lambda)$. This decomposition now represents a precise condition for locality in the context of Bell experiments. Note that no assumptions of determinism or of a "classical behavior" are being involved in equation 2.2: we assumed that a (and similarly b) is only probabilistically determined by the measurement x and the variable λ, with no restrictions on the physical laws governing this causal relation. Locality is the crucial assumption behind equation 2.2. In relativistic terms, it is the requirement that events in one region of space-time should not influence events in spacelike separated regions.

It is now straightforward to prove that the predictions of quantum theory for certain experiments involving entangled particles do not admit a decomposition of the form 2.2. To establish this result, we consider for simplicity an experiment where there are only two measurement choices per observer $x, y \in \{0, 1\}$ and where the possible outcomes take also two values labeled $a, b \in \{-1, +1\}$. Let $\langle a_x b_y \rangle = \sum_{a,b} ab P(ab|xy)$ be the expectation value of the product ab for a given measurement choice $(x; y)$ and consider the expression $S = \langle a_0 b_0 \rangle + \langle a_0 b_1 \rangle + \langle a_1 b_0 \rangle - \langle a_1 b_1 \rangle$, which is a function of the probabilities $P(ab|xy)$. If these probabilities satisfy the locality decomposition (2.2), we necessarily have that

$$S = \langle a_0 b_0 \rangle + \langle a_0 b_1 \rangle + \langle a_1 b_0 \rangle - \langle a_1 b_1 \rangle \leqslant 2 \tag{2.3}$$

which is known as the Clauser-Horne-Shimony-Holt (CHSH) inequality [21].

To derive this inequality, we can use equation 2.2 in the definition of $\langle a_x b_y \rangle$, which allows us to express this expectation value as an average $\langle a_x b_y \rangle = \int_\Lambda q(\lambda) \langle a_x \rangle_\lambda \langle b_y \rangle_\lambda d\lambda$ of a product of local expectations $\langle a_x \rangle_\lambda = \sum_a a P(a|x,\lambda)$ and $\langle b_y \rangle_\lambda = \sum_b b P(b|y,\lambda)$ taking values in $[-1, +1]$. Inserting these expressions into equation 2.3, we can write:

$$S = \int_\Lambda q(\lambda) S_\lambda d\lambda$$

with

$$S_\lambda = \langle a_0 \rangle_\lambda \langle b_0 \rangle_\lambda + \langle a_0 \rangle_\lambda \langle b_1 \rangle_\lambda + \langle a_1 \rangle_\lambda \langle b_0 \rangle_\lambda - \langle a_1 \rangle_\lambda \langle b_1 \rangle_\lambda$$

Since $\langle a_0 \rangle_\lambda, \langle a_1 \rangle_\lambda \in [-1, +1]$, this last expression is smaller than

$$S_\lambda \leqslant |\langle b_0 \rangle_\lambda + \langle b_1 \rangle_\lambda| + |\langle b_0 \rangle_\lambda - \langle b_1 \rangle_\lambda|$$

Without any loss of generality we can assume that $\langle b_0 \rangle_\lambda \geqslant \langle b_1 \rangle_\lambda \geqslant 0$ which yelds $S_\lambda = 2\langle b_0 \rangle_\lambda \leqslant 2$, and thus $S = \int_\Lambda q(\lambda) S_\lambda d\lambda \leqslant 2$.

If we consider now the quantum predictions for an experiment in which the two systems measured by *Alice* and *Bob* are two qubits in the singlet state $|\Psi^-\rangle = \frac{|01\rangle - |10\rangle}{\sqrt{2}}$, where $|0\rangle$ and $|1\rangle$ are the eigenstates of σ_z for the eigenvalues $+1$ and -1, respectively. Let the measurement choices x and y be associated with vectors $\mathbf{x}$ and $\mathbf{y}$ corresponding to the measurement of $\mathbf{x} \cdot \boldsymbol{\sigma}$ on the first qubit and of $\mathbf{y} \cdot \boldsymbol{\sigma}$ on the second qubit.

According to quantum theory, we then have the expectations $\langle a_x b_y \rangle = -\mathbf{x} \cdot \mathbf{y}$. If we choose the two measurement settings $x \in \{0, 1\}$ correspond to measurements in the orthogonal directions $\boldsymbol{e}_1$ and $\boldsymbol{e}_2$ respectively, and the two measurement settings $y \in \{0, 1\}$ correspond to measurements in the diagonal directions $-\frac{\boldsymbol{e}_1 + \boldsymbol{e}_2}{\sqrt{2}}$ and $\frac{\boldsymbol{e}_1 - \boldsymbol{e}_2}{\sqrt{2}}$, we get that:

$$\langle a_0 b_0 \rangle = \langle a_0 b_1 \rangle = \langle a_1 b_0 \rangle = \frac{1}{\sqrt{2}}$$
$$\langle a_1 b_1 \rangle = -\frac{1}{\sqrt{2}}$$

obtaining finally that:

$$S = 2\sqrt{2} > 2$$

in contradiction with equation 2.3 and thus with the locality constraint (2.2). This is the content of Bell's theorem, establishing the non-local character of quantum theory and of any model reproducing its predictions. The CHSH inequality (2.3) is an example of a Bell inequality, a linear inequality for the probabilities $P(ab|xy)$ that is necessarily verified by any model satisfying the locality condition (2.2), but which can be violated by suitable measurements on a pair of quantum particles in an entangled state. The violation of these inequalities and the predictions of quantum theory were first confirmed experimentally by Freedman and Clauser [22], then more convincingly by Aspect, Grangier, and Roger [23], and in many other experiments since then.

2.3.1 *Mathematical characterization of non-local correlations*

In the previous section we introduced the concept of non-locality, describing it as a characteristic property of entangled quantum system that emerges from the outcomes correlations. In this section we want to formalize the concept, showing how is possible to characterize the argument mathematically. We suggest to refer to [20] for an exhaustive treatment of the argument.

We start considering a situation similar to the one presented in the previous section. We consider two distant observers, *Alice* and *Bob*, performing measurements on a shared physical system, for instance, a pair of entangled particles. Each observer has a choice of m different measurements to perform on his system. Each measurement can yield Δ possible outcomes. Abstractly we describe the situation by saying that *Alice* and *Bob* have access to a "black box". Each party locally selects an input (a measurement setting) and the box produces an output (a measurement outcome). We refer to this scenario as a Bell scenario.

We label the inputs of *Alice* and *Bob* $x, y \in \{1, \ldots, m\}$ and their outputs $a, b \in \{1, \ldots, \Delta\}$ respectively. The labels attributed to the inputs and outputs are purely conventional, and the results presented here are independent of this choice.

Let $P(ab|xy)$ denote the joint probability to obtain the output pair (a, b) given the input pair (x, y). A Bell scenario is then completely characterized by $\Delta^2 m^2$ such joint probabilities, one for each possible pair of inputs and outputs. We refer to the set $\mathbf{P} = \{P(ab|xy)\}$ of all these probabilities as a *behavior*. Informally, we simply refer to them as the *correlations* characterizing the state shared by *Alice* and *Bob*. A behavior can be viewed as a point $\mathbf{P} \in \mathbb{R}^{\Delta^2 m^2}$ belonging to the probability space $\mathcal{P} \subset \mathbb{R}^{\Delta^2 m^2}$ defined by the positivity constraints $P(ab|xy) \geqslant 0$ and the normalization constraints $\sum_{a,b=1}^{\Delta} P(ab|xy) = 1$. Due to the normalization constraints $\mathcal{P}$ is a subspace of $\mathbb{R}^{\Delta^2 m^2}$ of dimension $\dim \mathcal{P} = (\Delta^2 - 1)m^2$.

The existence of a given physical model behind the correlations obtained in a Bell scenario translates into additional constraints on the behaviors $\mathbf{P}$. Three main types of correlations can be distinguished:

1. No-signaling correlations;
2. Local correlations;
3. Quantum correlations.

No-signaling correlations

The first natural limitation on behaviors $\mathbf{P}$ are the *no-signaling* constraints, formally expressed as:

$$\sum_{b=1}^{\Delta} P(ab|xy) = \sum_{b=1}^{\Delta} P(ab|xy') \qquad \text{for all} \quad a, x, y, y'$$

$$\sum_{a=1}^{\Delta} P(ab|xy) = \sum_{a=1}^{\Delta} P(ab|x'y) \qquad \text{for all} \quad b, y, x, x'$$

These constraints have a clear physical interpretation: they imply that the local marginal probabilities of *Alice* $P(a|x) \equiv P(a|xy) = \sum_{b=1}^{\Delta} P(ab|xy)$ are independent of *Bob*'s measurement setting y, and thus *Bob* cannot signal to *Alice* his choice of input (and the other way around). In particular, if Alice and Bob are spacelike separated, the no-signaling constraints guarantee that Alice and Bob cannot use their black box for instantaneous signaling, preventing a direct conflict with relativity.

We denote with $\mathcal{NS}$ the set of behaviors satisfying the no-signaling constraints.

Local correlations

A more restrictive constraint than the no-signaling condition is the locality condition. Formally, the set $\mathcal{L}$ of local behaviors is defined by the elements of $\mathcal{P}$ that can be written in the form (as already introduced in equation 2.2):

$$P(ab|xy) = \int_{\Lambda} q(\lambda) P(a|x, \lambda) P(b|y, \lambda) d\lambda$$

where the (hidden) variables λ are arbitrary variables taking value in a space Λ and distributed according to the probability density $q(\lambda)$ and where $P(a|x, \lambda)$ and $P(b|y, \lambda)$ are local probability response functions for *Alice* and *Bob*, respectively. Operationally, one can also think about λ as shared randomness; that is, some shared classical random bits, where *Alice* will choose an outcome a depending on both her measurement setting x and λ and similarly for *Bob*.

Whereas any local behavior satisfies the no-signaling constraint, the converse does not hold. There exist no-signaling behaviors which do not satisfy the locality conditions. Hence the set of local correlations is strictly smaller than the set of no-signaling correlations; that is, $\mathcal{L} \subset \mathcal{NS}$.

Quantum correlations

Finally, we consider the set of behaviors achievable in quantum mechanics. Formally, the set $\mathcal{Q}$ of quantum behaviors corresponds to the elements of $\mathcal{P}$ that can be written as:

$$P(ab|xy) = Tr(\rho_{AB}\ M_{a|x} \otimes M_{b|y}) \tag{2.4}$$

where ρ_{AB} is a quantum state in a joint Hilbert space $\mathscr{H}_A \otimes \mathscr{H}_B$ of arbitrary dimension, $M_{a|x}$ are measurement operators [positive operator valued measure (POVM) elements] on $\mathscr{H}_A$ characterizing *Alice*'s measurements (thus $M_{a|x} \geqslant 0$ and $\sum_{a=1}^{\Delta} M_{a|x} = \mathbb{1}$), and similarly $M_{b|y}$ are operators on $\mathscr{H}_B$ characterizing *Bob*'s measurements.

It can easily be shown that any local behavior admits a description in terms of equation 2.4 and thus belongs to $\mathcal{Q}$ ($\mathcal{L} \subset \mathcal{Q}$). Moreover, any quantum behavior satisfies the no-signaling constraints ($\mathcal{Q} \subset \mathcal{NS}$). However, there are quantum correlations that do not belong to the local set (this follows from the violation of Bell inequalities, $\mathcal{Q} \nsubseteq \mathcal{L}$) and, there are no-signaling correlations that do not belong to the quantum set ($\mathcal{NS} \nsubseteq \mathcal{Q}$).

Bell inequalities

The sets $\mathcal{L}$, $\mathcal{Q}$ and $\mathcal{NS}$ are closed, bounded, and convex. That is, if $\mathbf{P}_1$ and $\mathbf{P}_2$ belong to one of these sets, then the mixture $\mu\mathbf{P}_1 + (1-\mu)\mathbf{P}_2$ with $0 \leqslant \mu \leqslant 1$ also belongs to this set. By the hyper-plane separation theorem, it follows that for each behavior $\hat{\mathbf{P}} \in \mathbb{R}^{\Delta^2 m^2}$ that does not belong to one of the sets $\mathcal{K} = \mathcal{L}$, $\mathcal{Q}$, or $\mathcal{NS}$ there exists a hyperplane that separates this $\hat{\mathbf{P}}$ from the corresponding set (see figure 2.3). That is,

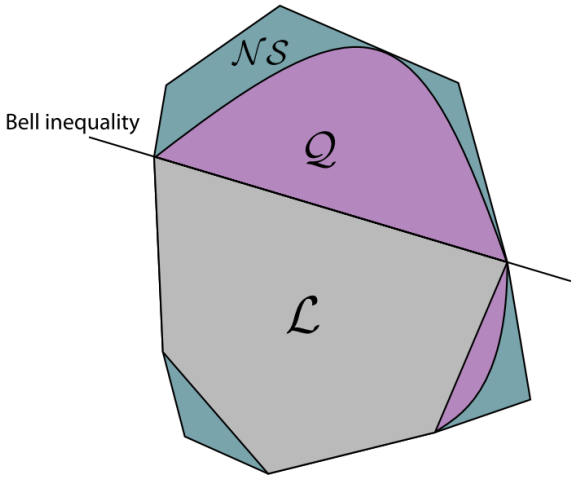

Figure 2.3.: Sketch of the no-signaling ($\mathcal{NS}$), quantum ($\mathcal{Q}$), and local ($\mathcal{L}$) sets. Notice the strict inclusions $\mathcal{L} \in \mathcal{Q} \in \mathcal{NS}$. Moreover, $\mathcal{NS}$ and $\mathcal{L}$ are polytopes, i.e., they can be defined as the convex combination of a finite number of extremal points. The set $\mathcal{Q}$ is convex, but not a polytope. The hyperplanes delimiting the set L correspond to Bell inequalities. [20]

if $\hat{\mathbf{P}} \notin \mathcal{K}$, then there exists an inequality of the form

$$\mathbf{s} \cdot \mathbf{P} = \sum_{a,b,x,y} s_{xy}^{ab} P(ab|xy) \leqslant S_k$$

that is satisfied by all $\mathbf{P} \in \mathcal{K}$ but which is violated by $\hat{\mathbf{P}}$: $\mathbf{s} \cdot \hat{\mathbf{P}} > S_k$.

In the case of the local set $\mathcal{L}$, such inequalities are simply Bell inequalities. Thus any non-local behavior violates a Bell inequality. An example of such an inequality is the CHSH inequality (see equation 2.3) introduced in section 2.3. The inequalities associated with the quantum set, which characterize the limits of $\mathcal{Q}$, are often called *quantum Bell inequalities* or *Tsirelson inequalities*.

We conclude here the introduction to the mathematical characterization of the possible physical correlations in a two observer scenario experiment. To the scope of this thesis is sufficient to have clear what we mean with the correlations sets $\mathcal{L}$, $\mathcal{Q}$ and $\mathcal{NS}$, and what we mean with *Classical bound* and *Tsirelson's bound*. For further studies and a more in depth understanding of the subject we refer to [20], where a very good introductory explanation and a comprehensive bibliography of the argument can be found.

2.4 WEAK MEASUREMENT

The last concept I want to introduce before discussing the main argument of this work is the concept of *weak measurement*. The first fact to point out is that there is no universally accepted definition of a weak measurement even though the idea at the basis of this concept is very simple: weak measurements are a type of quantum measurement where an observer obtains very little information about the system, but also disturbs the state very little. We know that any measurement on a system necessarily disturbs it (as formalized in the Busch's theorem [24]); with weak measurements we gain some informations about the system, without compromising (and then defining) completely its state. In this picture it is clear that:

- the more a measurement is weak, the less information we obtain about the system, and the less we perturb it;
- the less a measurement is weak, the more it is strong, and the more we approach a projective measurement, where we obtain all the possible information about the state (getting the outcome of the measurement) and where we drastically perturb it (projecting it onto the eigenspace of the measurement operator) [25].

The key aspect of the topic is the trade-off between the amount of information we can get about a quantum system and the amount of disturbance we introduce on it. Since the birth of quantum mechanics this has been a largely studied topic, and a lot of literature has been produced exploring the subject, even if the definition "weak measurement" is quite recent and was probably used for the first time in 1988 by Aharonov et al. [26].

The aim of this thesis is not that of reviewing exhaustively the subject, we are rather interested in giving an idea of what we mean by weak measurements, and how we can perform them, since our goal is to exploit them to correlate weakly two systems enabling for a double CHSH inequality violation. More information, and a deeper review of the argument, can be found in [27, 28, 29, 30]. In our exposition we will

closely follow the approach of B. E. Y. Svensson in his review [31].

Our explanation of weak measurements starts with a generalization of the quantum strong measurement (presented in 5 on page 76), that takes into account not only the quantum state under study, but also the practical implementation of the measurement, by introducing in our picture the measurement device (from now on called *ancilla* or *meter*) that couples with the studied system to allow the extraction of information. This ancilla-scheme goes a few steps in the direction of describing the very measurement process, highlighting some aspects of measurement that are classically left uncovered such as: what kind of measurement apparatus is used and what distinguishes measurements from other possible types of interactions.

It is the interaction of the ancilla with the *system* (called also the *object*) that constitutes the measurement: by reading off the meter one gets information about the value of the system observable. In some experimental situations, the meter can even be a property of the object under analysis different from than the one (*system*) we are interested into (like momentum and polarization for a photon).

2.4.1 *Modelling the ancilla measurement process*

The meter $\mathcal{M}$ will be modeled as a quantum device living in a Hilbert space $\mathscr{H}_{\mathcal{M}}$ having a complete, orthonormal set of basis states $|m_k\rangle$, $k = 1, 2, \ldots, d_{\mathcal{M}}$ that are eigenvectors of the operator $\hat{M}$. The intrinsic Hamiltonian of $\mathcal{M}$ is denoted $\hat{H}_{\mathcal{M}}$. The meter is assumed to be prepared in an initial pure state $|m^{(0)}\rangle$, so that the meter initial density matrix is $\hat{\mu}_0 = |m^{(0)}\rangle \langle m^{(0)}|$.

The object or system $\mathcal{S}$ has its Hilbert space $\mathscr{H}_{\mathcal{S}}$, and has its complete, orthonormal set of basis states $|s_i\rangle$, $s = 1, 2, \ldots, d_S$. Such set of vectors are eigenstates of the operator $\hat{S}$ in $\mathscr{H}_{\mathcal{S}}$ which corresponds to the observable S to be measured. The intrinsic Hamiltonian of the system is $\hat{H}_{\mathcal{M}}$. The system is assumed to be initially prepared (pre-selected) either in a pure state $|s\rangle$ (in which case its density matrix is $\hat{\sigma}_0 = |s\rangle \langle s|$) or in a more general state described by an arbitrary $\hat{\sigma}_0$.

The total system $\mathcal{T}$ comprises the object-system $\mathcal{S}$ and the meter $\mathcal{M}$. Its Hilbert space is $\mathscr{H}_{\mathcal{T}} = \mathscr{H}_{\mathcal{S}} \otimes \mathscr{H}_{\mathcal{M}}$ and the initial state of the total system is $\hat{\tau}_0 = \hat{\sigma}_0 \otimes \hat{\mu}_0$, the system and the meter are assumed to be initially uncorrelated (not entangled). The total Hamiltonian is

$$\hat{H}_{\mathcal{T}} = \hat{H}_{\mathcal{S}} + \hat{H}_{\mathcal{M}} + \hat{H}_{int}$$

and we consider that the only non vanishing term in $\hat{H}_{\mathcal{T}}$ is $\hat{H}_{int}$, the interaction Hamiltonian between $\mathcal{S}$ and $\mathcal{M}$.

2.4.2 *The pre-measurement*

The system and the meter are assumed to interact via a unitary time-evolution operator $\hat{U}$ in what is called a pre-measurement. This means that the total system $\mathcal{T}$ with its initial density matrix $\hat{\tau}_0$ will evolve unitarily into $\hat{\tau}_1$:

$$\hat{\tau}_0 = \hat{\sigma}_0 \otimes \hat{\mu}_0 \qquad \xrightarrow{\hat{U}} \qquad \hat{\tau}_1 = \hat{U}\hat{\sigma}_0 \otimes \hat{\mu}_0 \hat{U}^\dagger$$

where $\hat{U}^\dagger$ is the Hermitian conjugate of $\hat{U}$. For completeness we point out that the unitary time evolution operator $\hat{U}$ is linked to the Hamiltonian by:

$$\hat{U} = e^{-\frac{i}{\hbar}\int dt \hat{H}_T}$$

for $\hat{U}$ to be a pre-measurement of $\hat{S}$, $\hat{U}$ must be able to distinguishes between the different states $|s_i\rangle$. It is therefore assumed that an initial joint pure state $|s_i\rangle \otimes |m^{(0)}\rangle$ of the system and the meter is transformed by $\hat{U}$ into:

$$|s_i\rangle \otimes |m^{(0)}\rangle \quad \xrightarrow{\hat{U}} \quad \hat{U}\Big(|s_i\rangle \otimes |m^{(0)}\rangle\Big) = |s_i\rangle \otimes |m^{(i)}\rangle$$

where $i = 1, 2, \ldots, d_S$ and the meter states $|m^{(i)}\rangle$ act as markers for the system state $|s_i\rangle$; we will see in detail how this comes about later.

If this initial state is a superposition of eigenstates, the linearity of $\hat{U}$ gives:

$$|s\rangle \otimes |m^{(0)}\rangle \quad \xrightarrow{\hat{U}} \quad \hat{U}\Big(|s\rangle \otimes |m^{(0)}\rangle\Big) = \sum_{i=1}^{d_S} c_i |s_i\rangle \otimes |m^{(i)}\rangle \tag{2.5}$$

or, in the density matrix notation:

$$\begin{aligned}
\hat{\tau}_0 = \hat{\sigma}_0 \otimes \hat{\mu}_0 \quad \xrightarrow{\hat{U}} \quad \hat{\tau}_1 &= \hat{U}\hat{\sigma}_0 \otimes \hat{\mu}_0 \hat{U}^\dagger \\
&= \sum_{i,j} \Big(\langle s_i| \otimes \langle m^{(i)}| \langle s_i| \hat{\sigma}_0 |s_j\rangle \langle s_j| \otimes \langle m^{(j)}| \Big) \\
&= \sum_{i,j} \Big(\langle m^{(i)}| \hat{\mathbb{P}}_{s_i} \hat{\sigma}_0 \hat{\mathbb{P}}_{s_j} \langle m^{(j)}| \Big)
\end{aligned}$$

with $\hat{\mathbb{P}}_{s_i}$ projectors in the $\mathscr{H}_S$ space.

We note that:

- A system's pure eigenstate $|s_i\rangle$ is left unchanged under this operation.
- One of the most important consequences of the pre-measurement is that the system's state becomes correlated (entangled) with the meter state: $\hat{\tau}_1$ cannot be written as a product of one object state and one meter state (2.5).
- The meter states $|m^{(0)}\rangle$ and $|m^{(i)}\rangle$ are, in general, not eigenstates of the meter operator $\hat{M}$, but superpositions of such eigenstates. In particular, the states $|m^{(0)}\rangle$ and $|m^{(i)}\rangle$, $i = 1, 2, \ldots, d_S$, are normalized but in general not mutually orthogonal. Nor do they form a complete set in $\mathscr{H}_M$. Indeed, the dimensions d_S and d_M of the respective Hilbert spaces $\mathscr{H}_S$ and $\mathscr{H}_M$ need not be equal.
- The operation $\hat{U}$ thus correlates the system state $|s_i\rangle$ with the meter state $|m^{(i)}\rangle$ but not necessarily in a unique way: to each $|s_i\rangle$ there corresponds a definite $|m^{(i)}\rangle$, different for different $|s_i\rangle$, but there could be overlap between $|m^{(i)}\rangle$ and $|m^{(j)}\rangle$, expressed by $\langle m^{(i)}|m^{(j)}\rangle \neq 0$, for $i \neq j$.

The rule for obtaining the separate states $\hat{\sigma}_1$ for the system, and $\hat{\mu}_1$ for the meter, after this pre-measurement, is to take the partial trace over the non-interesting degrees of freedom (A.2.1). In case we want the state $\hat{\sigma}_1$ of the system, this means execute the partial trace over $\hat{H}_M$:

$$\begin{aligned}
\hat{\sigma}_0 \quad \xrightarrow{\hat{U}} \quad \hat{\sigma}_1 = Tr_M \hat{\tau}_1 &= \sum_k \langle m_k|\hat{\tau}_1|m_k\rangle \\
&= \sum_{i,j} \Big(\hat{\mathbb{P}}_{s_i} \hat{\sigma}_0 \hat{\mathbb{P}}_{s_j} \langle m^{(j)}|m^{(i)}\rangle \Big)
\end{aligned}$$

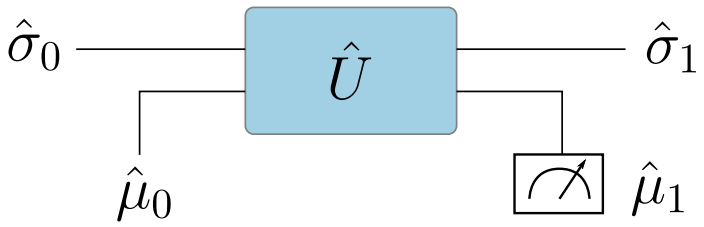

Figure 2.4.: Schematic diagram of a generalized measurement. The system of interest is coupled to an ancilla prepared in a known state $\hat{\mu}_0$ by the unitary evolution $\hat{U}$, and then a projective measurement is performed on the ancilla.

As is seen, in case of no overlap between different states $|m^{(i)}\rangle$, the ancilla-measurement scheme have the same consequences for the object-system as would a projective measurements scheme would have had. The general case, $\langle m(i)|m(j)\rangle \neq 0$ for $i \neq j$, does allow for interference between different eigenstates associated to the eigenvalues s_i, a fact which will have interesting measurable effects.

2.4.3 *The read-out*

So far, no real measurement has been performed in the sense of obtaining a record. The entangled system-meter is still in a quantum-mechanical superposition $\hat{\tau}_1$. One needs a recording, a read-out of the meter, in order to obtain information that constitutes a real measurement. Therefore, the next step in this ancilla measurement scheme is to subject the meter, and only the meter, to a projective measurement of the pointer observable M (see figure 2.4 for a schematic representation of the measurement process). Reading off the meter means obtaining an eigenvalue m_k of the corresponding operator $\hat{M}$ in a operation that is symbolized by the projector $\hat{O}_{m_k} = |m_k\rangle\langle m_k|$ onto the corresponding subspace of the meter Hilbert space $\mathscr{H}_M$. Since, as a result of the pre-measurement, the system is entangled with the meter, this will influence the system state too, and is therefore also a measurement of the object-system as will be evident shortly.

For the total density matrix, this projective measurement, implies:

$$\hat{\tau}_1 \xrightarrow{\hat{O}_{m_k}} \hat{\tau}_1(|m_k) = \frac{\left(\hat{\mathbb{I}}_S \otimes \hat{O}_{m_k}\right)\hat{\tau}_1\left(\hat{\mathbb{I}}_S \otimes \hat{O}_{m_k}\right)}{P(m_k)}$$

where with $\hat{\tau}_1(|m_k)$ we mean the total density matrix state $\hat{\tau}$ conditioned by the reading of the outcome m_k, $\hat{\mathbb{I}}_S$ is the unit operator in $\mathscr{H}_S$ and where $P(m_k) = P(m_k|\hat{\tau}_1)$ is the probability of obtaining the ancilla value m_k given the state $\hat{\tau}_1$.

The good question to ask now is if we have learned something concerning the system state from the read-out of the meter. To answer this question we have to look at the density matrix of the system $\hat{\sigma}_1(|m_k)$ after read-out, that tells what is the

system status after that action. Such density matrix matrix is obtained by partially tracing the overall system density matrix:

$$\hat{\sigma}_1(|m_k) = Tr_{\mathcal{M}}\,\hat{\tau}_1(|m_k) \tag{2.6}$$

$$= \frac{1}{P(m_k)} Tr_{\mathcal{M}}\left[\left(\hat{\mathbb{I}}_S \otimes \hat{\mathbb{O}}_{m_k}\right)\hat{\tau}_1\left(\hat{\mathbb{I}}_S \otimes \hat{\mathbb{O}}_{m_k}\right)\right] \tag{2.7}$$

$$= \frac{1}{P(m_k)} \langle m_k|\,\hat{U}\hat{\sigma}_0 \otimes \hat{\mu}_0\hat{U}^\dagger\,|m_k\rangle \tag{2.8}$$

$$= \frac{1}{P(m_k)} \langle m_k|\,\hat{U}\,|m^{(0)}\rangle\,\hat{\sigma}_0\,\langle m^{(0)}|\,\hat{U}^\dagger\,|m_k\rangle \tag{2.9}$$

$$= \frac{1}{P(m_k)} \hat{\Omega}_k\hat{\sigma}_0\hat{\Omega}_k^\dagger \tag{2.10}$$

where $\hat{\Omega}_k$ is an operator in $\mathscr{H}_S$ defined by:

$$\begin{aligned}\hat{\Omega}_k &= \langle m_k|\,\hat{U}\,|m^{(0)}\rangle \\ &= \sum_i \langle m_k|m^{(i)}\rangle\,|s_i\rangle\,\langle s_i| \\ &= \sum_i \langle m_k|m^{(i)}\rangle\,\hat{\mathbb{P}}_{s_i}\end{aligned}$$

The operators $\hat{\Omega}_k$ are called measurement operators and are often denoted $\hat{M}_k$ in literature (here we use $\hat{\Omega}_k$ since in our notation M entitles entities related to the meter).

At this point, the ancilla-scheme approach to the measurement theory allows us to easily understand the novel interesting properties of what we called weak measurement. A quantum mechanical measurement, in general implies that the object-system under study will suffer large changes (disturbances) in its state, even if the measurement is considered non-destructive; in our formalism, these disturbances appear in the change from the initial density matrix $\hat{\sigma}_0$ to a usually quite different matrix $\hat{\sigma}_1$ after the measurement (see 2.6). A weak measurement is a measurement that disturbs the state of the object of interest as little as possible. As we will see, a weak measurement is also such that the measurement results are less clear than in a strong or projective measurement. For example, there will be difficulties in distinguishing one eigenvalue of the observable under study from another. An interesting fact is that it has been shown that in certain conditions weak measurements allows for the emerging of new phenomena that can only be studied by weakening the interaction responsible for the measurement as much as possible [31].

In our work the result obtained in equation 2.5 is particularly meaningful; we saw that after the pre-measurement the two objects (system and ancilla) are entangled, and that this entanglement can be weakened as desired by appropriately choosing the $m^{(i)}$ basis. This result is the core idea of our work; our goal is in fact to weakly entangle a system and the ancilla in order to allow to share non-local correlations with a third system.

3

NON-LOCALITY SHARING AMONG MULTIPLE OBSERVERS

In this chapter we will discuss the topic of interest of this thesis. In the previous chapter we introduced the concepts of non-locality and weak measurement; we characterized non-locality mathematically, and we showed how this property basically qualifies a class of correlated measurements between two observers. All the discussions we made in section 2.3 had a two-observer scenario (*Alice* and *Bob*) as reference situation. This is not a casual aspect: generally scientific literature on the argument focus on characterizing non-locality properties in a two-observer (or at most multipartite) scenario. Only very recently the possibility of sharing non-locality among multiple observers has been taken into account.

The aim of this work is to explore experimentally the topic of non-locality sharing among multiple observers, building one of the first apparatuses capable of proving the possibility to establish multiple non-local correlation among three observers sharing the same spin-1/2 entangled state.

This work is inspired by the article *"Multiple Observers Can Share the Nonlocality of Half of an Entangled Pair by Using Optimal Weak Measurements"* by Silva, Ralph, et al. [7], which explored theoretically the possibility to observe such non-Locality sharing. In the following we will introduce the topic closely following their argument.

3.1 TRIPARTITE BELL INEQUALITY

In the previous chapter, talking about measurement, we already discussed about one of the fundamental traits of quantum mechanics: in order to probe the properties of a system one must perturb it. We distinguished among two different types of measures:

- "Strong" measurements which collapse the system into one of the eigenstates of the measured observable; this type of measurements give the maximum information about the system.
- "Weak" measurements that disturb the system infinitesimally, giving only a small amount of information about the state.

It is interesting to study the situation where the strength of the measurement can vary continuously from very weak to strong, analysing how the trade-off between the degree of disturbance on the system and the amount of information gained evolves with the measurement strength. We will explore this topic considering measurements on a pair of entangled spin-1/2 particles, focusing on a new fundamental question in non-locality: can the non-locality of an entangled pair of particles be distributed among multiple observers, considered a scenario where the observers act sequentially and independently of each other?

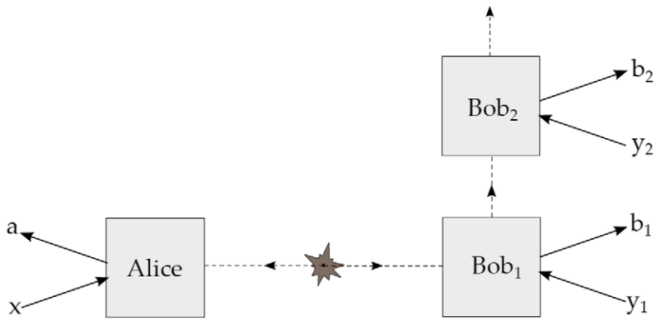

Figure 3.1.: Bell scenario involving a single Alice and multiple Bobs, where the dashed lines indicate a spin-1/2 particle being transmitted, and the solid lines the inputs and outputs. [7]

We consider the scenario where a single observer has access to one of the particles of an entangled pair, and a group of two of observers have access to the second particle. Each observer in the second group acts independently, so the first one performs a measurement on the particle before passing it to the second one. We address the question of whether the single observer with the first particle can see non-local correlations with both the two observers that have access to the second particle. This Bell-scenario is represented in figure 3.1.

In our scheme we will call *Alice* the observer that has exclusive access to one-half of the entangled pair of spin-1/2 particles, and we will call respectively Bob_1 and Bob_2 the two observers that have access to the other half of the the entangled pair. The Bobs are independent; i.e., Bob_2 is ignorant of the direction that Bob_1 measures his spin in as well as the outcome of his measurement.

We investigate whether the statistics of the measurements of Bob_1 and Bob_2 can both be non-local with *Alice* by testing the conditional probabilities $P(ab_1|xy_1)$ and $P(ab_2|xy_2)$ against the CHSH inequality.

At first one may think it impossible to have simultaneous violations *Alice*-Bob_1 and *Alice*-Bob_2 because of the monogamy of entanglement and of nonlocality [32]. However, these results assume no-signaling between all parties, while in our scenario Bob_1 implicitly signals to Bob_2 his choice of measurement on the state before he passes it on. Hence, no monogamy argument holds, and one has to look more closely at the situation.

We assume the measurements are unbiased; i.e., both *Bobs* choose the inputs 0 and 1 with equal probability. Clearly Bob_1 cannot perform a strong measurement, since he would destroy the entanglement, and prevent Bob_1 from being non-local with *Alice*. However, Bob_1 may not be able to observe non-locality with a very weak measurement either. To see this precisely, consider that *Alice* and the *Bobs* initially share a singlet state, and that they perform the standard measurements that attain Tsirelson's bound for the CHSH inequality: i.e., Alice measures in the $\bar{Z}$ or $\bar{X}$ direction, corresponding to inputs 0 or 1, respectively, and the *Bobs* measure in the directions $-\frac{\bar{Z}+\bar{X}}{\sqrt{2}}$ or $\frac{-\bar{Z}+\bar{X}}{\sqrt{2}}$, for their respective inputs 0 or 1.

The *Bobs* receive a spin-1/2 particle, whose spin in the $|H\rangle, |V\rangle$ polarization basis can be written:

$$|\psi\rangle = \alpha|H\rangle + \beta|V\rangle$$

Bob$_1$ is the first one to measure the particle, and he adopts a weak measurement scheme, coupling the state of the received system $|\psi\rangle$ with the state of an ancilla system that is initially in the state $|+\rangle$. *Bob*$_1$'s coupling follows is given by:

$$|\psi\rangle \otimes |+\rangle \longrightarrow \alpha\,|H\rangle \otimes |+\rangle + \beta\,|V\rangle \otimes \left(\cos\epsilon\,|+\rangle + i\sin\epsilon\,|-\rangle\right)$$

We will indicate with $|\phi_H\rangle$ the ancilla state associated to the $|H\rangle$ polarization of the entangled particle ($|\phi_H\rangle = |+\rangle$), and we will indicate with $|\phi_V\rangle$ the ancilla state associated to the $|V\rangle$ polarization ($|\phi_V\rangle = \cos\epsilon\,|+\rangle + i\sin\epsilon\,|-\rangle$). *Bob*$_1$ measures then on an orthonormal basis set $|+\rangle, |-\rangle$, obtaining the results $+, -$ with a probability:

$$P(+) = P\Big(|\psi\rangle = |H\rangle\Big)P\Big(+||\phi_H\rangle\Big) + P\Big(|\psi\rangle = |V\rangle\Big)P\Big(+||\phi_V\rangle\Big) \tag{3.1}$$

$$P(-) = P\Big(|\psi\rangle = |H\rangle\Big)P\Big(-||\phi_H\rangle\Big) + P\Big(|\psi\rangle = |V\rangle\Big)P\Big(-||\phi_V\rangle\Big) \tag{3.2}$$

where $P\Big(|\psi\rangle = |H\rangle\Big)$ and $P\Big(|\psi\rangle = |V\rangle\Big)$ represent respectively the probability of receiving an entangled particle with polarization $|H\rangle$ and $|V\rangle$, and the terms of the form $P\Big(+||\phi_H\rangle\Big)$ represent the conditional probability of obtaining a certain *Bob*$_1$ outcome given a certain ancilla state. The outcome probabilities 3.1 and 3.2 in the presented scheme are easy to calculate and read:

$$P(+) = \frac{1}{2}\Big(2 - \sin^2\epsilon\Big) \tag{3.3}$$

$$P(-) = \frac{1}{2}\sin^2\epsilon \tag{3.4}$$

From equations 3.4 and 3.3 we can easily see that both the outcome probabilities depend on the ϵ parameter by the function $\sin^2\epsilon$. We can call the quantity $\sin^2\epsilon = G$ *information gain*, we see in fact that G gives an idea of the quantity of information extracted from the entangled state by the ancilla:

- If $G = 0$, the read-out of the ancilla returns always the ancilla initial state, so basically the system behaves as if there was no interaction at all, and *Bob*$_1$ doesn't gain any information about the system state.
- If $G = 1$, the read-out of the ancilla allows to reconstruct exactly the system state, so it is like *Bob*$_1$ was performing a strong measurement on the system state.
- All the values for G between 0 and 1 characterize an intermediate situation between very weak (absent) *Bob*$_1$ measurement and strong measurement.

From the above consideration it is clear why we refer to G as the *information gain*.

Another quantity of interest is $F = \langle\phi_H|\phi_V\rangle = \cos\epsilon$ called the *quality factor*. The state after *Bob*$_1$ measurement (defined ρ' in the density matrix notation) reads:

$$\rho_0 = F\,|\psi\rangle\langle\psi| + (1-F)\Big(\pi^+\,|\psi\rangle\langle\psi|\,\pi^+ + \pi^-\,|\psi\rangle\langle\psi|\,\pi^-\Big)$$

From such equation it is clear why we refer the to F as the *quality factor*: F weights the proportion of the postmeasurement state that corresponds to the original state, while the remainder corresponds to the state decohered in the measurement eigenbasis, as it would have been if measured strongly.

At this point, using the standard form of the CHSH expression with the classical bound at 2 and the quantum bound at $2\sqrt{2}$, it is possible to calculate the CHSH expectation values[1] finding that the correlations between *Alice* and the *Bobs* are given by $I^{(1)}_{CHSH} = 2\sqrt{2}G$, and $I^{(2)}_{CHSH} = \sqrt{2}(1+F)$, where G and F are the precision and quality factor of Bob_1's measurement.

Studying such equations we find that there is a G-parameter region where both the CHSH inequalities can be violated, see the figure 5.3 on page 43 for a graphical representation of the CHSH inequalities trend in function of the information gain. From the figure we see that Bob_1 must tune the precision of his measurement, as either a strong or weak measurement would prevent Bob_2 or himself, respectively, from seeing a CHSH violation.

This discussion highlighted that in the scenario just described it should be possible (by optimizing Bob_1 measurement strength) to obtain simultaneous non-local correlation between *Alice-*Bob_1 and *Alice-*Bob_2. We want at this point prove this fact experimentally. In chapter 5 we will present an apparatus that implements the discussed idea, that should allow for experimental non-locality sharing among multiple observers.

1 The extended calculation can be found in chapter 5.

4

EXPERIMENTAL TECHNIQUES

As we have already seen in the first chapter, one of the most characteristic features of quantum mechanics is the phenomenon of *entanglement* (see section 2.2). Particles that are entangled in some of their degrees of freedom possess correlations that cannot be explicated within the classical framework (see section 2.3), a feature that makes entanglement one of the main obstacles in finding a convincing interpretation of quantum theory. Entanglement can exist between different degrees of freedom of a single particle, or in the same degree of freedom of multiple particles. The latter is the most interesting situation for quantum communication, since it allows non-classical correlations to travel along very long distances.

At the end of the previous chapter we saw that to demonstrate experimentally the possibility to obtain multiple non-local correlations from an entangled pair we need to manipulate a bipartite entangled quantum system. The first thing we will need to worry about to build our experiment is how to obtain an entangled photon-pair. In this chapter, we will deal with this aspect discussing:

- how it is possible to employ non-linear optical effects, in particular spontaneous parametric down-conversion (**SPDC**), to produce polarization entangled photons;
- how we can make use of such phenomenon to build an efficient entangled photon source;
- finally we will describe the design of the source used in our experiment, and we will characterize its properties.

4.1 SPONTANEOUS PARAMETRIC DOWN-CONVERSION

Spontaneous parametric down-conversion (also known as SPDC) is the physical process nowadays most commonly exploited in physics to produce entangled photon pairs. Such process is of extreme importance in quantum optics and quantum information, and is caused by nonlinear interactions between the electromagnetic field and a crystal (see figure 4.1 for a schematic representation of the phenomenon). To describe the process properly we will need then to study nonlinear optical effects; the starting point of such analysis will be obviously the Maxwell equations.

The set of equations B.1 on page 83, used to describe the free electromagnetic field, is no more adequate when we want to describe the interaction of the electromagnetic field with matter. This interaction happens at the atomic level, therefore it could be theoretically possible to describe the passage of an electromagnetic wave through some medium by explicitly treating atomic charges and currents within the theory. However, the high number of atoms in a general system makes this approach highly

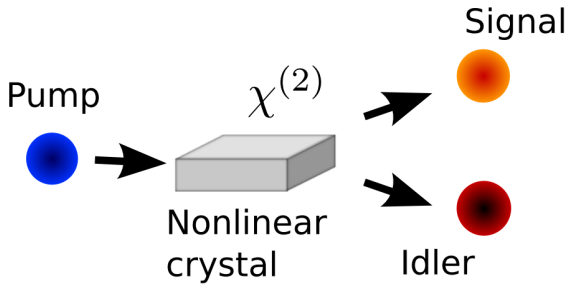

Figure 4.1.: In the process of SPDC a pump photon spontaneously decays, inside a medium exhibiting a $\chi^{(2)}$-nonlinearity, into two photons, for historical rea- sons, labelled signal and idler. [33]

impractical, making it preferable to find a model that approximates such interaction. The model used in electromagnetism splits currents and charges into "free" ones, that can move freely through the medium (like the electrons in a conductor), and "bound" ones, which are forced to oscillate around their atom. Bound charges and currents are described by electric and magnetic multi-poles [34]. Within this theory, Maxwell's equations become:

$$\nabla \cdot \mathbf{D}(\mathbf{r}, t) = \rho(\mathbf{r}, t) \tag{4.1}$$

$$\nabla \times \mathbf{H}(\mathbf{r}, t) - \frac{\partial \mathbf{D}(\mathbf{r}, t)}{\partial t} = \mathbf{J}(\mathbf{r}, t) \tag{4.2}$$

$$\nabla \times \mathbf{E}(\mathbf{r}, t) + \frac{\partial \mathbf{B}(\mathbf{r}, t)}{\partial t} = 0 \tag{4.3}$$

$$\nabla \cdot \mathbf{B}(\mathbf{r}, t) = 0 \tag{4.4}$$

where $\mathbf{D} = \varepsilon_0 \mathbf{E} + \mathbf{P}$ is the *displacement field* and $\mathbf{H} = \frac{1}{\mu_0}\mathbf{B} - \mathbf{M}$ is the *magnetizing field*. These fields capture the effects of the field on bound charges and currents, which are described by the *polarization vector* $\mathbf{P}$ and the *magnetization vector* $\mathbf{M}$, while the behaviour of free charges and currents is still described by the source terms ρ and $\mathbf{J}$. Most materials used in optics are uncharged non-conducting materials, therefore both free charges and currents are zero. Moreover, they are also non-magnetic materials, therefore the magnetization vector $\mathbf{M} \simeq 0$ and the interaction of the material with the field is completely captured by the polarization vector $\mathbf{P}$.

In the general case, the polarization vector can be expressed as a power series:

$$P_i = \varepsilon_0 \left(\sum_j \chi^{(1)}_{ij} E_j + \sum_{jk} \chi^{(2)}_{ijk} E_j E_k + \sum_{jkl} \chi^{(3)}_{ijkl} E_j E_k E_l + \cdots \right) \tag{4.5}$$

$$= P^{(1)}_i + P^{(2)}_i + P^{(3)}_i + \cdots \tag{4.6}$$

$$= P^{(1)}_i + P^{(NL)}_i \tag{4.7}$$

where the term $P^{(1)}_i$ is responsible for the linear response of the matter (such as refraction), while the higher order terms $P^{(NL)}_i$ are responsible for the nonlinear response of the matter. The relation between $\mathbf{P}$ and $\mathbf{E}$ (polarization vector and electric vector) is approximately linear when $\mathbf{E}$ is small, but becomes nonlinear when $\mathbf{E}$ acquires values comparable to interatomic electric fields [35]. The non linear terms

$P_i^{(NL)}$ act as a source of new components of the electromagnetic field. This is evident from the wave equation in a nonlinear optical medium [36]:

$$\nabla^2 \mathbf{E} - \frac{n^2}{c^2}\frac{\partial^2 \mathbf{E}}{\partial t^2} = \frac{1}{\varepsilon_0 c^2}\frac{\partial^2 P^{(NL)}}{\partial t^2} \tag{4.8}$$

where n is the index of refraction and c the speed of light. This expression can be regarded as a dipole emitting light $\mathbf{E}$ driven by the nonlinear polarization $\mathbf{P}^{(NL)}$ induced by the pump wave in the medium.

The **SPDC** emission stems from the $\chi^{(2)}$-nonlinearity. It features the advantage to be much stronger than the higher-order nonlinear terms and enables an efficient nonlinear interaction. Note that $\chi^{(2)}$-nonlinearity are only present in crystal materials featuring noncentrosymmetric crystal structures [36]. The most commonly used crystals for SPDC generation are BBO, $LiNbO_3$, and KTP.

Using the *Poynting theorem* [34], it is possible to write the field energy density (i.e., the Hamiltonian density) in the medium as

$$\mathcal{H}(\mathbf{r}, t) = \frac{1}{2}\left(\mathbf{E}\cdot\mathbf{D} + \mathbf{B}\cdot\mathbf{H}\right) \tag{4.9}$$

In our case we are not interested in the contribution by the magnetic component, since the SPDC interaction stems from the electric displacement field $\mathbf{D}$, obtaining (neglecting the time dependence from now on):

$$\begin{aligned}
H &= \int_V d^3r\, \mathcal{H}(\mathbf{r}) \\
&= \frac{1}{2}\int_V d^3r \left(\mathbf{E}^{(p)}\cdot\mathbf{D})\right) \\
&= \int_V d^3 \left(\frac{\varepsilon_0}{2}\chi^{(1)}\mathbf{E}^{(p)}\mathbf{E} + \frac{\varepsilon_0}{3}\chi^{(2)}\mathbf{E}^{(p)}\mathbf{E}\mathbf{E} + \dots\right) \\
&= \int_V d^3r \left(\frac{\varepsilon_0}{2}\sum_{ij}\chi^{(1)}_{ij}\mathbf{E}^{(p)}_i\mathbf{E}_j + \frac{\varepsilon_0}{3}\sum_{ijk}\chi^{(2)}_{ijk}\mathbf{E}^{(p)}_i\mathbf{E}_j\mathbf{E}_k + \dots\right) \qquad (4.10) \\
&= \int_V d^3r\, \left(\mathcal{H}_0(\mathbf{r}) + \mathcal{H}_I(\mathbf{r})\right) \qquad (4.11) \\
&= H_0 + H_I
\end{aligned}$$

where we explicitly labelled the incoming wave $\mathbf{E}^{(p)}$ and the ijk subscripts describe the polarization of the individual beams.

Once the classical Hamiltonian density has been written as a function of the classical fields (4.10), it is possible to obtain the corresponding quantum Hamiltonian by quantising the involved electric fields. Here we restrict ourselves to an interaction in one dimension, i.e. we assume a fully collinear propagation of the electric fields through the medium in a single spatial mode. We first separate the quantized electric field into its positive and negative frequency parts:

$$\hat{E} = \hat{E}^{(+)} + \hat{E}^{(-)}$$

The fields operator $\hat{E}^{(+)}$, $\hat{E}^{(-)}$ will be naturally associated to their quantum mechanical amplitude operator $\hat{a}_\lambda(\mathbf{k})$, $\hat{a}^\dagger_\lambda(\mathbf{k})$ that satisfy the commutation relations C.4, C.3 and that are the result of the same mode expansion as the free electric field.

The quantum interaction Hamiltonian density $\hat{\mathcal{H}}_I$ can therefore be written as:

$$\hat{\mathcal{H}}_I \propto \sum_{ij} \chi^{(1)}_{ij} \left(\hat{E}^{(+)}_i + \hat{E}^{(-)}_i\right)\left(\hat{E}^{(+)}_j + \hat{E}^{(-)}_j\right) + \sum_{ijk} \chi^{(2)}_{ijk} \left(\hat{E}^{(+)}_i + \hat{E}^{(-)}_i\right)\left(\hat{E}^{(+)}_j + \hat{E}^{(-)}_j\right)\left(\hat{E}^{(+)}_k + \hat{E}^{(-)}_k\right) + \dots \tag{4.12}$$

In the interaction picture, the evolution of the state is governed by operator

$$\hat{U} = \mathcal{T}\, exp\left[-\frac{i}{\hbar}\int_{-\infty}^{+\infty} \hat{H}_I\right] \tag{4.13}$$

where $\mathcal{T}$ it the time-ordered product [37], and the integration limits $-\infty$ and $+\infty$ are justified by the fact that the state is observed long after the non-linear interaction in the medium [33]. The interaction Hamiltonian is given by the spatial integration of the Hamiltonian density as in equation 4.11. The above integral can be evaluated using the rotating-wave approximation, which allows to neglect rapidly oscillating terms in the Hamiltonian $\hat{H}_I$ [33].

The linear $\chi^{(1)}$ term of the Hamiltonian density 4.12 gives rise to refractive effects (such as,for example, birefringence). The only linear surviving terms are those of the form $\hat{E}^{(+)}_i \cdot \hat{E}^{(-)}_j$ (and its complex conjugate), which produce a photon-number preserving Hamiltonian. These effects can be treated in a simple way by aligning the system of reference to the *principal axes* of the material, in which the $\chi^{(1)}$ tensor assumes a diagonal form (i.e., $\chi^{(1)}_{ij} \neq 0$ iff $i = j$) [35].

The $\chi^{(2)}$ term gives rise to a wide range of non-linear effects [36]. Spontaneous parametric down-conversion is the effect described by the interaction term of the form:

$$\hat{H}_{SPDC} = \int d^3\mathbf{r} \sum_{i_p j_s k_i} \chi^{(2)}_{i_p j_s k_i} \hat{E}^{(+)}_{i_p} \hat{E}^{(-)}_{j_s} \hat{E}^{(-)}_{k_i} + c.c. \tag{4.14}$$

where the term $\hat{E}^{(+)}_{i_p}$ corresponds to the annihilation of a *pump* photon of mode i_p and the terms $\hat{E}^{(-)}_{j_s}$ and $\hat{E}^{(-)}_{k_i}$ to the creation of two photons in modes j_s and k_i, called, respectively, *signal* and *idler* photons. By properly adjusting the pump field, it is possible to make the SPDC term the only one giving a considerable effect. In order to have this, however, it is necessary that the fields respect the so-called *phase-matching* conditions

$$\omega_{i_p} = \omega_{j_s} + \omega_{k_i} \tag{4.15}$$

$$\mathbf{k}_{i_p} = \mathbf{k}_{j_s} + \mathbf{k}_{k_i} \tag{4.16}$$

where the two conditions are due to energy conservation and momentum conservation respectively in the photons production (see figure 4.2).

The optimization of the SPDC process requires to study the form of the Hamiltonian (4.14) for different pump, signal and idler modes. The large number of variables required to describe these fields makes it preferable to perform some approximations about their form, in order to simplify the problem. The analysis of the SPDC process has been carried in a very lot of papers, each one considering a different approximation [38, 39, 40, 41, 42]. The most suitable analysis for our setup is the one by

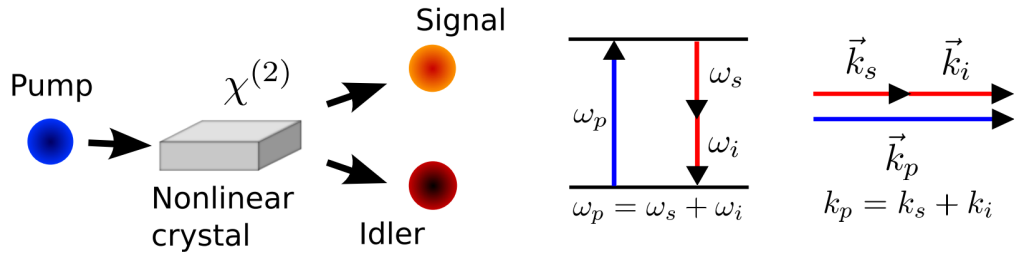

Figure 4.2.: In the SPDC process the spectral properties of the generated photon-pair are constrained by momentum and energy conservation between the three interacting photons. [33]

Bennink [38], that considers the interaction of a gaussian pump field with a non-linear crystal, leading to the production of two collinear photons in gaussian modes. Since in collinear propagation the phase-matching condition (4.16) is not obtainable, it is necessary adopt other strategies to give a considerable production of down-converted pairs, called *quasi phase-matching*. Quasi phase-matching consists in modulating the $\chi^{(2)}$ coefficient of the crystal, alternating its sign with spatial period Λ. In this way, it is possible to have a significant improvement of the down-conversion efficiency [35].

In Bennink's study [38], the field $E^{(+)}$ is expanded as a superposition of different frequency gaussian modes

$$\hat{\mathbf{E}}^{(+)}(\mathbf{r},t) = \int_0^\infty d\omega \sqrt{\frac{\hbar\omega}{2\varepsilon_0}} \mathbf{E}_\omega(\mathbf{r}) e^{-i\omega t} \hat{a}_\omega(t) + \textit{non gaussian terms}, \tag{4.17}$$

and similarly $\hat{\mathbf{E}}^{(-)}$. Furthermore, he assumes that the second-order interaction is weak, so that it is possible to perform a first-order expansion of the evolution operator of equation (4.13). The state after the SPDC process is therefore

$$|\psi_{SPDC}\rangle = \hat{U}\,|\text{initial}\rangle \simeq |\text{initial}\rangle - \frac{i}{\hbar}\int_{-\infty}^{\infty} \hat{H}_{SPDC}(t)\,|\text{initial}\rangle\,, \tag{4.18}$$

where $|\text{initial}\rangle$ is the state of the field prior to the interaction and $\hat{H}_{SPDC}(t)$ is the Hamiltoninan (4.14).

Since the crystal is pumped with a laser, he assumes the pump to be described as a classical coherent state, with spectral amplitude $s(\omega_p)$ and mean number of photons N_p. With these approximations, and assuming that the pump state is filtered out, equation (4.18) can be written as

$$|\psi_{SPDC}\rangle = -i\int_0^\infty d\omega_s d\omega_i \psi(\omega_s,\omega_i) \hat{a}^\dagger_{\omega_s} \hat{a}^\dagger_{\omega_i} |\Omega\rangle\,, \tag{4.19}$$

where $|\Omega\rangle$ is the vacuum state and

$$\psi(\omega_s,\omega_i) = \sqrt{\frac{2\pi^2\hbar N_p}{\varepsilon_0 \lambda_p \lambda_s \lambda_i}} s(\omega_p) \mathcal{O}(\omega_s,\omega_i), \tag{4.20}$$

where $\lambda_i = 2\pi c/\omega_j$ is the free-space wavelength of field j, and the photons respect the phase-matching condition (4.15). The term

$$\mathcal{O}(\omega_s,\omega_i) = \int_{medium} d^3\mathbf{r}\, \boldsymbol{\chi}^{(2)}(\mathbf{r}) : \mathbf{E}_{\omega_p}(\mathbf{r}) \mathbf{E}^*_{\omega_s}(\mathbf{r}) \mathbf{E}^*_{\omega_i}(\mathbf{r}) \tag{4.21}$$

gives the efficiency of the quasi-phase-matched down-conversion process, which depends both on the efficiency of quasi-phase matching and on the overlap of the different spatial modes (the : notation in the integral is used to indicate the tensor product of the non-linear coefficient $\chi^{(2)}$ with the polarization terms ϵ_{ω_p} of mode $\mathbf{E}_{\omega_p}$).

4.2 EXPERIMENTAL DESIGN OF THE SOURCE

The source is based on a polarization-based Sagnac interferometer. The scheme of the source is shown in figure 4.3, while its experimental realization on the optical bench is in figure 4.4.

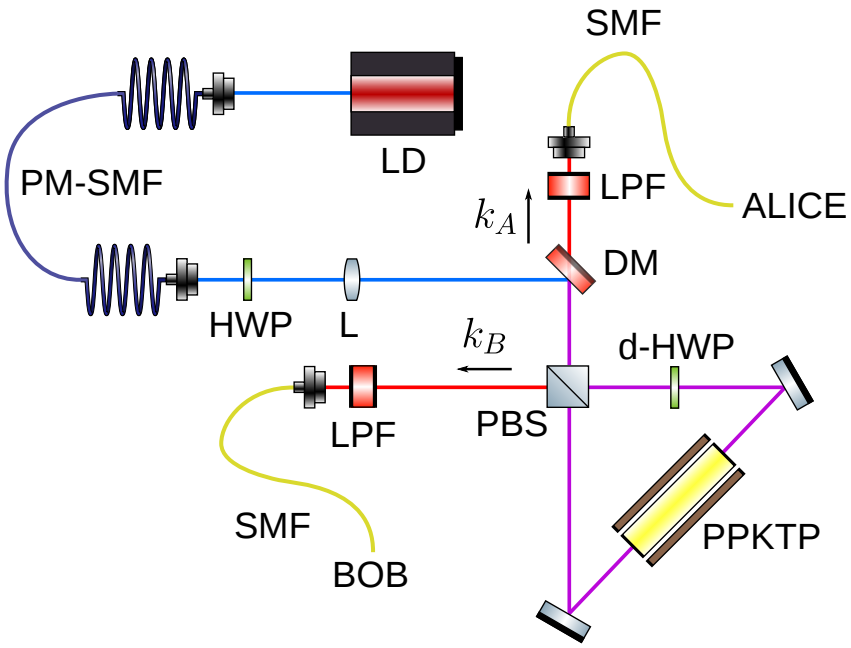

Figure 4.3.: Experimental scheme of the source of polarization-entangled photons based on a polarization Sagnac interferometer. The pump laser (LD) is injected into a polarization-maintaining single-mode fiber (PM-SMF) for mode filtering. The output of the fiber is sent onto a half-wave plate (HWP), that rotates the polarization state of the pump laser to $|+\rangle$. The state is then focused into a periodically-poled potassium titanyl phosphate (PPKTP) crystal placed at the center of a Sagnac interferometer. A polarizing-beam splitter (PBS) at the entrance of the interferometer splits the pump onto a superposition of clockwise (V) and counterclockwise (H) path. The clockwise pump beam crosses a dual-wavelength half-wave plate (d-HWP), that rotates its state from V to H. Both paths produce $|H\rangle_S |V\rangle_I$ couples, where the superscript indicates the signal and the idler photon. In the anticlockwise path, the d-HWP changes the couple to $|V\rangle_S |H\rangle_I$. At the PBS the photons are combined so that the resulting state is $|H\rangle_S |V\rangle_I + e^{i\theta} |V\rangle_S |H\rangle_I$, where θ is a phase term given by the different optical length of the two paths. The pump is removed using a long-pass filter (LPF) before injection into a single-mode fiber (SMF). This image uses elements from the ComponentLibrary by Alexander Franzen [43], licensed under CC BY-NC 3.0 [44].

The source is pumped with a CW laser diode (LD) at $\lambda_P = 404.5\,\text{nm}$. The beam emitted by the diode is collected onto a polarization-maintaining single-mode fiber (PM-SMF), used to clean its spatial mode. The PM-SMF is sent onto the optical breadboard, where the laser beam is collimated by an aspheric lens of focal length 11 mm into a beam of $\sim 1.5\,\text{mm}$ diameter. The polarization state of the beam is transformed into $\epsilon_+ = (\epsilon_H + \epsilon_V)/\sqrt{2}$ by a half-wave plate (HWP) and then focused

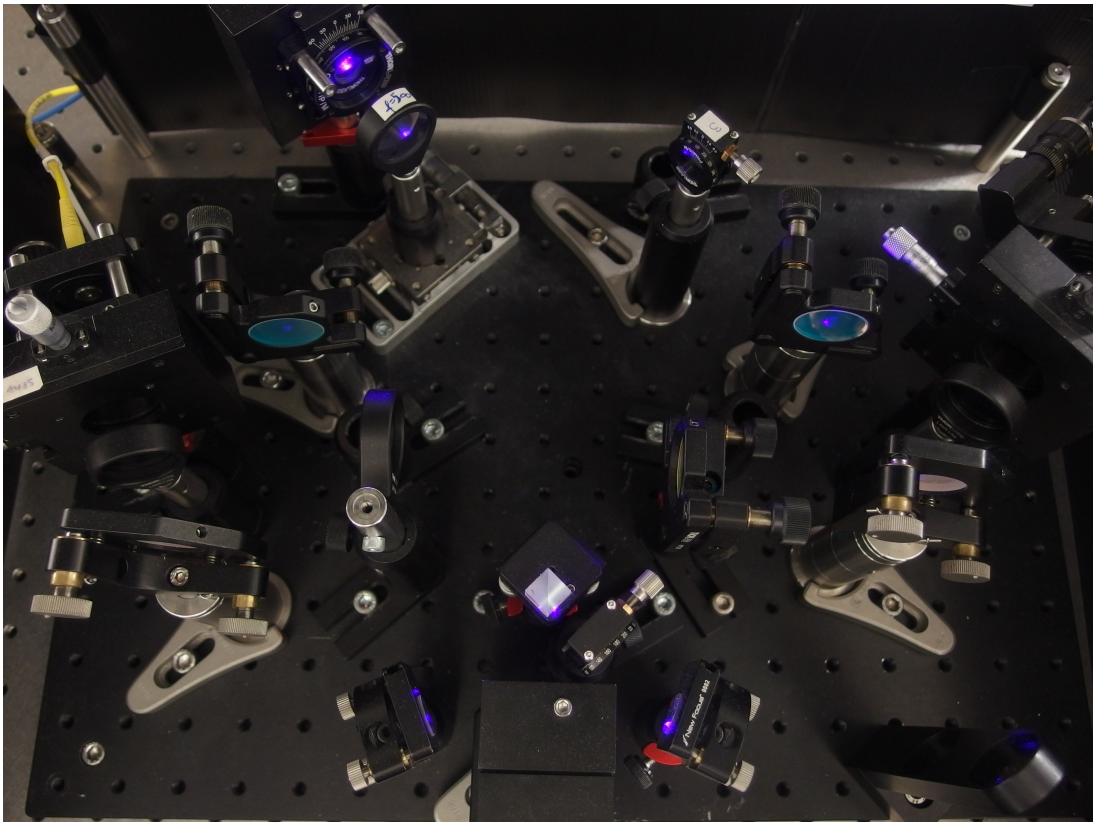

Figure 4.4.: Implementation of the scheme described in Figure 4.3 on the optical bench.

by a doublet with equivalent focal length 333 mm into the center of the Sagnac interferometer.

At the entrance of the interferometer, a polarizing-beam splitter (PBS) creates a superposition of clockwise $\mathbf{k}_C$ and counterclockwise $\mathbf{k}_{CC}$ path, by sending H polarization in the first path and V polarization in the second one. The state is then transformed, by the dual-wavelength half-wave plate (d-HWP) into $(E_H(\mathbf{k}_C) + E_H(\mathbf{k}_{CC}))/\sqrt{2}$. This state travels through a periodically-poled $KTiOPO_4$ (PPKTP) crystal[1], that outputs the state

$$\hat{a}^\dagger_{\mathbf{k}_C,H}\hat{b}^\dagger_{\mathbf{k}_C,V} + \hat{a}^\dagger_{\mathbf{k}_{CC},H}\hat{b}^\dagger_{\mathbf{k}_{CC},V} \tag{4.22}$$

where $\hat{a}^\dagger$ and $\hat{b}^\dagger$ are the mode functions of, respectively, the signal and the idler photon (they can have different wavelength and are, in general, not temporally superposed due to the temporal walk-off introduced by crystal birefringence). The pair in the counterclockwise path, then, crosses the d-HWP, being transformed into $\hat{a}^\dagger_{\mathbf{k}_{CC},V}\hat{b}^\dagger_{\mathbf{k}_{CC},H}$.

Just before the polarizing beam-splitter (PBS), the state is

$$\hat{a}^\dagger_{\mathbf{k}_C,H}\hat{b}^\dagger_{\mathbf{k}_C,V} + e^{i\theta}\hat{a}^\dagger_{\mathbf{k}_{CC},V}\hat{b}^\dagger_{\mathbf{k}_{CC},H} \tag{4.23}$$

where the phase term $e^{i\theta}$ takes into account the different path length of the two arms of the interferometer. The PBS transforms the state into

$$|\text{out}\rangle = \frac{1}{\sqrt{2}}\left(\hat{a}^\dagger_{\mathbf{k}_A,H}\hat{b}^\dagger_{\mathbf{k}_B,V} + e^{i\theta}\hat{a}^\dagger_{\mathbf{k}_A,V}\hat{b}^\dagger_{\mathbf{k}_B,H}\right)|\Omega\rangle \tag{4.24}$$

1 The crystal is a 30 mm PPKTP by Raicol, with a $\chi^{(2)}$ grating of period $\Lambda = 10^{-}$m.

where $|\Omega\rangle$ is the vacuum state. The output polarization state is therefore

$$|\psi\rangle = \frac{|H\rangle_A |V\rangle_B + e^{i\theta} |V\rangle_A |H\rangle_B}{\sqrt{2}} \tag{4.25}$$

In order to produce the maximally entangled state $|\Psi^-\rangle$, therefore, it is necessary to adjust the value of the phase θ in the state (4.25). In addition to this, it is also necessary to compensate the birefringence effect of optical fibers. Indeed, let U_A be the effect of *Alice*'s fiber and U_B the effect of *Bob*'s one, the state at the output of the fibers is

$$|\psi_{fiber}\rangle = (U_A \otimes U_B) \frac{|H\rangle_A |V\rangle_B + e^{i\theta} |V\rangle_A |H\rangle_B}{\sqrt{2}} \tag{4.26}$$

To produce the singlet state $|\Psi^-\rangle$, it is sufficient to implement a general unitary transformation in one of the two output photons. Indeed, the singlet state has the property that $(U \otimes U) |\Psi^-\rangle = |\Psi^-\rangle$. The transformation that must be implemented on the output state is therefore $I_2 \otimes U$, with

$$U = U_A \begin{pmatrix} 1 & 0 \\ 0 & -e^{i\theta} \end{pmatrix} U_B^{-1} \tag{4.27}$$

Indeed, the applications of this transformation gives

$$\begin{aligned} (I_2 \otimes U)(U_A \otimes U_B)|\psi\rangle &= \frac{U_A |H\rangle_A (-e^{i\theta}) U_A |V\rangle_B + e^{i\theta} U_A |V\rangle_A U_A |H\rangle_B}{\sqrt{2}} \\ &= (U_A \otimes U_A) |\Psi^-\rangle = |\Psi^-\rangle \end{aligned} \tag{4.28}$$

5

EXPERIMENT

In this chapter (that is the most important of all the thesis) all the experimental aspects will be discussed in detail. The description will be organized as follow:

- In the first section 5.1 we will describe a physical system $\mathfrak{S}$ which can led to a tripartite Bell inequality when adequately prepared.
- In the second section 5.2 we will present an experimental design $\mathfrak{D}$ which in certain conditions produces the same results of the physical system $\mathfrak{S}$. In this section is thus given the idea and the theoretical description of a physical set-up that allows for a tripartite Bell inequality.
- In the third section 5.3 we will describe the experimental apparatus $\mathfrak{A}$ as mounted in laboratory. The analogy between the apparatus $\mathfrak{A}$ and the experimental design $\mathfrak{D}$ will be stressed precisely.

5.1 THEORETICAL MODEL

In this section the instruments of modern information theory (particularly quantum information theory) will be widely used to describe a physical system which can lead to a tripartite Bell inequality. See appendix A on page 75 for a brief review of these instruments.

As already introduced in section 2.3, it's generally convenient to describe quantum information problems as problems about the information exchanged among different parties (normally called the *observers*). To obtain a tripartite Bell inequality we'll necessarily need to consider a problem with three observers involved; we name these observers[1] *Alice*, *Bob* and *Charlie*. As explained in section 2.3 a tripartite Bell inequality occurs when non-local correlations are shared among multiple observers, more specifically, when an observer (in this case *Alice*) has non-local correlations with both the other two observers (in this case *Bob* and *Charlie*). For an easier connection between our experimental model and the model presented in the previous section, we stress the fact that $\mathtt{Bob}_1$ and $\mathtt{Bob}_2$ of section 3.1 are respectively *Charlie* and *Bob* of our model. In this model each observer is associated to a different Hilbert space on which he solely can perform measures as follows:

$$\begin{aligned} \mathtt{Alice} &\longrightarrow \mathscr{H}_A \\ \mathtt{Bob} &\longrightarrow \mathscr{H}_B \\ \mathtt{Charlie} &\longrightarrow \mathscr{H}_C \end{aligned}$$

1 The chosen names follow the convention generally adopted in quantum information theory.

Figure 5.1.: Scheme of a trivial circuit where the three observers *Alice*, *Bob* and *Charlie*, referred respectively as A, B and C at the left of the circuit, are associated to a different communication channel (or equivalently, Hilbert space) and where no interaction is present between the channels. The measurement on the channels operated by the observer is represented on the right by the measurement box.

The Hilbert spaces considered in our model are discrete 2-dimensional spaces, and the association of each observer to a specific Hilbert space represents the binding of every observer to a specific communication channel (such association is the foundation of the logical circuit notation in quantum information theory). From section 2.1 we know that any unit vector in a 2-dimensional complex vector state is a qubit, therefore in our discussion we'll often refer to any of the states of the system we are analysing as a qubit.

5.1.1 *Trivial circuit example*

Before starting to describe the system $\mathfrak{S}$ we provide a description of a trivial system to gain some confidence with the basic instruments (logic circuits and state density matrix) used to in quantum information theory. We keep considering a three observer system and we call the generic physical states on the different Hilbert spaces Ψ_A, Ψ_B and Ψ_C. Suppose to consider a system with no initial correlation between the various Ψ_I (with $I \in \{A, B, C\}$) states and without any interaction among the different $\mathscr{H}_I$ spaces. The state of such system is described by the simple density matrix (see A.2)

$$\rho_{ABC} \in \mathscr{H}_A \otimes \mathscr{H}_B \otimes \mathscr{H}_C$$
$$\rho_{ABC} = |\Psi_A\rangle \langle\Psi_A| \otimes |\Psi_B\rangle \langle\Psi_B| \otimes |\Psi_C\rangle \langle\Psi_C|$$

and the logic circuit scheme of such a system is the one shown in figure 5.1 and it's basically constituted by three quantum wires (see A.3.1) associated respectively to the three communication channels. In this situation where the states on the different Hilbert spaces are completely independent and where every observer has access only to the state on its own Hilbert space, nothing more interesting than measuring independently each state can be done.

5.1.2 *System circuit*

The situation starts to be interesting when correlations among the different spaces and manipulation on the states are made. Let's consider now the circuit showed in

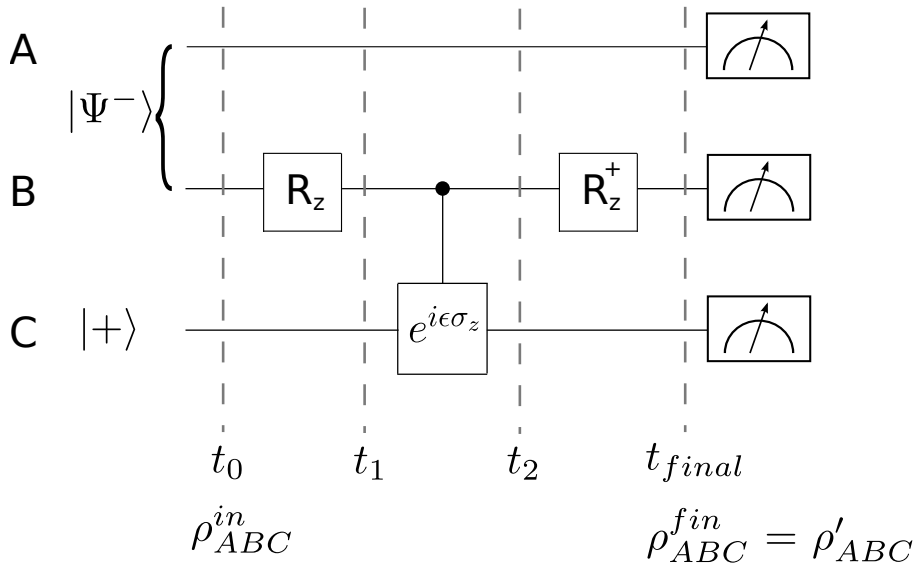

Figure 5.2.: Scheme of the analysed physical system. On the left the observer communication channel are indicated with an obvious convention with A, B and C. On the left of the scheme are shown the initial states entering in the circuit, and on the bottom are marked the evolution steps. ρ^{in}_{ABC} and ρ'_{ABC} are the initial and final total system state respectively.

figure 5.2, that is the system $\mathfrak{S}$ we are interested in. The considered circuit presents both state correlation among different Hilbert spaces (an entangled pair enters at channel A and B) and state manipulation. Let's first analyse the circuit elements and then describe the evolution of the state across the circuit.

R boxes

The $\boxed{R_z}$ and $\boxed{R_z^\dagger}$ boxes are two single-qubit gates (see A.3.2 for a fererence on quantum gates) that represent a rotation operated on the state. Such rotation depends on the variable z which can assume two values $z = 1, 0$. The action of the rotation maps the initial Hilbert space base to a new base depending on the z value:

$$R_z^\dagger |0\rangle = |w_z\rangle \tag{5.1}$$
$$R_z^\dagger |1\rangle = |w_z^\perp\rangle \tag{5.2}$$

The z variable is then simply a variable that selects between two possible state rotations.

Controlled gate box

The $\boxed{e^{i\epsilon\sigma_z}}$ box represent a controlled operation. With controlled operation we basically intend an operation that is executed on a *target qubit* just in the case a certain condition on a *control qubit* is satisfied (the logic of this operation is simply: "if `condition` is true than do `operation`"). In this specific case the control qubit is the state on the $\mathscr{H}_B$ space while the target qubit is the state on the $\mathscr{H}_C$ space. The control condition is that the B-qubit must be in the $|1\rangle$ state, while $e^{i\epsilon\sigma_z}$ is a single qubit

unitary operation to execute on the *C*-qubit in case the control condition is satisfied. It is easy to prove that the 2-dimensional matrix representation of the $e^{i\epsilon\sigma_z}$ operator is

$$e^{i\epsilon\sigma_z} = \begin{bmatrix} e^{i\epsilon} & 0 \\ 0 & e^{-i\epsilon} \end{bmatrix}$$

The action of the $\boxed{e^{i\epsilon\sigma_z}}$ box on the C-qubit can therefore be summarized as an addiction of a relative phase (valued 2ϵ) between the two $\mathscr{H}_C$ space base vectors. It is straightforward to see that the ϵ value measures the intensity of the state modification of the *C*-qubit. For $\epsilon = 0$ there is no modification of the *C*-qubit state, while for increasing ϵ values we have an increasing relative phase between the two $\mathscr{H}_C$ base vectors.

5.1.3 *State evolution*

After the description of the elements in the circuit we are now going to study the evolution of the system state through the circuit. To track more easily the state evolution in figure 5.2 are shown the different time steps through which the state evolves.

At the circuit entrance a qubit couple entangled in a singlet state $|\Psi^-\rangle_{AB}$ enters in channels *A* and *B* while a single qubit in a precise state $|+\rangle$ enters in channel *C*. The $|+\rangle$ state in the $\mathscr{H}_C$ space is often referred as the *ancilla* state, i.e., a new element that is entangled with the system and then measured, in order to obtain information without completely destroying the system state.

At time t_0 the system state (described in the density matrix notation) is simply the composition of the entrance states:

$$\rho^{in}_{ABC} = \rho^{in}_{AB} \otimes |+\rangle\langle+|_C$$
$$\text{with} \qquad \rho^{in}_{AB} = |\Psi^-\rangle\langle\Psi^-|_{AB}$$

where *in* apex stands for *initial*. It is convenient to stress here an important property of the singlet state that will be widely employed in the following. The form of the singlet state $|\Psi^-\rangle_{AB}$ representation is invariant on the basis chosen for the spaces $\mathscr{H}_A$ and $\mathscr{H}_B$, so we will often substitute the classic representation

$$|\Psi^-\rangle_{AB} = \frac{|0_A 1_B\rangle - |1_A 0_B\rangle}{\sqrt{2}}$$

that implies the choice of a specific $\mathscr{H}_A$ and $\mathscr{H}_B$ state base, with the more general:

$$|\Psi^-\rangle_{AB} = \frac{|s\rangle_A |s^\perp\rangle_B - |s^\perp\rangle_A |s\rangle_B}{\sqrt{2}}$$

that leaves the freedom of choice of the basis $(|s\rangle, |s^\perp\rangle)$ for the singlet representation.

Between time t_0 and t_1 the R_z rotation is applied to the state on the $\mathscr{H}_B$ space. This operation is represented by the unitary operator

$$U_1(z) = \mathbb{1}_A \otimes R_{zB} \otimes \mathbb{1}_C$$

acting on the system density matrix. All the identity operators $\mathbb{1}$ considered in our work are obviously representable with 2-dimensional unitary matrices $\mathbb{1}_2$ therefore from now on we will drop the obvious dimension subscript 2.

Between time t_1 and t_2 the controlled operation $e^{i\epsilon\sigma_z}$ with the state on $\mathscr{H}_B$ as control qubit and the state on $\mathscr{H}_C$ as target qubit is applied to the state. Such operation is represented by the unitary operator

$$U_2(\epsilon) = \mathbb{1}_A \otimes |0\rangle\langle 0|_B \otimes \mathbb{1}_C + \mathbb{1}_A \otimes |1\rangle\langle 1|_B \otimes e^{i\epsilon\sigma_z}_C$$

acting on the system density matrix.

At the end of the circuit, between time t_2 and t_3, the inverse $R_z^\dagger$ rotation is applied to the state on the $\mathscr{H}_B$ space, and the operator on the system state is

$$U_3(z) = \mathbb{1}_A \otimes R^\dagger_{zB} \otimes \mathbb{1}_C$$

The overall action of the circuit on the state is then representable by the concatenation of the U_i evolution operators $U_{total} \equiv U_z(\epsilon)$ (in the following we'll drop the Hilbert space subscript when obvious thanks to the operator order)

$$\begin{aligned} U_z(\epsilon) \equiv U_{total} &= U_3(z) \circ U_2(\epsilon) \circ U_1(z) \\ &= \left(\mathbb{1} \otimes R_z^\dagger \otimes \mathbb{1}\right)\left(\mathbb{1} \otimes |0\rangle\langle 0| \otimes \mathbb{1} + \mathbb{1} \otimes |1\rangle\langle 1| \otimes e^{i\epsilon\sigma_z}\right)\left(\mathbb{1} \otimes R_z \otimes \mathbb{1}\right) \\ &= \mathbb{1} \otimes R_z^\dagger\left(|0\rangle\langle 0|\right)R_z \otimes \mathbb{1} + \mathbb{1} \otimes R_z^\dagger\left(|1\rangle\langle 1|\right)R_z \otimes e^{i\epsilon\sigma_z} \end{aligned}$$

Remembering the definition of the rotation operators given in 5.1, $U_z(\epsilon)$ can be written:

$$U_z(\epsilon) = \mathbb{1} \otimes |w_z\rangle\langle w_z| \otimes \mathbb{1} + \mathbb{1} \otimes |w_z^\perp\rangle\langle w_z^\perp| \otimes e^{i\epsilon\sigma_z}$$

And recognizing that $|w_z\rangle\langle w_z|$ and $|w_z^\perp\rangle\langle w_z^\perp|$ are projectors

$$\begin{aligned} |w_z\rangle\langle w_z| &= \pi_B^{+z} \\ |w_z\rangle\langle w_z| &= \pi_B^{-z} \end{aligned}$$

One can write $U_z(\epsilon)$ as:

$$U_z(\epsilon) = \mathbb{1} \otimes \pi_B^{+z} \otimes \mathbb{1} + \mathbb{1} \otimes \pi_B^{-z} \otimes e^{i\epsilon\sigma_z}$$

The final state at the end of the circuit is then (where *fin* stands for *final*)

$$\begin{aligned} \rho'_{ABC} = \rho^{fin}_{ABC} &= U_z(\epsilon)\rho^{in}_{ABC}U_z^\dagger(\epsilon) \\ &= \left(\pi_B^{+z} + \pi_B^{-z}\left(e^{i\epsilon\sigma_z}\right)_C\right)\rho_{ABC}\left(\pi_B^{+z} + \pi_B^{-z}\left(e^{-i\epsilon\sigma_z}\right)_C\right) \\ &= \pi_B^{+z}\rho_{ABC}\pi_B^{+z} && (5.3a) \\ &+ \pi_B^{+z}\rho_{ABC}e_C^{-i\epsilon\sigma_z}\pi_B^{-z} && (5.3b) \\ &+ \pi_B^{-z}e_C^{i\epsilon\sigma_z}\rho_{ABC}\pi_B^{+z} && (5.3c) \\ &+ \pi_B^{-z}e_C^{i\epsilon\sigma_z}\rho_{ABC}e_C^{-i\epsilon\sigma_z}\pi_B^{-z} && (5.3d) \end{aligned}$$

Note that the evolution depends both on the variable z that selects one of the two possible rotations and on the variable ϵ which quantifies the intensity of the state manipulation on the $\mathscr{H}_C$ space.

5.1.4 *State measurement and probability*

In the scheme presented in figure 5.2 each observer can perform measurements only on its own channel (or, equivalently, Hilbert space); we suppose that the only direct information any observer can gain about the system state comes from projective measurements on its own part of the system. Being in a 2-dimensional Hilbert space, the projective measurement consists in projecting the state onto 2 orthogonal vectors; every *Alice*, *Bob* and *Charlie* measurement will be associated to a particular 2-dimension basis set.

Measurement basis

We label with $x \in \{0, 1\}$ the two possible basis on which Alice can measure. Each basis set *Alice* can choose from will be associated to two orthogonal vectors as follows:

$$\begin{aligned} x = 0 \quad &\Longrightarrow \quad \left\{ |u_0\rangle_A \,, \quad |u_0^\perp\rangle_A \right\} \\ x = 1 \quad &\Longrightarrow \quad \left\{ |u_1\rangle_A \,, \quad |u_1^\perp\rangle_A \right\} \end{aligned}$$

We then label with *a Alice*'s measurement outcome and we associate to the projection onto the vector $|u_x\rangle$ the result $a = 1$ and to the projection onto the vector $|u_x^\perp\rangle$ the result $a = -1$.This scheme can be summarized as follows:

$$\begin{aligned} x = 0 \quad &\Longrightarrow \quad \left\{ |u_0\rangle_A \to a = 1, \quad |u_0^\perp\rangle_A \to a = -1 \right\} \\ x = 1 \quad &\Longrightarrow \quad \left\{ |u_1\rangle_A \to a = 1, \quad |u_1^\perp\rangle_A \to a = -1 \right\} \end{aligned}$$

In exactly the same fashion we label with $y \in \{0, 1\}$ the two possible basis *Bob* can chose from, with $|v_y\rangle$ and $|v_y^\perp\rangle$ the two orthogonal vectors of each base, and we associate the each base the measurement outcome *b* as follows:

$$\begin{aligned} y = 0 \quad &\Longrightarrow \quad \left\{ |v_0\rangle_B \to b = 1, \quad |v_0^\perp\rangle_B \to b = -1 \right\} \\ y = 1 \quad &\Longrightarrow \quad \left\{ |v_1\rangle_B \to b = 1, \quad |v_1^\perp\rangle_B \to b = -1 \right\} \end{aligned}$$

Charlie, conversely to *Alice* and *Bob*, disposes only of one orthogonal base on which he can project the $\mathscr{H}_C$ state. We indicate the two orthogonal base vectors for *Charlie* measure $|t\rangle_C$ and $|t^\perp\rangle_C$, and we associate to each projection result the measurement outcome *c* as follows:

$$|t\rangle_C \to c = 1, \qquad |t^\perp\rangle_C \to c = -1$$

A fundamental aspect of this scheme is that *Charlie* is the one who chooses what rotation R_z and $R_z^\dagger$ to apply on the state on the $\mathscr{H}_B$ space having two possible rotations $z \in \{0, 1\}$ to chose from:

$$\begin{aligned} z = 0 \quad &\Longrightarrow \quad \left\{ R_0^\dagger |0\rangle_B = |w_0\rangle_B \,, \quad R_0^\dagger |1\rangle_B = |w_0^\dagger\rangle_B \right\} \\ z = 1 \quad &\Longrightarrow \quad \left\{ R_1^\dagger |0\rangle_B = |w_1\rangle_B \,, \quad R_1^\dagger |1\rangle_B = |w_1^\dagger\rangle_B \right\} \end{aligned}$$

Measurement operators and probabilities

Now that we have characterized all the measurement basis we can build the objects needed for a CHSH inequality (see section 2.3). First of all we define the operators associated to the projective measurements as:

$$\begin{aligned} A_x^a &= |u_x^a\rangle \langle u_x^a|_A \\ B_y^b &= |v_y^b\rangle \langle v_y^b|_B \\ C^c &= |t^c\rangle \langle t^c|_C \end{aligned}$$

As already introduced, the CHSH inequalities are build upon the conditioned probabilities to obtain a certain correlated outcome between two observer in a precise measurement configuration. In our case these conditioned probability reads $P(ab|xy)$ for *Alice* and *Bob* and $P(ac|xz)$ for *Alice* and *Charlie*. The $P(ab|xy)$ probability is computed as:

$$P(ab|xy) = \sum_z P(z) \mathrm{Tr}(A_x^z B_y^b \rho'_{AB}(z)) \qquad \text{with} \qquad \rho'_{AB}(z) = \mathrm{Tr}_C(\rho'_{ABC}(z)) \tag{5.4}$$

The sum over the possible values of the variable z is due to the dependence of the *AB*-system state over the rotation z-choice; the sum over all the $\rho'_{AB}(z)$ weighted by their probability makes the calculated probability independent from the z value.

$P(ac|xz)$ probability is simply computed as:

$$P(ac|xz) = \mathrm{Tr}(A_x^a C_z^c \rho'_{AC}(z)) \qquad \text{with} \qquad \rho'_{AC}(z) = \mathrm{Tr}_B(\rho'_{ABC}(z)) \tag{5.5}$$

Before proceeding with the probability calculation it is convenient to calculate explicitly the $\rho'_{AB}(c) = \mathrm{Tr}_C\left(\rho'_{ABC}(c)\right)$ and $\rho'_{AC}(c) = \mathrm{Tr}_B\left(\rho'_{ABC}(c)\right)$ partial system states.

Partial trace calculation

Below we show some steps of the partial trace calculation on the *C* space in order to get the ρ'_{AB} state. We start calculating the Tr_C on the four addends shown respectively in equation 5.3a, 5.3b, 5.3c, 5.3d:

$$\mathrm{Tr}_C\left(\pi_B^{+z} \rho_{ABC} \pi_B^{+z}\right) = \pi_B^{+z} \rho_{AB} \pi_B^{+z} \tag{5.6}$$

$$\mathrm{Tr}_C\left(\pi_B^{+z} \rho_{ABC} e_C^{-i\epsilon\sigma_z} \pi_B^{-z}\right) = \pi_B^{+z} \rho_{AB} \pi_B^{-z} \cos\epsilon \tag{5.7}$$

$$\mathrm{Tr}_C\left(\pi_B^{-z} e_C^{i\epsilon\sigma_z} \rho_{ABC} \pi_B^{+z}\right) = \pi_B^{-z} \rho_{AB} \pi_B^{+z} \cos\epsilon \tag{5.8}$$

$$\mathrm{Tr}_C\left(\pi_B^{-z} e_C^{i\epsilon\sigma_z} \rho_{ABC} e_C^{-i\epsilon\sigma_z} \pi_B^{-z}\right) = \pi_B^{-z} \rho_{AB} \pi_B^{-z} \tag{5.9}$$

Consequently, summing the four contributes one get:

$$\begin{aligned} \rho'_{AB} &= \mathrm{Tr}_C\left(\rho'_{ABC}\right) \\ &= \rho_{AB} \cos\epsilon + (1 - \cos\epsilon)\left(\pi_B^{+z} \rho_{AB} \pi_B^{+z} + \pi_B^{-z} \rho_{AB} \pi_B^{-z}\right) \end{aligned} \tag{5.10}$$

Looking at equation 5.10, it is clear what is the role played by the ϵ parameter on the determination of the ρ'_{AB} state. Let's consider the following three example cases:

- $\boxed{\epsilon = 0}$ In this case the controlled gate acts as an identity, the evolution operator becomes an identity $U_z(\epsilon) = \mathbb{1}_A \circ \mathbb{1}_B \circ \mathbb{1}_C$ and $\rho'_{AB} = \rho_{AB}$;
- $\boxed{0 < \epsilon < \frac{\pi}{2}}$ For intermediate ϵ values the state becomes a linear combination of the singlet state and the decohered state weighted by a function of the ϵ value;
- $\boxed{\epsilon = \frac{\pi}{2}}$ In this case ρ'_{AB} is a completely decohered state.

In order to calculate the ρ'_{AC} system state we repeat the procedure above tracing this time on the B space:

$$\mathrm{Tr}_B\left(\pi_B^{+z}\rho_{ABC}\pi_B^{+z}\right) = \frac{1}{2}\pi_A^- \otimes |+\rangle\langle+|_C \tag{5.11}$$

$$\mathrm{Tr}_B\left(\pi_B^{+z}\rho_{ABC}e_C^{-i\epsilon\sigma_z}\pi_B^{-z}\right) = 0 \tag{5.12}$$

$$\mathrm{Tr}_B\left(\pi_B^{-z}e_C^{i\epsilon\sigma_z}\rho_{ABC}\pi_B^{+z}\right) = 0 \tag{5.13}$$

$$\mathrm{Tr}_B\left(\pi_B^{-z}e_C^{i\epsilon\sigma_z}\rho_{ABC}e_C^{-i\epsilon\sigma_z}\pi_B^{-z}\right) = \frac{1}{2}\pi_A^+ \otimes \left(e^{i\epsilon\sigma_z}|+\rangle\langle+|e^{-i\epsilon\sigma_z}\right)_C \tag{5.14}$$

Where

$$\pi_A^+ = |w_z\rangle\langle w_z|_A$$
$$\pi_A^- = |w_z^\perp\rangle\langle w_z^\perp|_A$$

are projectors on the $\mathscr{H}_A$ space with $|w_z\rangle_A$, $|w_z^\perp\rangle_A$ defined as the conjugate of the $|w_z\rangle_B$, $|w_z^\perp\rangle_B$ rotation base vector in $\mathscr{H}_B$ for the R_z operator. Summing the previous four contributes one get:

$$\begin{aligned}\rho'_{AC} &= \mathrm{Tr}_B\left(\rho'_{ABC}\right)\\ &= \frac{1}{2}\pi_A^- \otimes |+\rangle\langle+|_C + \frac{1}{2}\pi_A^+ \otimes \left(e^{i\epsilon\sigma_z}|+\rangle\langle+|e^{-i\epsilon\sigma_z}\right)_C\end{aligned} \tag{5.15}$$

Probability calculation

It is now possible to calculate the conditional probabilities showed in equations 5.4 and 5.5. We start with $P(ab|xy)$.

$$\begin{aligned}P(ab|xy) &= \sum_z P(z)\mathrm{Tr}_{AB}\left(A_x^a B_y^b \rho'_{AB}(z)\right)\\ &= \mathrm{Tr}_{AB}\left(\left(|u_x^a\rangle\langle u_x^a|_A \otimes |v_y^b\rangle\langle v_y^b|_B\right)\left(\rho_{AB}\cos\epsilon + (1-\cos\epsilon)\left(\pi_B^{+z}\rho_{AB}\pi_B^{+z} + \pi_B^{-z}\rho_{AB}\pi_B^{-z}\right)\right)\right)\end{aligned} \tag{5.16}$$

Ignoring for a while the multiplicative factors, keeping in mind the possibility to write a pure state with a unitary Bloch state vector notation and splitting this computation into smaller parts one finds:

$$\mathrm{Tr}\left(A_x^a B_y^b \rho_{AB}(z)\right) = \frac{1}{4}\left(1 - \bar{u}_x^a \cdot \bar{v}_y^b\right) \tag{5.17}$$

$$\mathrm{Tr}\left(A_x^a B_y^b \pi_B^{+z}\rho_{AB}(z)\pi_B^{+z}\right) = \frac{1}{8}\left(1 - \bar{u}_x^a \cdot \bar{w}_z\right)\left(1 + \bar{v}_y^b \cdot \bar{w}_z\right) \tag{5.18}$$

$$\mathrm{Tr}\left(A_x^a B_y^b \pi_B^{-z}\rho_{AB}(z)\pi_B^{-z}\right) = \frac{1}{8}\left(1 + \bar{u}_x^a \cdot \bar{w}_z\right)\left(1 - \bar{v}_y^b \cdot \bar{w}_z\right) \tag{5.19}$$

It follows, composing the results in 5.17, 5.18, 5.19 as in 5.16, and keeping in mind the property of Bloch state vectors[2] for which we can convert the outcome apexes a and b into multiplying factors, we have:

$$P(ab|xy) = \sum_z P(z)\frac{1}{4}\Big(\cos\epsilon\Big(1 - ab(\bar{u}_x \cdot \bar{v}_y)\Big) + (1-\cos\epsilon)\Big(1 - ab(\bar{u}_x \cdot \bar{w}_z)(\bar{v}_y \cdot \bar{w}_z)\Big)\Big) \tag{5.20}$$

While the $P(ac|xz)$ probability reads:

$$P(ac|xz) = \mathrm{Tr}_{AC}\Big(A_x^a C^c \rho'_{AC}(z)\Big) =$$
$$\mathrm{Tr}_{AC}\Big(\Big(|u_x^a\rangle\langle u_x^a|_A \otimes |t^c\rangle\langle t^c|_C\Big)\Big(\frac{1}{2}\pi_A^- \otimes |+\rangle\langle+|_C + \frac{1}{2}\pi_A^+ \otimes \big(e^{i\epsilon\sigma_z}|+\rangle\langle+|e^{-i\epsilon\sigma_z}\big)_C\Big)\Big) \tag{5.21}$$

and again splitting the trace into smaller parts and recomposing them together:

$$\mathrm{Tr}\Big(A_x^a \pi_A^-\Big) = \frac{1}{2}(1 - \bar{u}_x^a \cdot \bar{w}_z) \tag{5.22}$$
$$\mathrm{Tr}\Big(C^c |+\rangle\langle+|_C\Big) = \delta_{c,+} \tag{5.23}$$
$$\mathrm{Tr}\Big(A_x^a \pi_A^+\Big) = \frac{1}{2}(1 + \bar{u}_x^a \cdot \bar{w}_z) \tag{5.24}$$
$$\mathrm{Tr}\Big(C^c \big(e^{i\epsilon\sigma_z}|+\rangle\langle+|e^{-i\epsilon\sigma_z}\big)_C\Big) = \delta_{c,+} - c\sin^2\epsilon \tag{5.25}$$

Where in equations 5.23 and 5.25 we are assuming that the projective measurement on the $\mathscr{H}_C$ space are made on the same base used for the initial state definition in the $\mathscr{H}_C$ space, namely: $|t^+\rangle_C = |+\rangle_C$ and $|t^-\rangle_C = |-\rangle_C$ (the $+$ and $-$ apex indicate the $c = 1$ and $c = -1$ outcomes respectively). Composing the different terms together we obtain:

$$\begin{aligned} P(ac|xz) &= \frac{1}{2}\Big(\frac{1}{2}\Big(1 - \bar{u}_x^a \cdot \bar{w}_z\Big)\delta_{c,+} + \frac{1}{2}\Big(1 + \bar{u}_x^a \cdot \bar{w}_z\Big)\Big(\delta_{c,+} - c\sin^2\epsilon\Big)\Big) \\ &= \frac{1}{4}\Big(1 + c + -c\sin^2\epsilon\big(1 + a\bar{u}_x \cdot \bar{w}_z\big)\Big) \end{aligned} \tag{5.26}$$

5.1.5 *CHSH correlations and inequalities*

We look now at the E_{xy} and E_{xz} correlations that compose the CHSH inequalities of interest. Reminding that the correlations factor are in the form:

$$E_{xy} = \sum_{\substack{a=\pm1 \\ b=\pm1}} ab \cdot P(ab|xy) \qquad\qquad E_{xz} = \sum_{\substack{a=\pm1 \\ c=\pm1}} ac \cdot P(ac|xz)$$

And noting that given probabilities in the form

$$P(ab|xy) = \Gamma_0 + a\Gamma_1 + b\Gamma_2 + ab\Gamma_3$$
$$P(ac|xz) = \Gamma_0^* + a\Gamma_1^* + c\Gamma_2^* + ac\Gamma_3^*$$

2 In Bloch representation orthogonal states in the direct space are represented by opposite vectors.

(where Γ_i and Γ_i^* are the appropriate coefficients in equation 5.20 and 5.26) the sum over the *a*, *b* and *c* indexes gives $E_{xy} = 4\Gamma_3$, $E_{xz} = 4\Gamma_3^*$. It follows that the correlation factors are simply:

$$E_{xy} = -\sum_z P(z)\Big(\cos\epsilon(\bar{u}_x \cdot \bar{v}_y) + (1-\cos\epsilon)(\bar{u}_x \cdot \bar{w}_z)(\bar{v}_y \cdot \bar{w}_z)\Big)$$
$$E_{xz} = -\sin^2\epsilon(\bar{u}_x \cdot \bar{w}_z)$$

At this point summing up the correlations to obtain the CHSH inequality[3] we get for *Alice* and *Bob*:

$$I^{AB}_{CHSH} = \Theta_1 \cos\epsilon + \Theta_2(1-\cos\epsilon) = \Theta_2 + (\Theta_1 - \Theta_2)\cos\epsilon \leqslant 2 \tag{5.27}$$

with

$$\Theta_1 = -(u_0 \cdot v_0 + u_1 \cdot v_0 + u_0 \cdot v_1 - u_1 \cdot v_1) \tag{5.28}$$
$$\Theta_2 = -\sum_z P(z)\Big((u_0 \cdot w_z)(v_0 \cdot w_z) + (u_0 \cdot w_z)(v_1 \cdot w_z) + (u_1 \cdot w_z)(v_0 \cdot w_z) - (u_1 \cdot w_z)(v_1 \cdot w_z)\Big) \tag{5.29}$$

and for *Alice* and *Charlie* we get:

$$I^{AC}_{CHSH} = \Theta_3 \sin^2\epsilon \leqslant 2 \tag{5.30}$$

with

$$\Theta_3 = -(u_0 \cdot w_0 + u_0 \cdot w_1 + u_1 \cdot w_0 - u_1 \cdot w_1) \tag{5.31}$$

Summarizing, we have finally obtained in equations 5.27 and 5.30 both the CHSH inequality expectation values as function of the measurement basis for the system under study.

Best set of measurements

At this point we want to find the best set of measurement basis for a double CHSH violation. Defining $x = \sin^2\epsilon$ and substituting it into the equations 5.27 and 5.30 the CHSH inequalities read:

$$I^{AB}_{CHSH} = \Theta_2 + (\Theta_1 - \Theta_2)\sqrt{1-x} \leqslant 2$$
$$I^{AC}_{CHSH} = \Theta_3 x \leqslant 2$$

It is convenient to make some consideration on the Θ_1, Θ_3, Θ_3 parameters in order to get some information about the measurement basis. In particular:

- Considering the I^{AB}_{CHSH} expression we note that if $\Theta_1 \leqslant \Theta_2$ than I^{AB}_{CHSH} would be an increasing function in ϵ. From the system description we know that when $x = 1$ ($\epsilon = \pi/2$), *Charlie* is performing a strong measurement on the state in the $\mathscr{H}_B$ space, and consequently *Charlie* is extracting all the information about the state, thus for $x = 1$ necessarily *Bob* can't observe a CHSH violation. In the $\Theta_1 \leqslant \Theta_2$ case we therefore have: $I^{AB}_{CHSH}(x) \leqslant I^{AB}_{CHSH}(1) \leqslant 2$, so follows that to get a CHSH violation for *Alice* and *Bob* we must constraint $\Theta_1 > \Theta_2$.

3 We remind that the general formulation for a CHSH inequality is: $I = E_{00} + E_{01} + E_{10} - E_{11} \leqslant 2$

- Studying now the I^{AC}_{CHSH} expression we find immediately that to obtain a CHSH violation we can impose the constraint $\Theta_1 > 0$. It follows that I^{AC}_{CHSH} is an increasing function of ϵ.

From the two previous observations, since I^{AB}_{CHSH} must be a monotonically increasing function, and I^{AC}_{CHSH} must be a monotonically decreasing function of x, and since we expect both functions to variate in the $x \in [0,1]$ interval from CHSH violation to CHSH non-violation (and thus from $I_{CHSH} < 2$ to $I_{CHSH} > 2$) and vice-versa, it follows that there will be only one x value such that I^{AB}_{CHSH} and I^{AC}_{CHSH} are equal. We will call this value $\tilde{x} := \{x \in [0,1] \,|\, I^{AB}_{CHSH}(x) = I^{AC}_{CHSH}(x)\}$. It follows naturally that if both the CHSH inequality are violated, at $\tilde{x}$ we have the stronger simultaneous violation. It is therefore convenient to maximize the values $I^{AB}_{CHSH}(\tilde{x})$ and $I^{AC}_{CHSH}(\tilde{x})$. First of all we find now $\tilde{x}$, being the solution of $I^{AB}_{CHSH}(x) = I^{AB}_{CHSH}(x)$. We get:

$$\tilde{x} = \beta - \frac{1}{2}(\alpha-\beta)^2 + \frac{1}{2}\sqrt{(2\beta-(\alpha-\beta)^2)^2 - 4(\beta^2-(\alpha-\beta)^2)}$$

with $\alpha = \Theta_1/\Theta_3$ and $\beta = \Theta_2/\Theta_3$. In all generality, this is an optimization problem over *11* free real parameters. *10* parameters come from the vectors in the Bloch sphere that define the Θ_i variables: two parameter per each of the vectors u_1, v_0, v_1, w_0, w_1; u_0 is omitted since Θ_i are invariant for a rotation in the Bloch sphere so u_0 can be fixed. The last real parameter comes from the probability $P(z)$.

This problem is computationally intensive, but we may simplify it making some assumptions. The first assumption we make is on Θ_3. Since I^{AC}_{CHSH} depends only on Θ_3, it is natural to require that there is an ϵ configuration where such CHSH parameter gets the highest possible, equal to the Tsirelson's bound: $\Theta_3 = 2\sqrt{2}$ (see section 2.3.1 for reference). This is accomplished choosing for example:

$$u_0 = Z \qquad w_0 = -\frac{Z+X}{\sqrt{2}}$$
$$u_1 = X \qquad w_1 = \frac{-Z+X}{\sqrt{2}}$$

At this point we are left with 5 free real parameters: v_0, v_1 and $P(0)$. The numerical optimization leads to the final choice

$$u_0 = Z \qquad w_0 = v_0 = -\frac{Z+X}{\sqrt{2}} \tag{5.32}$$
$$u_1 = X \qquad w_1 = v_1 = \frac{-Z+X}{\sqrt{2}} \tag{5.33}$$

and $P(y_1 = 0)$ being any number between 0 and 1. We notice that the basis set just found is equivalent to the following:

$$w_0' = v_0' = Z \qquad u_0' = -\frac{Z+X}{\sqrt{2}}$$
$$w_1' = v_1' = X \qquad u_1' = \frac{-Z+X}{\sqrt{2}}$$

which has the advantage to be easier to implement experimentally (such equivalence becomes clear looking at the definitions of Θ_1 (5.28), Θ_2 (5.29), and Θ_3 (5.31)).

Given the first set of measurements (equations 5.32 and 5.33), the corresponding Bloch vectors are:

$$\begin{aligned} \vec{u}_0 &= (0,0,1) & \vec{u}_0^{\perp} &= (0,0,-1) \\ \vec{u}_1 &= (1,0,0) & \vec{u}_1^{\perp} &= (-1,0,0) \\ \vec{w}_0 = \vec{v}_0 &= \left(-\frac{1}{\sqrt{2}},0,-\frac{1}{\sqrt{2}}\right) & \vec{w}_0^{\perp} = \vec{v}_0^{\perp} &= \left(\frac{1}{\sqrt{2}},0,\frac{1}{\sqrt{2}}\right) \\ \vec{w}_1 = \vec{v}_1 &= \left(\frac{1}{\sqrt{2}},0,-\frac{1}{\sqrt{2}}\right) & \vec{w}_1^{\perp} = \vec{v}_1^{\perp} &= \left(-\frac{1}{\sqrt{2}},0,\frac{1}{\sqrt{2}}\right) \end{aligned}$$

and we set probability $P(z) = \frac{1}{2}$.

CHSH expression

At this point, having explicitly expressed the u, w and v base vectors, it is now easy to calculate the Θ_i values. Since u, w and v lie on the same two-dimensional space we have

$$\sum_z P(z)(u_x \cdot w_z)(v_y \cdot w_z) = \frac{1}{2} u_x \cdot v_y$$

and consequently $\Theta_2 = \frac{1}{2}\Theta_1$. The inequalities in 5.27, 5.30 at this point read:

$$\begin{aligned} I^{AB}_{CHSH} &= \frac{1}{2}\Theta_1(1+\cos\epsilon) \\ I^{AC}_{CHSH} &= \Theta_3 \sin^2\epsilon \end{aligned}$$

Considering that we also have:

$$\begin{aligned} u_0 \cdot w_0 = u_1 \cdot w_0 = u_0 \cdot w_1 &= -\frac{1}{\sqrt{2}} & u_1 \cdot w_1 &= \frac{1}{\sqrt{2}} \\ u_0 \cdot v_0 = u_1 \cdot v_0 = u_0 \cdot v_1 &= -\frac{1}{\sqrt{2}} & u_1 \cdot v_1 &= \frac{1}{\sqrt{2}} \end{aligned}$$

we get that $\Theta_0 = \Theta_1 = 2\sqrt{2}$ and finally:

$$I^{AB}_{CHSH} = \sqrt{2}(1+\cos\epsilon) \tag{5.34}$$

$$I^{AC}_{CHSH} = 2\sqrt{2}\sin^2\epsilon \tag{5.35}$$

These are finally the CHSH inequalities expectation values for *Alice-Bob* and *Alice-Charlie* as a function of the parameter ϵ for the system showed in figure 5.2. Studying these last equations emerges that there exist an ϵ-interval where both I^{AB}_{CHSH} and I^{AC}_{CHSH} are violated.

We have therefore reached the goal we fixed at the beginning of this section, showing that the system under investigation $\mathfrak{S}$, under certain constraints (namely, an appropriate choice of the measurement basis and the selection of adequate ϵ values) is capable of a tripartite Bell inequality. In figure 5.3 the functions 5.34 and 5.35 are plotted: it is easy to identify the ϵ-interval where both violations occur. The maximum violation is found at $\sin^2\epsilon = 3/4$ where both the CHSH functions are greater than 2. At $\tilde{x}$ the functions are equal to $I^{AB}_{CHSH}(\tilde{x}) = I^{AC}_{CHSH}(\tilde{x}) = \frac{3}{2}\sqrt{2} \sim 2.12$.

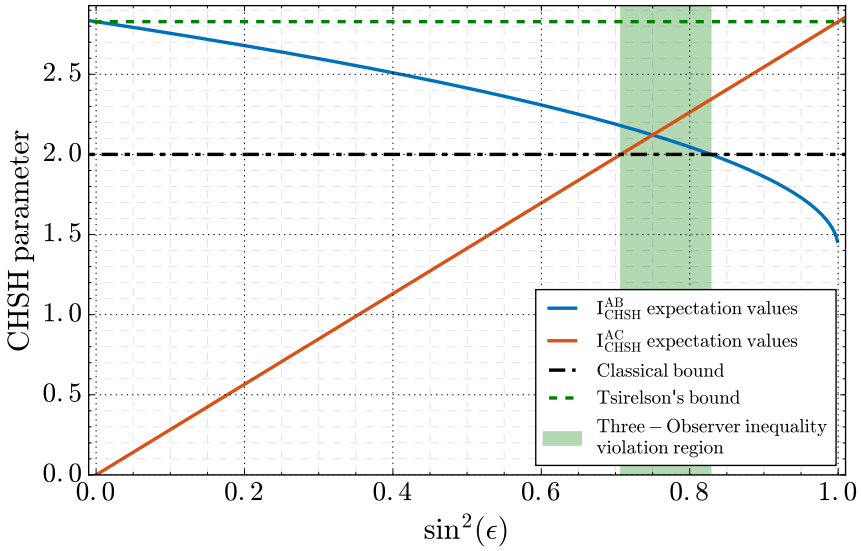

Figure 5.3.: *Alice-Bob* (I^{AB}_{CHSH}) and *Alice-Charlie* (I^{AC}_{CHSH}) CHSH inequality expectation values for the best measurements set as function of $\sin^2(\epsilon)$. The three-observer CHSH violation region is marked in green in the graph. The maximum multiple-observer violation is achived at $\sin^2 \epsilon = 3/4$.

5.2 EXPERIMENTAL DESIGN

In the previous section, we described a physical system capable of double CHSH violation, and we labelled it with $\mathfrak{S}$. The above description in terms of a logic circuit composed by ideal operators has the feature to be fully general and easily understandable but lacks of a intuitive connection with a real physical situation, that is, a connection with an experiment capable of such double CHSH violation. In the following, we will translate the previous description in terms of physical elements and operations, we will introduce hence the experiment design $\mathfrak{D}$.

The first thing to chose in order to design the experiment is the typology of the quantum objects we want to employ for our analysis. We've chosen photons as the tool of our investigation; we will thus exploit intensively the photons-manipulation-techniques proper of Quantum Optics to design the experiment (for a brief review of the fundamental tools of quantum optics see C on page 93). In our experiment we will use in particular two different information encoding schemes proper of quantum optics, polarization and path encoding schemes.

5.2.1 *Experimental scheme*

The experimental design is showed in figure 5.4. In such scheme we see different objects, which represent:

- The yellow circle is the starting point of our apparatus and it represents the entangled photons source that produces a singlet state $|\Psi^-\rangle$. The two photons composing the singlet are sent one to the left of the source, and the other to the right.
- On the left side of the source the $\boxed{A}$ box represents *Alice*'s measurement apparatus that receive one half of the singlet state.

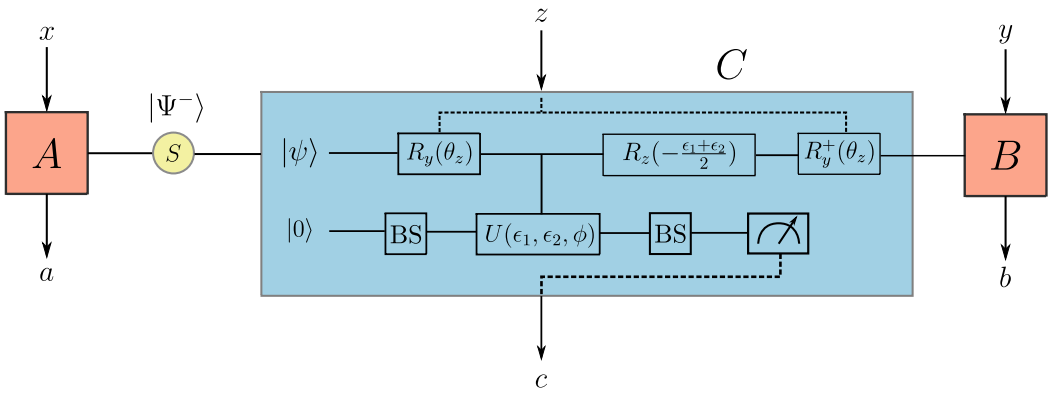

Figure 5.4.: Experiment design $\mathfrak{D}$. The yellow circle represents the entangled photons source that produces a singlet state $|\Psi^-\rangle$, the red boxes marked with letter **A** and **B** represent *Alice*'s and *Bob*'s measurement apparatus respectively, the light blue area identifies *Charlie*'s measurement apparatus. On the top of the schemes there are the setup inputs, on the bottom the setup outputs.

- On the right side of the source the light blue area identifies *Charlie*'s measurement apparatus which receives the second half of the singlet state.
- On the right of *Charlie*'s apparatus the $\boxed{B}$ box represents *Bob*'s measurement apparatus.

Alice and *Bob*'s measurement apparatuses consist simply in two devices that project the photon polarization onto a selected polarization base. The x and y variables allow to chose the measurement base of the two observers (x and y in the scheme are inputs of the measurement devices); a and b are the outcomes of the measurement (and in fact are represented as output of the measurement apparatus in the scheme).

The most interesting element of the design is *Charlie*'s apparatus, which we will deeply analyse in the following. Looking at the scheme we see that two objects ($|\psi\rangle$ and $|0^*\rangle$) enter separately in the circuit. These objects are subsequently manipulated and coupled together by a series of operators ($\boxed{R_y(\theta_z)}$, $\boxed{R_y^+(\theta_z)}$, $\boxed{U(\epsilon_1,\epsilon_2,\phi)}$, $\boxed{BS}$), and finally measured by *Charlie* or sent to *Bob*. We will now focus on the characterization of all the various elements (states and operators) and on the evolution of the states through the apparatus.

$|\psi\rangle$ represent an half of a polarization-entangled singlet state; recalling the multiple observer model given in 5.1 this is exactly the half of the entangled singlet on which *Bob* and *Charlie* act through manipulations and measurements. Such state can always be decomposed on an orthonormal polarization base, we choose here a vertical $|H\rangle$ and horizontal $|V\rangle$ polarization base, so we can express $|\psi\rangle = \alpha|H\rangle + \beta|V\rangle$. The coefficient of such decomposition will depend on the state of the other half of the singlet sent to *Alice* and on the measurement base chosen by *Charlie*. This fact can be easily seen as follows: the entangled photon source emits a singlet state that can be written as $|\Psi^-\rangle = \frac{|0\rangle|1\rangle - |1\rangle|0\rangle}{\sqrt{2}}$. Every time *Alice* measures the photon polarization using one of her basis ($x \in \{0,1\}$), she gets one out of two outcomes $\{|u_x\rangle, |u_x^\perp\rangle\}$. Labelling these outcomes $a = +$ (if she measures $|u_x\rangle$) and $a = -$ (if she measures $|u_x^\perp\rangle$), and expressing the singlet state in terms of the *Alice* measurement base as

$|\Psi^-\rangle = \frac{|u_x^\perp\rangle|u_x\rangle - |u_x\rangle|u_x^\perp\rangle}{\sqrt{2}}$, we can write the state at *Bob* and *Charlie* side as $|\psi\rangle = |u_x^{-a}\rangle$, where

$$|u_x^{-a}\rangle = \begin{cases} |u_x^\perp\rangle & \text{if } a = 1 \\ |u_x\rangle & \text{if } a = -1 \end{cases}.$$

So $|\psi\rangle = |u_x^{-a}\rangle$ is the definition of the state entering in *Charlie* apparatus expressed in *Alice*'s measurement basis. $|\psi\rangle$ in the *Charlie* chosen polarization base ($\{|w_z\rangle, |w_z^\perp\rangle\}$, with $z \in \{0, 1\}$) reads:

$$|\psi\rangle = |w_z\rangle \langle w_z|u_x^{-a}\rangle + |w_z^\perp\rangle \langle w_z^\perp|u_x^{-a}\rangle = \alpha |w_z\rangle + \beta |w_z^\perp\rangle$$

The first operator this state encounters in its evolution is the $\boxed{R_y(\theta_z)}$ box which represents a state rotation in the Bloch sphere conditioned by the variable z that maps the *Charlie* chosen measurement base $\{|w_z\rangle, |w_z^\perp\rangle\}$ to a reference $\{|H\rangle, |V\rangle\}$ polarization base:

$$R_z |w_z\rangle \to |H\rangle$$
$$R_z |w_z^\perp\rangle \to |V\rangle$$

The state at this point can be expressed as: $|\psi\rangle = (\alpha |H\rangle + \beta |V\rangle)$.

The other element entering Charlie circuit is $|0^*\rangle$; this is the ancilla state, a new degree of freedom (a path d.o.f.) that, coupled with the $|\psi\rangle$ polarization d.o.f., allows the double CHSH violation. In path encoding, the computational basis corresponds to two non-overlapping spatial modes of the electromagnetic field, such as two gaussian beams with different approximate wave-vector $\mathbf{k_1} \perp \mathbf{k_2}$. In our scheme the ancilla at the entrance of *Charlie* represents simply the initial direction of the entangled-photon laser beam. The first operator $|0^*\rangle$ encounters is $\boxed{BS}$, a quantum gate that reproduce the action of a beam splitter and whose action maps the initial path state to the new ones as:

$$|0^*\rangle \mapsto \frac{|1\rangle + i|0\rangle}{\sqrt{2}}$$

where $|0\rangle, |1\rangle$ are the new path states introduced by the beam splitter. At this point the overall state inside *Charlie* apparatus is given by:

$$|\psi_0\rangle = (\alpha |H\rangle + \beta |V\rangle) \otimes \frac{|1\rangle + i|0\rangle}{\sqrt{2}}$$

At this point the overall state encounters the $\boxed{U(\epsilon_1, \epsilon_2, \phi)}$ conditional gate; this is the element responsible for the degrees of freedom coupling. This operator acts differently on the polarization degree of freedom depending on the path state introduced by $\boxed{BS}$. This is the action that in practice enables non-locality correlation sharing between multiple observers. Coupling the two different degrees of freedom in fact allows the ancilla state to extract some information from the entangled half singlet state, enabling for a double CHSH inequality violation. The action of the $\boxed{U(\epsilon_1, \epsilon_2, \phi)}$ operator on the system state is the following:

- it adds a relative phase displacement ϵ_1 between the vertical and horizontal polarization vectors on the $|1\rangle$ path;
- while on the $|0\rangle$ path it adds a relative phase displacement ϵ_2 between the vertical and horizontal polarization vectors, and an overall phase displacement ϕ between the paths.

The overall system state at this point reads:

$$|\psi_1\rangle = \frac{1}{\sqrt{2}}\left(\left(\alpha|H\rangle + e^{i\epsilon_1}\beta|V\rangle\right)|1\rangle + ie^{i\phi}\left(\alpha|H\rangle + e^{i\epsilon_2}\beta|V\rangle\right)|0\rangle\right)$$

The state then encounters another $\boxed{BS}$ operator which mixes the two path degree of freedom and maps:

$$|0\rangle \longmapsto \frac{|2\rangle + i|3\rangle}{\sqrt{2}} \qquad\qquad |1\rangle \longmapsto \frac{|3\rangle + i|2\rangle}{\sqrt{2}}$$

So the state at this point reads:

$$\begin{aligned}
|\psi_2\rangle &= \frac{1}{2}\left\{\left[ie^{i\phi}\left(\alpha|H\rangle + e^{i\epsilon_2}\beta|V\rangle\right)\otimes\left(|2\rangle + i|3\rangle\right)\right] + \left[\left(\alpha|H\rangle + \beta e^{i\epsilon_1}|V\rangle\right)\otimes\left(|3\rangle + i|2\rangle\right)\right]\right\} \\
&= \frac{1}{2}\left\{\left[\alpha i\left(e^{i\phi}+1\right)|H\rangle + \beta i\left(e^{i(\phi+\epsilon_2)} + e^{i\epsilon_1}\right)|V\rangle\right]\otimes|2\rangle\right. \\
&\qquad\left. + \left[\alpha\left(-e^{i\phi}+1\right)|H\rangle + \beta\left(-e^{i(\phi+\epsilon_2)} + e^{i\epsilon_1}\right)|V\rangle\right]\otimes|3\rangle\right\} \\
&= ie^{i\frac{\phi}{2}}\left\{\left[\alpha\cos\frac{\phi}{2}|H\rangle + \beta e^{i\frac{(\epsilon_1+\epsilon_2)}{2}}\cos\left(\frac{\epsilon_1-\epsilon_2-\phi}{2}\right)|V\rangle\right]\otimes|2\rangle\right. \\
&\qquad\left. + \left[-\alpha\sin\frac{\phi}{2}|H\rangle + \beta e^{i\frac{(\epsilon_1+\epsilon_2)}{2}}\sin\left(\frac{\epsilon_1-\epsilon_2-\phi}{2}\right)|V\rangle\right]\otimes|3\rangle\right\} \\
&= \beta e^{i\frac{(\epsilon_1+\epsilon_2)}{2}}|V\rangle\otimes\left[\cos\left(\frac{\epsilon_1-\epsilon_2-\phi}{2}\right)|2\rangle + \sin\left(\frac{\epsilon_1-\epsilon_2-\phi}{2}\right)|3\rangle\right] \\
&\qquad + \alpha|H\rangle\otimes\left(\cos\frac{\phi}{2}|2\rangle - \sin\frac{\phi}{2}|3\rangle\right) \\
&\equiv U_\phi|\psi_3(\epsilon_1,\epsilon_2)\rangle\,.
\end{aligned}$$

It's immediate to see how the final state depends on the ϕ, ϵ_1 and ϵ_2 phase displacements; we stress particularly the dependence on the ϕ displacement writing the final state of this step as a function of ϕ: $U_\phi|\psi_1\rangle$. We notice that if $\phi = 0$ we obtain

$$U_0|\psi_3(\epsilon_1,\epsilon_2)\rangle = \alpha|H\rangle\otimes|2\rangle + \beta e^{i\frac{\epsilon_1+\epsilon_2}{2}}|V\rangle\otimes\left[\cos\frac{\epsilon_1-\epsilon_2}{2}|2\rangle + \sin\frac{\epsilon_1-\epsilon_2}{2}|3\rangle\right] \tag{5.36}$$

while for $\phi = \pi$ we have

$$U_\pi|\psi_3(\epsilon_1,\epsilon_2)\rangle = -\alpha|H\rangle\otimes|3\rangle + \beta e^{i\frac{\epsilon_1+\epsilon_2}{2}}|V\rangle\otimes\left[\sin\frac{\epsilon_1-\epsilon_2}{2}|2\rangle - \cos\frac{\epsilon_1-\epsilon_2}{2}|3\rangle\right] \tag{5.37}$$

The last two operations executed on the state are:

1. the compensation of the relative displacement ($e^{i\frac{\epsilon_1+\epsilon_2}{2}}$) between $|H\rangle$ and $|V\rangle$ that appears in 5.36, 5.37 on both the path degree of freedom introducing an opposite phase displacement $e^{-i\frac{\epsilon_1+\epsilon_2}{2}} = e^{-i\epsilon'}$;
2. the application of inverse polarization transformation executed at the beginning on $|\psi\rangle$ in order to return to the chosen *Charlie* measurement base: $\boxed{R_y^+(\theta_z)}$.

The final state obtained before the measurement is therefore:

$$U_0 |\psi_3(\epsilon_1, \epsilon_2)\rangle = \alpha |w_z\rangle \otimes |2\rangle + \beta |w_z^\perp\rangle \otimes \left[\cos\frac{\epsilon_1 - \epsilon_2}{2} |2\rangle + \sin\frac{\epsilon_1 - \epsilon_2}{2} |3\rangle\right] \quad (5.38)$$

$$U_\pi |\psi_3(\epsilon_1, \epsilon_2)\rangle = -\alpha |w_z\rangle \otimes |3\rangle + \beta |w_z^\perp\rangle \otimes \left[\sin\frac{\epsilon_1 - \epsilon_2}{2} |2\rangle - \cos\frac{\epsilon_1 - \epsilon_2}{2} |3\rangle\right] \quad (5.39)$$

5.2.2 *Equivalence between experiment design and theoretical model*

The only things we miss now is describe how the measurement is executed and show how the experiment design $\mathfrak{D}$ is equivalent to the system $\mathfrak{S}$. The two observers execute measurements in the two different degrees of freedom:

- *Bob* measures on the polarization d.o.f.
- *Charlie* measures on the path d.o.f.

In our scheme we will measure only the outputs at the port $|2\rangle$.

We start describing *Charlie* measurement. The fundamental fact is that defining a POVM measurement on our system characterized by the operators $\left\{(I \otimes |2\rangle\langle 2|) U_0, (I \otimes |2\rangle\langle 2|) U_\pi\right\}$ (with result $c = +$ and $c = -$ associated respectively to the first and second operator), we get exactly the same results of the measurement $C^c = |t^c\rangle\langle t^c|_C$ calculated in 5.26. In the following we prove this fact. Calling ρ_0^{final} the final state density matrix in the case $\phi = 0$, and ρ_π^{final} the final state density matrix in the case $\phi = \pi$, we easily find that:

$$\begin{aligned} P(+|xza) &= Tr_{pol}\left((I \otimes |2\rangle\langle 2|)\ \rho_0^{final}\right) = \alpha^2 + \beta^2 \cos^2\frac{\epsilon_1 - \epsilon_2}{2} \\ &= \left|\langle w_z | u_x^{-a}\rangle\right|^2 + \cos^2\frac{\epsilon_1 - \epsilon_2}{2}\left|\langle w_z^\perp | u_x^{-a}\rangle\right|^2 \\ &= \frac{1}{4}(1 + a u_x w_z)\left[1 + \cos^2\frac{\epsilon_1 - \epsilon_2}{2}\right] \end{aligned} \quad (5.40)$$

$$\begin{aligned} P(-|xza) &= Tr_{pol}\left((I \otimes |2\rangle\langle 2|)\ \rho_\pi^{final}\right) = \beta^2 \sin^2\frac{\epsilon_1 - \epsilon_2}{2} \\ &= \sin^2\frac{\epsilon_1 - \epsilon_1}{2}\left|\langle w_{y_1}^\perp | u_x^{-a}\rangle\right|^2 \\ &= \frac{1}{4}(1 + a u_x w_z)\sin^2\frac{\epsilon_1 - \epsilon_2}{2} \end{aligned} \quad (5.41)$$

That is exactly what we obtained in 5.26 if we substitute $\frac{\epsilon_1 - \epsilon_2}{2}$ to ϵ. So we can conclude that detecting a photon on the path $|2\rangle$ when $\phi = 0$ is equivalent to the measurement of $|+\rangle_C$, while detecting a photon on the path $|2\rangle$ when $\phi = \pi$ is equivalent to the measurement of $|-\rangle_C$.

We describe now *Bob* measurement. The final state density matrix for *Bob* (considering the polarization of the beam on the path $|2\rangle$) reads:

$$\rho_{Bob,\phi=0}^{final} = \left[\alpha |w_z\rangle + \beta \cos\frac{\epsilon_1 - \epsilon_2}{2} |w_z^\perp\rangle\right] \cdot \left[\langle w_z| \alpha + \langle w_z^\perp| \beta \cos\frac{\epsilon_1 - \epsilon_2}{2}\right]$$

$$\rho_{Bob,\phi=\pi}^{final} = \left[\beta \sin\frac{\epsilon_1 - \epsilon_2}{2} |w_z^\perp\rangle\right] \cdot \left[\langle w_z^\perp| \beta \sin\frac{\epsilon_1 - \epsilon_2}{2}\right]$$

Recalling that *Bob's* measurement session is executed for one half with $\phi = 0$, and the other half with $\phi = \pi$ (this realizes the independence of *Bob* outcome from *Charlie*

measurement setting), and that *Bob's* measurement operator is $B_y^b = |v_y^b\rangle \langle v_y^b|_B$ (where $|v_y^b\rangle$ are a polarizaion vectors) we have that the measurement outcome probability reads:

$$\begin{aligned} P(b|xya) &= \frac{1}{2}Tr\left(B_y^b \rho_{Bob,\phi=0}^{final}\right) + \frac{1}{2}Tr\left(B_y^b \rho_{Bob,\phi=\pi}^{final}\right) \\ &= \frac{1}{2}Tr\Bigg(B_y^b \Big(|\alpha|^2 |w_z\rangle \langle w_z| + |\beta|^2 \cos^2 \frac{\epsilon_1 - \epsilon_2}{2} \|w_z^\perp\rangle\rangle \langle w_z^\perp| \\ &\qquad + \alpha\bar{\beta} \cos \frac{\epsilon_1 - \epsilon_2}{2} |w_z\rangle \langle w_z^\perp| + \bar{\alpha}\beta \cos \frac{\epsilon_1 - \epsilon_2}{2} |w_z^\perp\rangle \langle w_z|\Big)\Bigg) \\ &\qquad + \frac{1}{2}Tr\left(B_y^b \left(|\beta|^2 \sin^2 \frac{\epsilon_1 - \epsilon_2}{2} |w_z^\perp\rangle \langle w_z^\perp|\right)\right) \end{aligned} \tag{5.42}$$

and developing eq. 5.42, we obtain:

$$P(b|xya) = \frac{1}{2}\left(1 + \cos\frac{\epsilon}{2}(u \cdot v) + (w \cdot v)(w \cdot u)(1 - \cos\frac{\epsilon}{2})\right) \tag{5.43}$$

that is exactly what we obtained in 5.20 if we substitute $\frac{\epsilon_1 - \epsilon_2}{2}$ to ϵ.

Concluding, we have proved that the experimental design depicted in figure 5.4 give exactly the same results in terms of outcome probability than the theoretical model presented at the beginning of this chapter both for *Bob* and for *Charlie*. Consequently, using the results of the previous section, we know that there exist a set of basis for the measurement of the three observers that leads to a multiple CHSH inequality violation for such experimental design. The only thing we miss at this point is to build an apparatus that reproduces experimentally the operations and the manipulations on the initial state described in $\mathfrak{D}$, that is what we are going to explain in the next section.

5.3 APPARATUS

In this section we will describe precisely the experiment: what components we used to perform the operations on the system state required by $\mathfrak{D}$, in which configuration we mounted them and how we performed the measurements on the state. In this section we will often use the properties of optical elements such as Beam Splitters (BSs), Polarizing Beam Splitters (PBSs), Half Wave Plates (HWPs) and Quarter Wave Plates (QWPs) discussed in C on page 93.

The optical circuit described in section 5.2 is implemented using the setup showed in Figure 5.5. In our setup the polarization-entangled photons are produced by the Sagnac source described in section 4.2 and sent to *Alice*, *Bob* and *Charlie* through optical fibers.

Alice's and Bob's measurements

Alice and *Bob* have the same simple implementation scheme, highlighted in orange and green respectively in the figure. The measurement scheme consists of an Half Wave Plate (**HWP1** and **HWP6** respectively) followed by a Polarizing Beam Splitter (**PBS**) with two single-photon avalanche photo-diodes (SPADs) detectors placed at its output ports. This scheme allows for any strong polarization

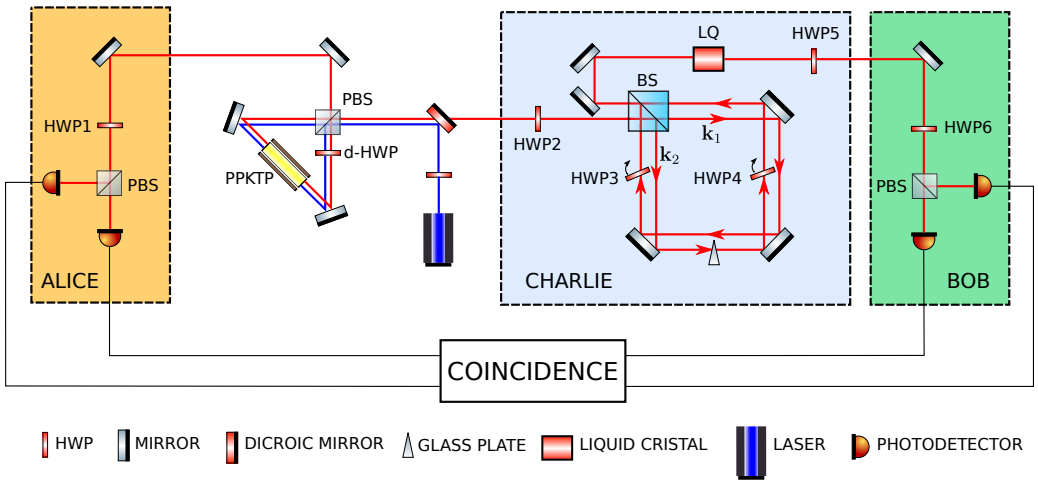

Figure 5.5.: Scheme of the experimental setup. The polarization-entangled photon-pair source comprises a PPKTP crystal, in a Sagnac interferometer, pumped by a laser diode at 404.5 nm. The entangled photons are collected and sent to *Alice*, *Bob* and *Charlie* apparatuses. *Alice* and *Bob* implement a scheme, consisting of a HWP (**HWP1** and **HWP6**) and a **PBS**, to measure the polarization on two linear basis. The transmitted and reflected photons from the **PBS** are detected by single photon avalanche diodes. *Charlie*'s apparatus performs the weak measurement. **HWP2** and **HWP5** implement the transformations $R_y(\theta_z)$ and $R_y^+(\theta_z)$, respectively. **HWP3** and **HWP4** are placed in a sagnac interferometer with clockwise and anticlockwise paths spatially separated. In particular, **HWP3** (**HWP4**) is placed in the clockwise (anticlockwise) path, and is used as a phase retarder between horizontal and vertical polarization. The phase difference between the two paths is adjusted by tilting a thin glass plate. Finally, a liquid crystal is used as a phase retarder between horizontal and vertical polarization.

measurement on the X-Z plane of the Bloch sphere. It is straightforward to see that keeping the HWPs with the fast axis parallel to the reference $|H\rangle$ polarization direction *Alice* and *Bob* execute a polarization measurement on the computational basis $\{|H\rangle, |V\rangle\}$. In order to measure on an arbitrary polarization basis $\left\{|a\rangle = \cos\frac{\alpha}{2}|H\rangle + \sin\frac{\alpha}{2}|V\rangle, |a^\perp\rangle = -\sin\frac{\alpha}{2}|H\rangle + \cos\frac{\alpha}{2}|V\rangle\right\}$ on the X-Z plane of the Bloch sphere, it is necessary to perform a polarization rotation around the y-axis $R_y(\theta)$ before the PBSs, such that

$$R_y(\theta_a)|a\rangle = |H\rangle, \text{ and } R_y(\theta_a)|a^\perp\rangle = |V\rangle$$

where $\theta_a = -\alpha = 2\arccos(\langle H|a\rangle)$. This state rotation can be implemented by rotating a HWP of an angle $\theta_a/4$, since the HWP characteristic equation is: $\Lambda_{HWP}(\theta_a/4) = R_y(\theta_a)\sigma_z$. It is worth notice that the presence of the σ_z after the HWP rotation matrix has no effect in our polarization measurement (that is insensitive to the relative phase between $|H\rangle$ and $|V\rangle$).

Charlie's measurement

Charlie's apparatus performs the general measurement. We list in the following how the circuit elements in figure 5.4 are practically implemented by the elements in figure 5.5.

- Two HWPs (**HWP2** and **HWP5** in figure) are used to rotate and reset the polarization base vectors of the incoming state $|\psi\rangle$ and of the state outgoing the

interferometer, implementing thus the transformations $\boxed{R_y(\theta_z)}$ and $\boxed{R_y^+(\theta_z)}$ in figure 5.4 that allow for *Charlie*'s measurement base choice.

- A beam splitter (the only **BS** in figure) is used both to split the initial path degree of freedom in two and to mix at the output the two *Charlie*'s path degrees of freedom thanks to the Sagnac configuration of the interferometer. **BS** therefore implements the action of both the operators $\boxed{BS}$ in figure 5.4.
- Two HWPs (**HWP3** and **HWP4** in figure) are used to introduce the two relative phase ϵ_1 and ϵ_2 difference between $|H\rangle$ and $|V\rangle$ polarization inside the interferometer on the two different path. ϵ_1 and ϵ_2 are adjusted by tilting **HWP3** and **HWP4** along their fast axis.
- A thin glass plate intercepting only one of the two path of the interferometer is used to introduce the phase difference ϕ between the two paths. ϕ is adjusted by tilting the glass slide.
- A liquid crystal (**LQ** in figure) is used as the phase retarder of $e^{-i\epsilon'}$ between horizontal and vertical polarization that is necessary in order to obtained the desired final state.

5.3.1 *Apparatus description*

The experimental scheme just described is mounted on the optical bench and exploit the polarization-entangled photons generated by a sagnac interferometer equipped with a 30 mm PPKTP crystal, pumped with a 404.5 nm CW laser that produces pairs of photons at 809 nm. Both the outputs of the interferometer are collected with a single-mode optical fiber, and one fiber outcome is sent to *Alice*, while the other is sent to *Bob* and *Charlie*.

In figure 5.6 we show a photo of Alice's setup. Alice's measurement setup is preceded by a three-coil polarization controller and a half-wave plate (HWP), with horizontal fast axis, which tilts around its vertical axis. These elements implement an arbitrary and easily manipulable unitary transformation on the photon sent to *Alice* that is fundamental to correct the source-phase and the transformation induced by fiber birefringence. Manipulating these two elements, we can obtain comfortably a singlet state $|\Psi^-\rangle$, as pointed out in section 4.2. The elements needed to implement *Alice*'s measuremet scheme (visible in picture) are listed below:

- the half-wave plate (**HWP1**) needed to implement the basis choice, that is mounted on a mechanized rotation mount controlled by a personal computer;
- the **PBS** that allows for a measurement in the computational basis $\{|H\rangle, |V\rangle\}$, whose outputs are collected by two multi-mode optical fibers and directed into the SPADs.

A linear polariser is used to filter out the residual $|H\rangle$ polarization present in the reflected beam.

Bob's measurement apparatus is shown in figure 5.7 and is very similar to *Alice*'s one. The only difference with respect to *Alice*'s setup are the collection fibers, which in this case are single-mode fibers. This is needed by *Charlie* which uses *Bob*'s side counts to measure his outcomes; *Charlie* requires beam spatial mode filtering in order to obtain a good interference visibility between the clockwise and the anticlockwise arms of the interferometer.

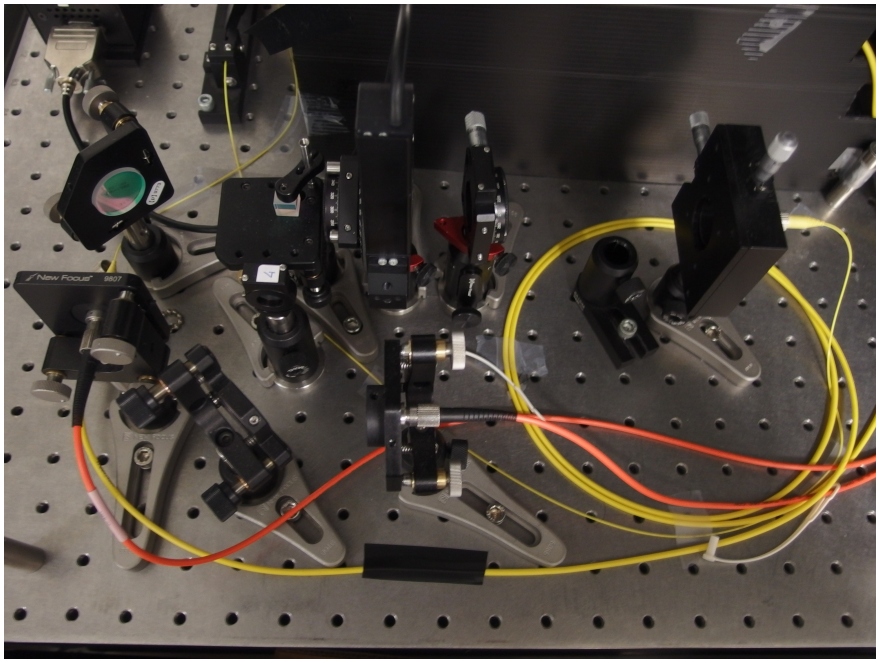

Figure 5.6.: Setup used for *Alice*'s measurement. Alice's measurement setup consists of a half-wave plate (**HWP1**) and a polarizing beam-splitter (**PBS**) whose outputs are collected by multi-mode fibers and sent to two SPADs. The reflected arm of the **PBS** is filtered by a linear polariser.

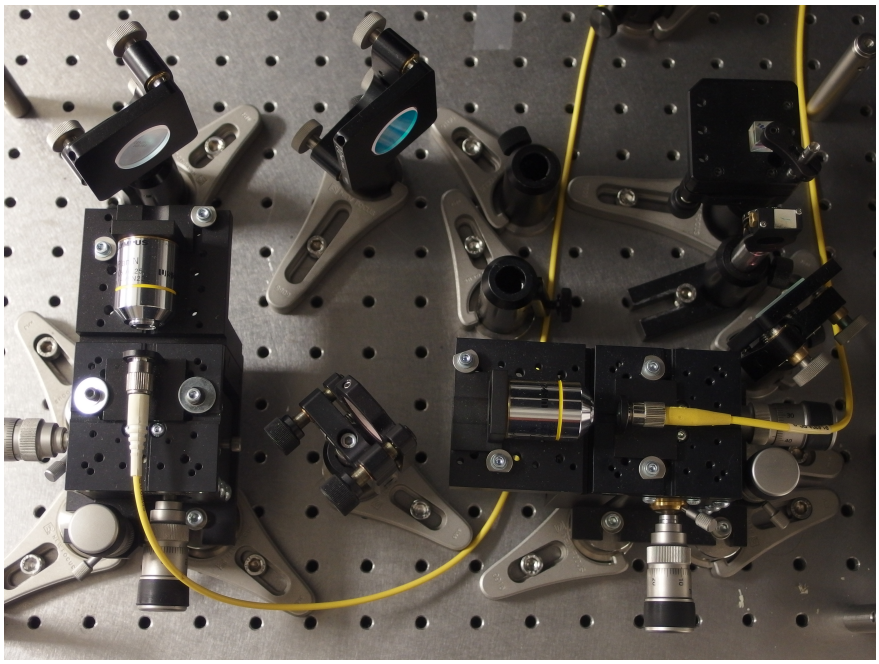

Figure 5.7.: Setup used for *Bob*'s measurement. Even in this case **HWP6** is placed on a mechanized rotation mount, followed by a **PBS** that performs the measurement in the $\{|H\rangle, |V\rangle\}$ basis. The reflected arm of the **PBS** is filtered by a linear polariser.

In figure 5.8 we show the practical implementation of the sagnac interferometer showed in the scheme 5.5. The computational basis of *Charlie*'s path encoding are implemented using the clockwise and anticlockwise beam propagation direction inside the interferometer.

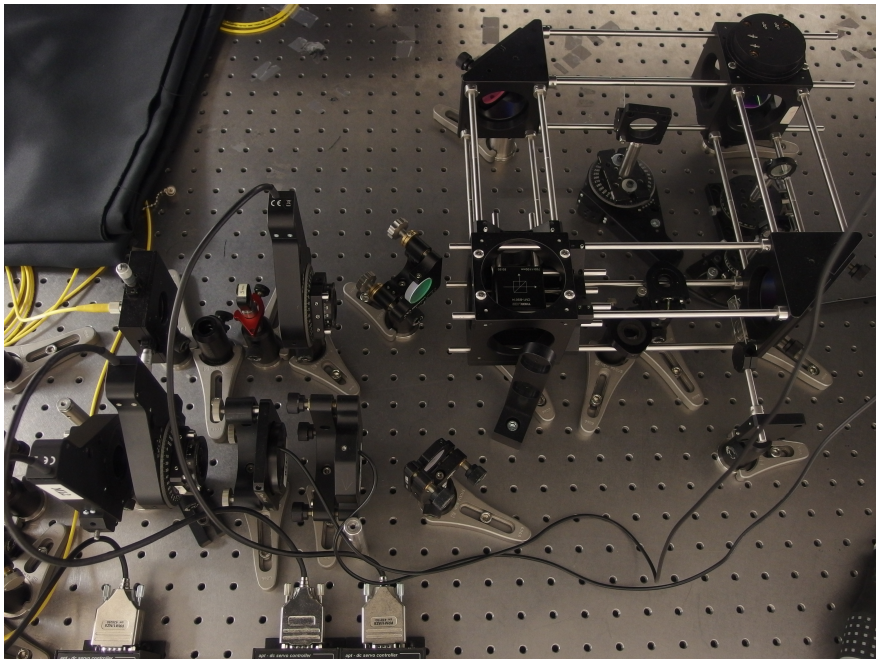

Figure 5.8.: Charlie's measurement setup. The beam coming out from the fiber crosses a 3 nm band-filter and an half-wave plate (**HWP2**) before entering into the Sagnac interferometer. A **BS** generates the clockwise and anticlockwise arms of the interferometer, the two arms inside the interferometer are separated by 1 cm. Both arms are equipped with a half-wave plate (**HWP3** and **HWP4**) and a glass. At the output of the interferometer, the beam crosses a couple of liquid crystals (**LQ**) and a half-wave plate (**HWP5**). At the bottom-left side of the figure is possible to see before **HWP6**, the element that start Bob measurement apparatus.

Before entering *Charlie*'s setup, the photon spectrum is filtered by a band-pass filter centred at 808 nm and 3 nm-wide. This is done in order to remove unwanted wave-length photons virtually produced by the source[4] whose presence would be harmful to our purposes. Different wave-length photons would in fact face different phase transformations interacting with the various optical elements in our circuit, preventing us to obtain the desired photon manipulation and interference. After passing the band-pass filter the beam pass through an **HWP2** placed on a motorized rotation mount, such waveplate is used to select the measurement basis. The beam then encounters a beam-splitter (**BS**), which creates a superposition of clockwise and anticlockwise arm. The two arms are separated by 1 cm in order to make it possible to place different optical elements on the two arms. Because of the short coherence length of the photons produced by the source, it is necessary to maintain as equal as possible the optical path length of the beams on the two arms of the interferometer in order to see interference at the exit of the **BS**. This practically translates into placing the same optical elements on both the arms of the interferometer.

Each arm has a half-wave plate, with the fast and slow axes correspondent to the $|H\rangle$-$|V\rangle$ basis, which is tilted around its vertical axis in order to introduce a phase

4 The production of photons at a different wavelength than the 809 nm expected by our source was not predicted at all. Nevertheless testing and characterizing the apparatus we obtained unexpected results that we were unable to justify. We solved that situation only placing this band-filter on the incoming beam, so that became experimentally evident that photons at different wavelength that the one expected were produced by the source, and were compromising the experiment outcome. We didn't investigate further this different wavelength photons production and we solved the problem by keeping the band-pass filter for all the duration of our measurements.

displacement between the $|H\rangle$ and the $|V\rangle$ polarization. The cumulative effect of these plates, the mirrors and the beam-splitter gives a relative phase ϵ_1 (ϵ_2) between the two polarizations for the two arms.

Both arms are also equipped with an equal-thick glass plate. The one that intercept the anticlockwise beam is fixed and kept perpendicular to the beam, while the one that intercept the clockwise beam is mounted on a mechanized rotator stage which allows to tilt the wave plate around its vertical axis. By tilting this glass plate, it is possible to control the relative phase displacement ϕ between the two arms of the interferometer.

At the output of the interferometer, two liquid-crystals are placed in order to implement the $e^{-i\epsilon'}$ transformation required to obtain the desired final state.
Finally, **HWP5**, placed on a motorized rotation mount implements the inverse of the basis selection transformation applied before the entrance of the interferometer. This concludes *Charlie*'s state manipulation.

As previously said, photons are detected using four SPADs, two at *Alice*'s side and two at *Bob*'s and *Charlie*'s side, whose detection events are tagged using a 81 ps resolution time-tagger. Both the acquisition of the time-tags and the control of the experiment is implemented using a personal computer, equipped with a Linux operating system and a custom software implemented in Python.

6

EXPERIMENTAL RESULTS

In this chapter, we discuss the experimental results obtained. We will organize the discussion as follows:

- In the first section, we will discuss the apparatus characterization, that is, all the preliminary tests made on the apparatus that are necessary to check its correct functioning.
- In the second section, we will discuss the state preparation procedure to follow in order to correctly set the apparatus before any run of the experiment.
- In the third section, the obtained experimental results will be presented and discussed.

6.1 APPARATUS CHARACTERIZATION

After mounting the apparatus the first thing we have done was testing it. We firstly have checked the interferometer, modelling in the first place the expected behaviour of the various optical elements that compose it, and subsequently testing them experimentally. As already stressed in the previous chapter, to reach the scope of the experiment it is fundamental to be able to control the global phase displacement between the two arms of the interferometer ϕ, and the relative phase displacement between $|H\rangle$ and $|V\rangle$ polarizations on both arms (ϵ_1, ϵ_2).
The optical elements responsible for the introduction of the ϕ phase displacement are the two glass slides mounted inside the interferometer. In section 6.1.1 we have modelled and tested the glasses slide behaviour.
The optical elements responsible for the introduction of the ϵ_1 and ϵ_2 relative phase displacement are the HWPs mounted inside the interferometer. In section 6.1.2 we have modelled and tested the HWPs behaviour.

6.1.1 *Glass Slide Characterization*

Every material is characterized by a specific refractive index n. A laser beam can be modelled very easily as a monochromatic electromagnetic wave characterized by a certain frequency and amplitude (for a brief review of classical optics instruments and results see B on page 83). An electromagnetic wave, that is characterized by a vacuum wavelength λ_0, when passing trough a material with refractive index n, changes its wavelength to $\lambda = \frac{\lambda_0}{n}$. The phase ϕ^* of a time independent EM wave is linked to its wavelength and to its propagation distance x by the relation $\phi^* = \frac{2\pi}{\lambda}x$. It is clear then that varying one of the two quantities x or λ (this second is manipulable via n), is

possible to adjust the EM wave phase (and thus a generic laser beam phase). Since our goal is to add a phase displacement between the clockwise and the anticlockwise laser beams inside the interferometer we inserted two glass slides that intercept the two paths; tilting the glass that intercepts the clockwise beam we are able to modify the Optical Path Length Difference between the two beams and thus we can introduce the desired phase displacement ϕ^*.

This fact can be modelled easily: the phase introduced by a tilted glass with thickness d and inclination angle θ_g (that is the angle between the glass slide and the plane perpendicular to the laser beam) to the laser beam propagating through it[1], and the phase introduced by the fixed glass to the other laser beam read respectively:

$$\phi_{clockwise} = \frac{2\pi}{\lambda_0}\frac{d}{\cos\theta_g}n_g \qquad \phi_{cunterclockwise} = \frac{2\pi}{\lambda_0}d\,n_g$$

where n_g is clearly the refraction index of the glass, and λ_0 the EM vacuum wavelength. The phase displacement between the two beams introduced by the glass slide is then:

$$\begin{aligned}\Delta\phi &= \phi_{clockwise} - \phi_{cunterclockwise}\\ &= \frac{2\pi}{\lambda_0}\left(\frac{1}{\cos\theta_g} - 1\right) d\,(n_g - n_a)\\ &= \left(\frac{\xi_g}{\cos\theta_g} + \Delta\phi_0\right)\end{aligned}$$

with n_a the refraction index of air, $\xi_g = \frac{2\pi}{\lambda_0} d\,(n_g - n_a)$ and $\Delta\phi_0$ a phase factor that collect the initial phase difference multiplied by ξ_g. We can now express the intensity of the interference between the two beams at the output of the interferometer as a function of θ_g:

$$I(\theta) = I_0 \sin^2\left(\frac{\xi_g}{\cos\theta_g} + \Delta\phi_0\right) \tag{6.1}$$

where I_0 is the maximum intensity. Considering the indicative values of the quantities characterizing our system ($\lambda \sim 10^{-6}$m, $d \sim 10^{-3}$m and $n_g - n_0 \sim 0.4$) we expect $\xi_g \sim 10^3$.

Experimental characterization

In an experiment we inject photons in a mixed state of polarization $|H\rangle$ and $|V\rangle$ inside the interferometer, and we then measure at the output port on the basis $|H\rangle$ and $|V\rangle$. We observe the variation of the intensity while changing the incident angle of the glass slide; this is shown in figure 6.1.

Fitting the experimental data with the following ansatz

$$I(\theta) = I_0 \sin^2\left(\frac{\xi_g}{\cos(\theta_g - \theta_0)} + \Delta\phi_0\right) + N_0 \tag{6.2}$$

per each channel, we get a very good agreement with the model (N_0 in the equation is kept to take into account the noise).

We note the following facts:

1 In the following we approximated the beam inside the glass as a straight line, neglecting thus the beam refraction inside the glass. This happens to be a good approximation in cases of small θ_g.

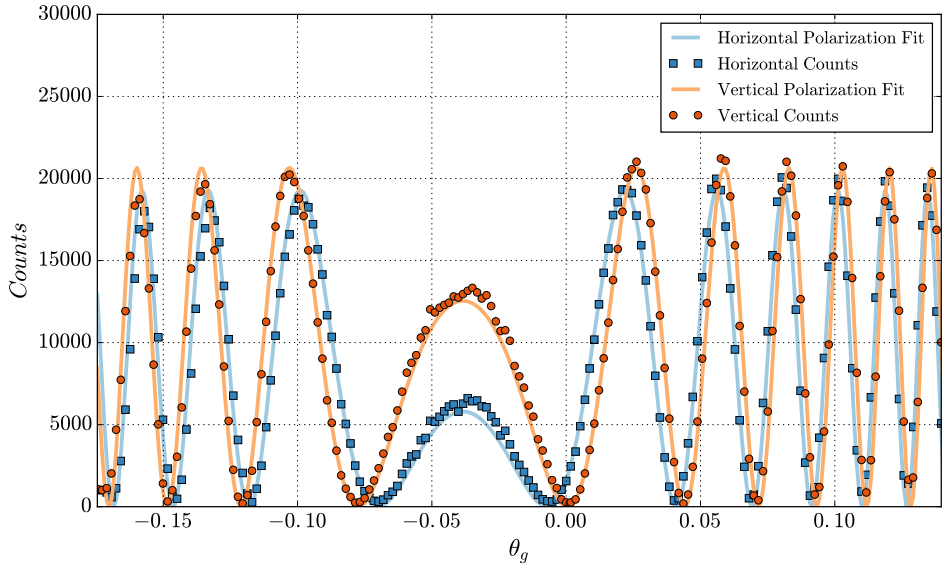

Figure 6.1.: Photon counts measured on $|H\rangle$ (blue squares in the figure) and $|V\rangle$ (orange circles in the figure) polarization base for several glass slide θ_g angles expressed in radians. In this measurement the interferometer was equipped with only the two glass slides. In this example the horizontal polarization counts are fitted by the function $P_H = 19000 \cdot \sin^2(\frac{1180}{\cos(\theta_g + 2.21)} + 2.62)$, while the vertical polarization counts are fitted by $P_V = 20000 \cdot \sin^2(\frac{1180}{\cos(\theta_g + 2.21)} + 2.21)$.

- ξ_g is of the order of 10^3 and is independent on the polarization which is consistent with the isotropy of the glass;
- $\Delta\phi_0$ is slightly different in the two channel, probably due the action of the mirrors and of the beam splitter which introduce a phase displacement between the two polarizations.
- The maximum visibility is around 98% for both channels, and it is obtained for angles $[0, 0.05]$ in figure 6.1.

We concluded than the two glass slides were suitable for the implementation of the phase displacement between the two interferometer arms.

6.1.2 *Half Wave Plate Characterization*

This time our aim is to test an optical element capable of adding a tunable relative phase displacement between the two polarization $|H\rangle$ and $|V\rangle$ of the beam. To implement such operation we use an HWP endorsable around the $|H\rangle$ axis with fast axis parallel to $|H\rangle$. Since the HWP is birefringent with the two different refractive indexes n_H and n_V, follows immediately that tilting it we can change the phase difference between the $|H\rangle$ and $|V\rangle$ polarizations.

The mathematical model of the HWP behaviour is very similar to the glass slide one, we only have to consider the two polarizations separately. The phases introduced

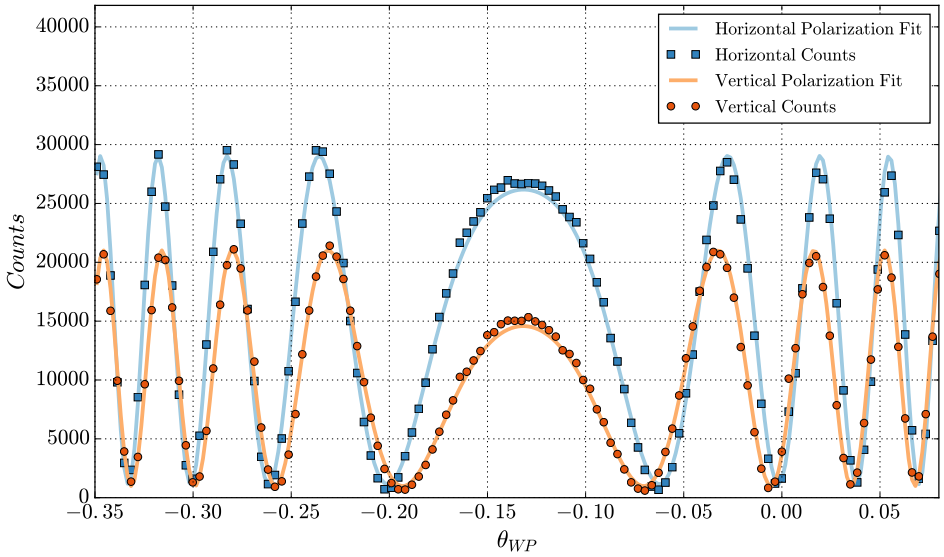

Figure 6.2.: Photon counts measured on $|H\rangle$ (blue squares in the figure) and $|V\rangle$ (orange circles in the figure) polarization base for several half wave plate θ_{WP} angles expressed in radians. In this measure the interferometer was equipped with two glass slides and two wave plates. In this example the horizontal polarization counts are fitted by the function $P_H = 28000 \cdot \sin^2(\frac{518.7}{\cos(\theta_{WP}-0.132)} - 1.55) + 1016$, while the vertical polarization counts are fitted by $P_V = 20000 \cdot \sin^2(\frac{514.5}{\cos(\theta_{WP}-0.132)} - 2.94) + 883$.

by an HWP tilted by an angle θ_{WP} with respect to the same beam propagating though air are:

$$\phi_H = \frac{\xi_H}{\cos\theta_{WP}} + \phi_{0H} \qquad \xi_H = \frac{2\pi}{\lambda} d(n_H - n_0)$$
$$\phi_V = \frac{\xi_V}{\cos\theta_{WP}} + \phi_{0V} \qquad \xi_V = \frac{2\pi}{\lambda} d(n_V - n_0)$$

and the expected intensities at the output of the interferometer when the arms are interfering are:

$$I_H(\theta) = I_{0H} \sin^2\left(\frac{\xi_H}{\cos\theta_{WP}} + \Delta\phi_H\right) \tag{6.3}$$
$$I_V(\theta) = I_{0V} \sin^2\left(\frac{\xi_V}{\cos\theta_{WP}} + \Delta\phi_V\right) \tag{6.4}$$

Experimental characterization

In an experiment, we injected photons in a mixed state of polarization $|H\rangle$ and $|V\rangle$ inside the interferometer, measuring at the output port on the basis $|H\rangle$ and $|V\rangle$. We observe the variation of the intensity while changing the incident angle of the half wave plate; this is shown in figure 6.2. Fitting the experimental data with the following ansatzs

$$I_H(\theta) = I_{0H} \sin^2\left(\frac{\xi_H}{\cos(\theta_{WP} - \theta_{0H})} + \Delta\phi_H\right) + N_{0H}$$
$$I_V(\theta) = I_{0V} \sin^2\left(\frac{\xi_V}{\cos(\theta_{WP} - \theta_{0V})} + \Delta\phi_V\right) + N_{0V}$$

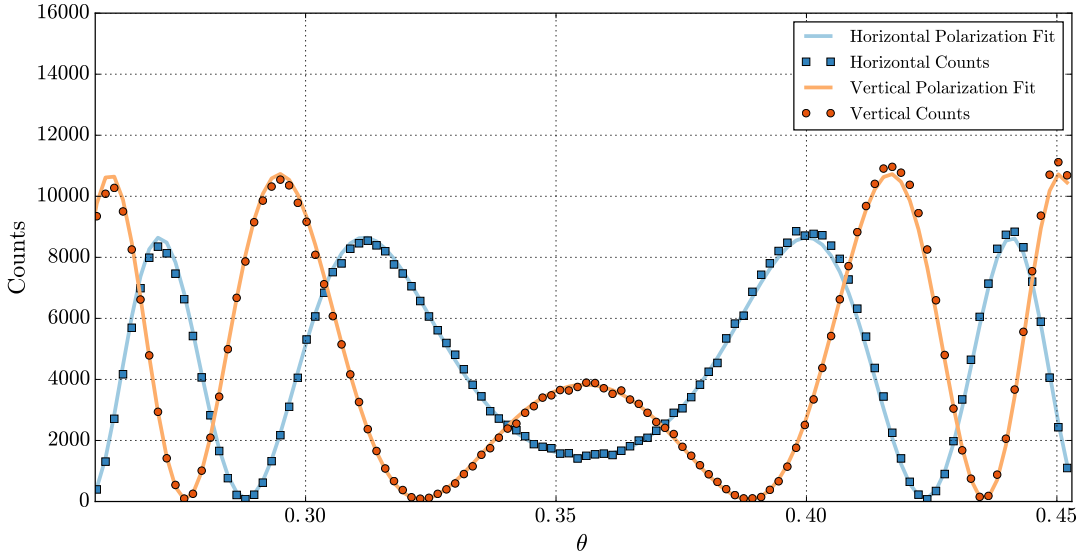

Figure 6.3.: Example of the procedure to evaluate the relative phase difference ϵ^* given by the interferometer between the horizontal (blue squares in figure) and vertical polarization (orange circles in figure). In this example the horizontal polarization counts are fitted by the function $P_H = 8600 \cdot \sin^2(\frac{1185.5}{\cos(\theta - 0.356)} + 2.45) + 98$, while the vertical polarization counts are fitted by $P_V = 11000 \cdot \sin^2(\frac{1185.5}{\cos(\theta - 0.356)} + 1.40) + 68$. θ is the rotation angle of the glass plate expressed in radians. The phase difference ϵ is thus 1.049 ± 0.004. The glass angle θ is expressed in radians.

where N_{0H} and N_{0V} take into account the noise, we get a very good agreement with the model. We note the following facts:

- ξ_H and ξ_V are of the order of 10^3 and depend on the polarization, in particular $\xi_H - \xi_V \approx 4$;
- with this method we can identify the fast axis of the HWP that in this case is horizontal, since $\xi_H < \xi_V$.

6.1.3 *Polarization shift characterization*

Thanks to the equations 6.3 and 6.4 the polarization phase displacement ϵ^* can be straightforwardly be expressed as a function of θ_{WP} through

$$\epsilon^* = \Delta\phi_H - \Delta\phi_V = \frac{\xi_H - \xi_V}{\cos\theta_{WP}} + \phi_{0H} - \phi_{0V} \tag{6.5}$$

It follows that tilting the HWPs we can control the polarization phase displacement on the two arms and we can set ϵ^* (via θ_{WP}) to be equal to the desired ϵ of our model. Experimentally, we retrieve the ϵ^* value of a certain HWPs configuration by fixing the HWPs in a certain position, and then fitting with equation 6.2 the $|H\rangle$ and $|V\rangle$ polarization interference pattern obtained moving the tiltable glass in order to obtain $\Delta\phi_{0,H}$ and $\Delta\phi_{0,H}$. ϵ^* is at this point simply the difference between the two polarization phase offset:

$$\epsilon^* = \Delta\phi_{0,V} - \Delta\phi_{0,H}$$

In figure 6.3 we show an example of the interference pattern used to retrieve ϵ^*. In figure 6.4 we give a visual representation of the ϵ^* dependence on θ_{WP} showing several interference patterns obtained at increasing θ_{WP} inclination angle. The graphs

are obtained keeping fixed the position of one of the two HWP and tilting the second HWP of 5° at every measurement, starting from a condition where both the HWPs are perpendicular to the laser beam. Finally, in figure 6.5 we have tested our model plotting the ϵ^* values obtained with the analysis shown in figure 6.4 in function of the tilting angle θ_{WP}, and then fitting the data with the equation 6.5. The obtained results are in good agreement with our model.

We finally remember here a fundamental result that we already obtained in 5.2.2 that is the link between the experimental phase shift on the two arm of the interferometer ϵ_1 and ϵ_2, and the measurement strength parameter ϵ:

$$\epsilon = \frac{\epsilon_1 - \epsilon_2}{2} \tag{6.6}$$

6.1.4 *System stability*

Since our experiment heavily depends on the ϵ value esteem to characterize the strength of the measurement executed by *Charlie*, it's clear that this is a very sensible parameter of our experiment, on witch we want a good confidence.

In the previous section we explained how the procedure used to evaluate ϵ relies basically on the difference between two parameters retrieved from a fit over the interference of $|H\rangle$ and $|V\rangle$ polarizations. The error associated to the ϵ in this way evaluated would be given by a simple $\Delta\phi_{0,V}$ and $\Delta\phi_{0,H}$ error propagation. This procedure takes into account just the fit errors but totally ignores other important factors such as possible movement systematic errors (offsets, rotation inaccuracies) or fluctuations of the environment conditions.

In order to better evaluate the ϵ parameter error and to estimate its stability (we are particularly concerned about the stability because of the repeated CHSH measurements we want to do), we executed a repeated ϵ parameter evaluation for a period of time of thirteen hours. We set up the apparatus to repeat an interference measurement over a whole night keeping fixed all the experimental parameters (except for the tilting glass angle that had to move to execute the interference measurement) and we subsequently esteemed the ϵ parameter for all the measurements and looked at the parameter stability. In figure 6.6, we show the result of such measurement. The ϵ parameter distribution so obtained was used to evaluate its error. The statistical error in fact, differently from the one obtained by the fit error propagation, keeps in regard all the aspects of the experiment and it is therefore considered the more accurate.

In figure 6.7, we show another interesting graph related to the night measurement. In the graph, the trends over the night of all the equation 6.2 fit parameters are plotted. Looking at the graph, we notice that $\Delta\phi_{0,H}$ and $\Delta\phi_{0,V}$ are pretty stable (and consequently the same holds for the phase difference ϵ as already seen in figure 6.6). Conversely the intensity (I_0) and the offset angle (θ_0) show an evident variation during the night. The I_0 variation highlights a beam polarization variation probably due to the relaxation and to the effect of the environment stabilization on the optical fiber, while the θ_0 variation highlights a fine (and negligible) dependence of the rotator offset from the environment conditions. Both the variations just pointed out are of no importance to the purpose of our experiment.

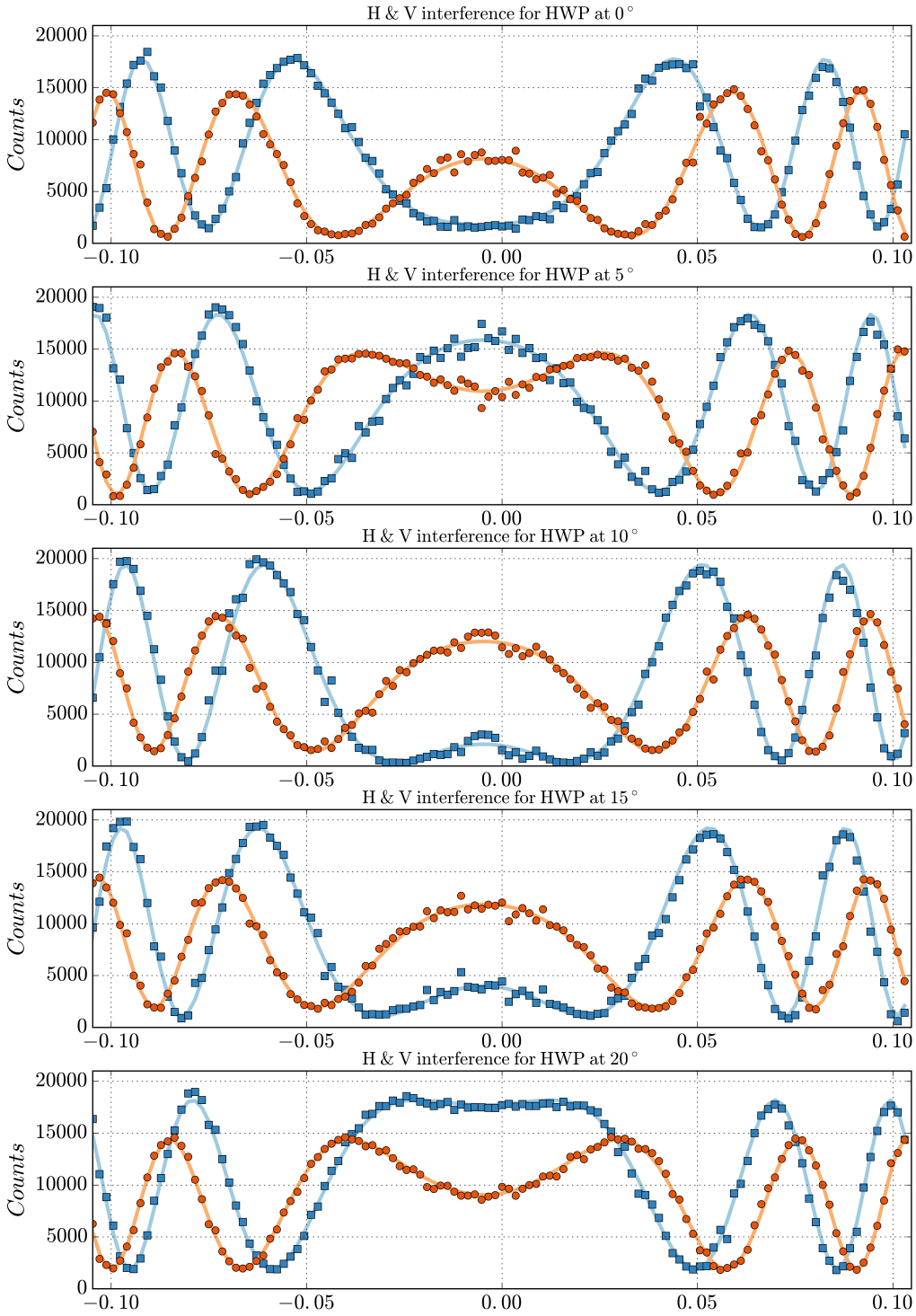

Figure 6.4.: $|H\rangle$ (blue squares) and $|V\rangle$ (orange circles) interference patterns obtained keeping fixed one HWP and tilting the second HWP of 5° more at every subsequent measure. The interferometer was equipped with two glass slides and two wave plates. On the x-axis is represented the glass slide angle expressed in radians. The interference pattern are fitted with equation 6.2.

6.2 STATE PREPARATION PROCEDURE

Now that we have characterized the apparatus, showing that is capable of all the optical state manipulations required by the model in section 5.2, we need to prepare

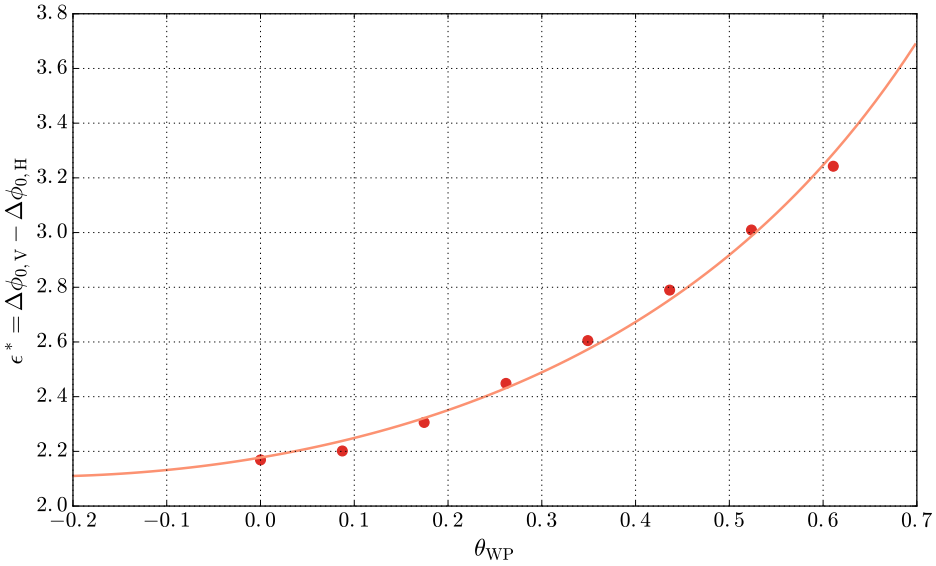

Figure 6.5.: ϵ^* phase displacement between $|H\rangle$ and $|V\rangle$ polarizations in function of the HWP inclination angle θ_{WP}. The ϵ^* value plotted are those obtained by the analysis shown in figure 6.4 (it is worth notice that in this graph we cover a wider θ_{WP} range than the previous figure for a matter of graph dimension). The interferometer was equipped with two glass slides and two wave plates, and the curve that fits the data is: $\epsilon^* = \epsilon = \frac{2.24}{\cos(\theta_{WP}+0.25)} - 0.13$.

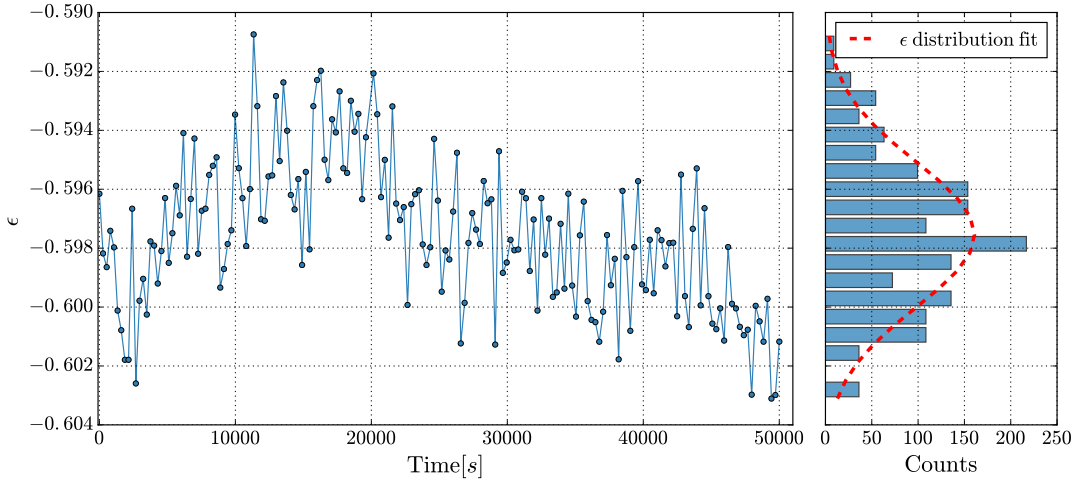

Figure 6.6.: Estimation of the ϵ phase displacement over several measurements lasting for a period of thirteen hours. (**Left**) Each point in the graph represents a different estimation of ϵ (**Right**) ϵ value distribution. The gaussian curve that fits the data is characterized by a mean value $\mu = -0.5975$ and a standard deviation $\sigma = 0.0025$. The standard deviation of the distribution was used to evaluate the error on the estimation of ϵ.

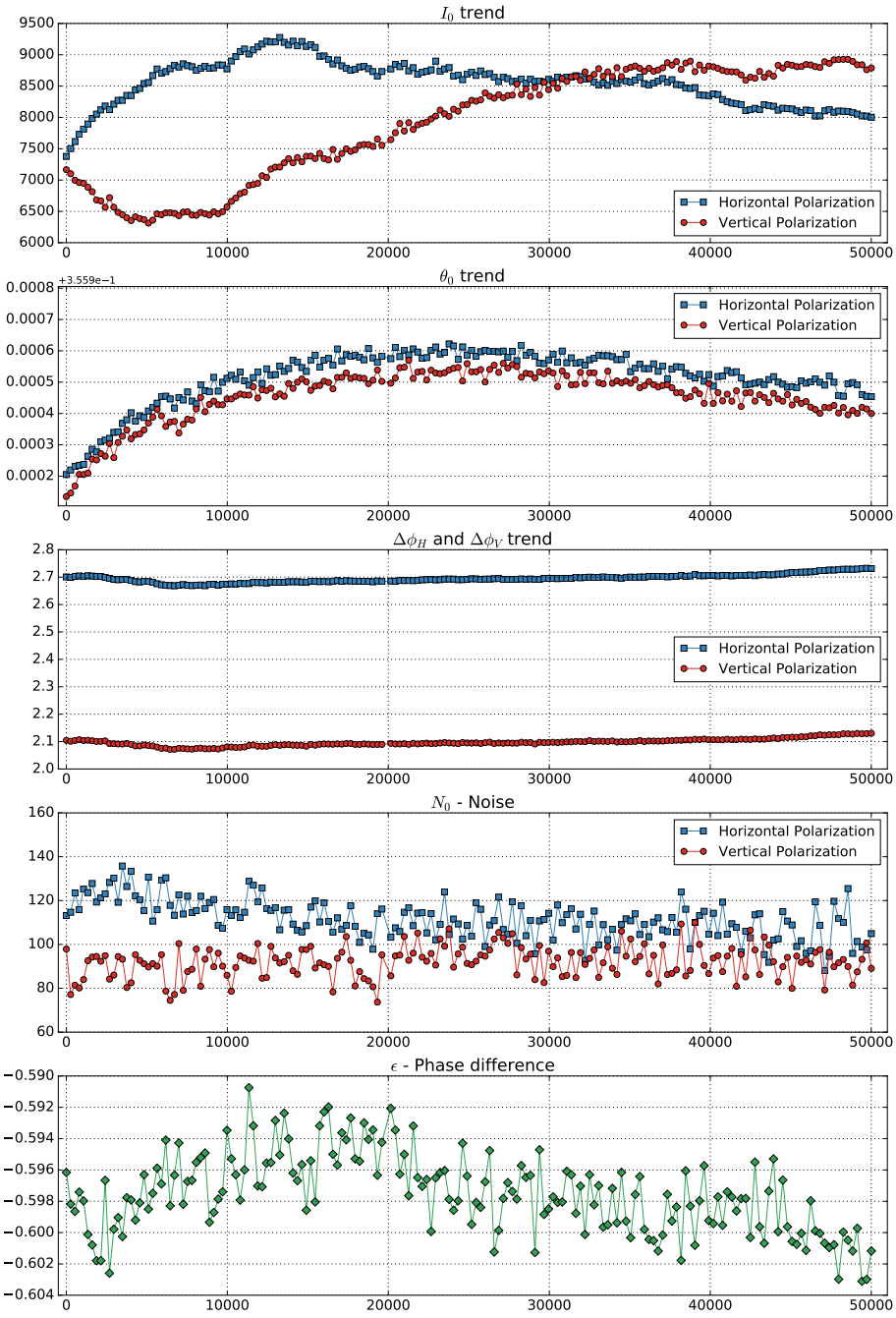

Figure 6.7.: Fit parameter variation over a thirteen hours time interval. The blue squares in the graphs represent the $|H\rangle$ polarization parameters, the red circle represent the $|V\rangle$ polarization parameters. On the x-axis is represented the time interval (in second) from the first measure performed. Looking at the graph we notice that while $\Delta\phi_{0,H}$, $\Delta\phi_{0,V}$ and ϵ are stable over the night, I_0 and θ_0 are not.

the state for the actual multiple observer CHSH inequality violation. In the theoretical model we saw that the starting point of all the analysis was a maximally entangled double photon singlet state. Such state is produced by the Sagnac source described in 4.2 and the two entangled photons are transmitted to *Alice* and *Bob & Charlie* through two optical fibers.

In our experiment, we have to take into account that the various optical elements of the apparatus are not ideal, and thus they modify the photon state interacting with them with manipulations that can be represented by unitary matrices acting on the photon state. The interferometer, for example, introduces a generic phase displacement between $|H\rangle$ and $|V\rangle$ polarization due to the action of the mirrors inside it, while the optical fibers introduce a generic unitary transformation to the photons that pass through them, adding both a random polarization phase displacement ϕ' between $|H\rangle$ and $|V\rangle$ ($\alpha|H\rangle + \beta|V\rangle \mapsto \alpha|H\rangle + e^{i\phi'}\beta|V\rangle$) and rotating the $|H\rangle$ and $|V\rangle$ reference polarization base to a new generic orthogonal base ($\alpha|H\rangle + e^{i\phi'}\beta|V\rangle \mapsto \alpha|w\rangle + e^{i\phi'}\beta|w^{\perp}\rangle$).

Experimentally we have to take into account these effects and, in order to get some results, we must correct them performing a state preparation procedure. The state preparation is divided in two steps:

Source alignment Here we prepare the initial singlet state using only one arm of the interferometer. We correct the phase displacement introduced by the interferometer to the photon passing through it and we retrieve the singlet state manipulating *Alice* photons while looking at *Alice* and *Bob* coincidences.

Interferometer optimization Here we prepare the state we want to analyse setting the desired ϵ strength parameter and removing the $e^{i\epsilon}$ phase displacement between $|H\rangle$ and $|V\rangle$.

6.2.1 *Source alignment*

To align the source we use a single arm of the interferometer (the one with the fixed wave plate). First of all we need to compensate the phase shifts between $|H\rangle$ and $|V\rangle$ introduced by the mirrors of the interferometer operating as follows:

- we send to *Bob* a 20 mW 808 nm laser whose high intensity eases the procedure;
- we block the interferometer arm that pass through the endorsable HWP;
- we polarize vertically the laser beam using a linear polarizer placed before **HWP2** (see figure 5.5);
- we set the **HWP2** 22.5° to have the $|+\rangle$ state entering the interferometer;
- we set the **HWP6** at 22.5° so that *Bob* is measuring on the basis $\{|+\rangle, |-\rangle\}$.

The unitary operator describing the action of the interferometer's arm plus the liquid crystal before **HWP6** has the form

$$U = |H\rangle\langle H| + e^{i\phi'}|V\rangle\langle V|$$

for some angle ϕ. The state before *Bob*'s measure is then

$$|\psi\rangle = \frac{1}{2}(|H\rangle + e^{i\phi'}|V\rangle)$$

and the outcomes probability for *Bob* are

$$|\langle\pm|\psi\rangle|^2 = \frac{1}{2}(1 \pm \cos\phi')$$

Varying the phase displacement given by the liquid crystal to the state (by tuning the electric voltage on the **LC**) we can control the value of ϕ'. Since we want $\cos\phi' = 1$, we tune the **LC** action until we find the minimum for the $|\langle -|\psi\rangle|^2$ probability.

The following step consist in manipulating *Alice*'s photon state in order to retrieve the best possible singlet state shared between *Alice* and *Bob*. This is achieved by following this procedure:

- first of all we send both to *Alice* and *Bob* the output of the Sagnac source, and we remove the polarizer before the interferometer used in the previous procedure;
- using a software specifically developed, we check the detected photons coincidences between *Alice* and *Bob* in all the possible measurement basis configuration (rotating **HWP1**, **HWP6** and **HWP2** & **HWP5**);
- we manipulate *Alice*'s photon by tuning the *Alice*'s three-coil polarization controller and the endorsable half wave plate until we get the best singlet state visibility in all the measurement basis.

Once prepared the singlet state we proceed then with the interferometer optimization.

6.2.2 *Interferometer optimization*

Once the source has been aligned, we proceed firstly tilting the HWPs inside the interferometer to get the desired phase shift between $|H\rangle$ and $|V\rangle$, and then tuning the **LC** voltage in order to compensate the relative phase $e^{i\frac{\epsilon_1-\epsilon_2}{2}}$. The relative phase displacement can be compensated performing the following steps:

- for the first time we let look at the interference between the two arms of the interferometer removing the stopper used for the previous procedures;
- we set *Alice* to measure on the $|+\rangle$ and $|-\rangle$ basis, therefore, since the state has been prepared to be a singlet, *Bob* knows what is the state entering the interferometer (either $|-\rangle$ or $|+\rangle$);
- the **HWP2** is rotated at 45 degrees, to left unaltered the obliquely polarized entering state;
- we set *Bob* to measure on the $|+\rangle$ and $|-\rangle$ basis.

The action of the interferometer for a global phase shift $\phi = 0$ is given by equation (5.36), and, looking only at the port $|2\rangle$, the output state is

$$|\psi\rangle = |H\rangle \pm e^{i\frac{\epsilon_1+\epsilon_2}{2}} \cos\frac{\epsilon_1-\epsilon_2}{2}|V\rangle \qquad \text{for Alice's outcome} \mp$$

Suppose that the **LC** apply a phase retardation of χ, then *Bob* receives

$$|\psi\rangle = |H\rangle \pm e^{i(\chi+\frac{\epsilon_1+\epsilon_2}{2})} \cos\frac{\epsilon_1+\epsilon_2}{2}|V\rangle \qquad \text{for Alice's outcome} \mp$$

The outcome probabilities of *Bob*'s measurement, conditioned on the Alice's outcome $\pm$, are:

$$P(b=+|a=\mp) = |\langle +|\psi\rangle|^2 = \frac{1}{2}\left(1+\cos^2\frac{\epsilon_1+\epsilon_2}{2} \pm 2\cos\frac{\epsilon_1+\epsilon_2}{2}\cos\left(\chi+\frac{\epsilon_1+\epsilon_2}{2}\right)\right)$$
$$P(b=-|a=\mp) = |\langle +|\psi\rangle|^2 = \frac{1}{2}\left(1+\cos^2\frac{\epsilon_1+\epsilon_2}{2} \mp 2\cos\frac{\epsilon_1+\epsilon_2}{2}\cos\left(\chi+\frac{\epsilon_1+\epsilon_2}{2}\right)\right)$$

Since we want $\cos(\chi + \frac{\epsilon_1+\epsilon_2}{2}) = 1$, we act on χ to maximize $P(b = +|a = -)$ and minimize $P(b = -|a = -)$ or minimize $P(b = +|a = +)$ and maximize $P(b = -|a = +)$.

We conclude in this way the state preparation procedure and we are ready to run the experiment.

6.3 EXPERIMENT PROCEDURE

Once completed the singlet state preparation and the interferometer optimization, we can start to collect the necessary data to evaluate the CHSH parameter of a certain ϵ-configuration.

The experimental evaluation of the CHSH parameter is obtained calculating the conditional probabilities $P(ab|xy)$ and $P(ac|xz)$. These two conditional probabilities are calculated as follow:

$$P(ab|xy) = \frac{N(xy)}{N(ab|xy)} \qquad \text{with} \qquad N(xy) = \sum_{\substack{a=\pm1 \\ b=\pm1}} N(ab|xy)$$

$$P(ac|xz) = \frac{N(xz)}{N(ac|xz)} \qquad \text{with} \qquad N(xz) = \sum_{\substack{a=\pm1 \\ c=\pm1}} N(ax|xz)$$

Where $N(ab|xy)$ and $N(ac|xz)$ are respectively the number of coincidences with outcome ab, ac detected while measuring in the xy and xz basis configuration. Hence, for every experiment run, we have to record the coincidences of 32 basis configurations. In order to obtain comparable coincidence counts, the period of measurement was kept equal for all the basis configurations.

The two CHSH parameters read:

$$I^{AB}_{CHSH} = E^{AB}_{00} + E^{AB}_{01} + E^{AB}_{10} - E^{AB}_{11} \leqslant 2$$
$$I^{AC}_{CHSH} = E^{AC}_{00} + E^{AC}_{01} + E^{AC}_{10} - E^{AC}_{11} \leqslant 2$$

with:

$$E^{AB}_{xy} = \sum_{\substack{a=\pm1 \\ b=\pm1}} ab \cdot P(ab|xy) \qquad E^{AC}_{xz} = \sum_{\substack{a=\pm1 \\ c=\pm1}} ac \cdot P(ac|xz)$$

It is worth remembering that *Alice-Bob* correlation parameters are calculated considering the polarization coincidences between the two photons composing the singlet. *Alice-Charlie* instead, calculate their correlations considering a polarization-path coincidence scheme.

6.4 EXPERIMENT RESULTS

After the apparatus characterization and state preparation, we are finally ready for the correlation measurement.

We have performed two different type of measurements: one explores the CHSH correlation values in function of the measurement strength ϵ, and the second consists of a series of measurements to prove the multiple simultaneous CHSH violation for both *Alice & Bob* and *Alice & Charlie*. The first type of measurements were performed

to test our theoretical model, in order to prove our comprehension of the phenomenon and the maneuverability of our apparatus, while the second type is the goal of our work.

6.4.1 *CHSH correlation values VS* ϵ

In the first type of measurement we ran the experiment several times at different ϵ values. In table 6.4.1 we show the results obtained for ϵ in the range $[0, \pi/2]$.

	ϵ	I^{AC}_{CHSH}	I^{AB}_{CHSH}
	0.060 ± 0.002	0.045 ± 0.007	2.733 ± 0.007
	0.060 ± 0.002	0.031 ± 0.007	2.738 ± 0.007
*	0.060 ± 0.002	0.035 ± 0.007	2.748 ± 0.007
	0.060 ± 0.002	0.018 ± 0.007	2.730 ± 0.007
*	0.060 ± 0.002	0.029 ± 0.007	2.737 ± 0.007
	0.548 ± 0.002	0.778 ± 0.008	2.492 ± 0.008
	0.548 ± 0.002	0.901 ± 0.008	2.489 ± 0.008
	0.548 ± 0.002	0.884 ± 0.008	2.485 ± 0.008
	0.570 ± 0.002	0.482 ± 0.008	2.474 ± 0.008
	0.570 ± 0.002	0.588 ± 0.008	2.490 ± 0.008
	0.570 ± 0.002	0.551 ± 0.008	2.481 ± 0.008
	0.873 ± 0.002	1.398 ± 0.009	2.227 ± 0.009
	0.873 ± 0.002	1.468 ± 0.009	2.238 ± 0.009
*	0.873 ± 0.002	1.485 ± 0.009	2.239 ± 0.009
*	$\mathbf{1.049 \pm 0.002}$	$\mathbf{2.119 \pm 0.007}$	$\mathbf{2.101 \pm 0.007}$
*	$\mathbf{1.049 \pm 0.002}$	$\mathbf{2.131 \pm 0.007}$	$\mathbf{2.112 \pm 0.007}$
*	$\mathbf{1.049 \pm 0.002}$	$\mathbf{2.133 \pm 0.007}$	$\mathbf{2.103 \pm 0.007}$
*	$\mathbf{1.049 \pm 0.002}$	$\mathbf{2.130 \pm 0.007}$	$\mathbf{2.105 \pm 0.007}$
*	$\mathbf{1.049 \pm 0.002}$	$\mathbf{2.126 \pm 0.007}$	$\mathbf{2.102 \pm 0.007}$
*	$\mathbf{1.049 \pm 0.002}$	$\mathbf{2.121 \pm 0.007}$	$\mathbf{2.091 \pm 0.007}$
*	$\mathbf{1.049 \pm 0.002}$	$\mathbf{2.129 \pm 0.007}$	$\mathbf{2.085 \pm 0.007}$
*	$\mathbf{1.049 \pm 0.002}$	$\mathbf{2.112 \pm 0.007}$	$\mathbf{2.075 \pm 0.007}$
	$\mathbf{1.053 \pm 0.002}$	$\mathbf{2.104 \pm 0.007}$	$\mathbf{2.060 \pm 0.007}$
	$\mathbf{1.053 \pm 0.002}$	$\mathbf{2.117 \pm 0.007}$	$\mathbf{2.069 \pm 0.007}$
	$\mathbf{1.053 \pm 0.002}$	$\mathbf{2.121 \pm 0.007}$	$\mathbf{2.066 \pm 0.007}$
	$\mathbf{1.053 \pm 0.002}$	$\mathbf{2.119 \pm 0.007}$	$\mathbf{2.066 \pm 0.007}$
	$\mathbf{1.053 \pm 0.002}$	$\mathbf{2.110 \pm 0.007}$	$\mathbf{2.057 \pm 0.007}$
*	1.256 ± 0.002	2.514 ± 0.008	1.753 ± 0.008
	1.256 ± 0.002	2.527 ± 0.008	1.762 ± 0.008
	1.256 ± 0.002	2.518 ± 0.008	1.768 ± 0.008
	1.535 ± 0.002	2.668 ± 0.007	1.298 ± 0.007
*	1.535 ± 0.002	2.727 ± 0.007	1.359 ± 0.007

Table 6.1.: Experiment results. In the table are listed the experimental CHSH parameter evaluation between *Alice* & *Bob* (I^{AB}_{CHSH}), and between *Alice* & *Charlie* (I^{AC}_{CHSH}) at different ϵ values. The double CHSH inequality violation ran are highlighted by bold type. The experimental outcomes marked by * are plotted in figure 6.8.

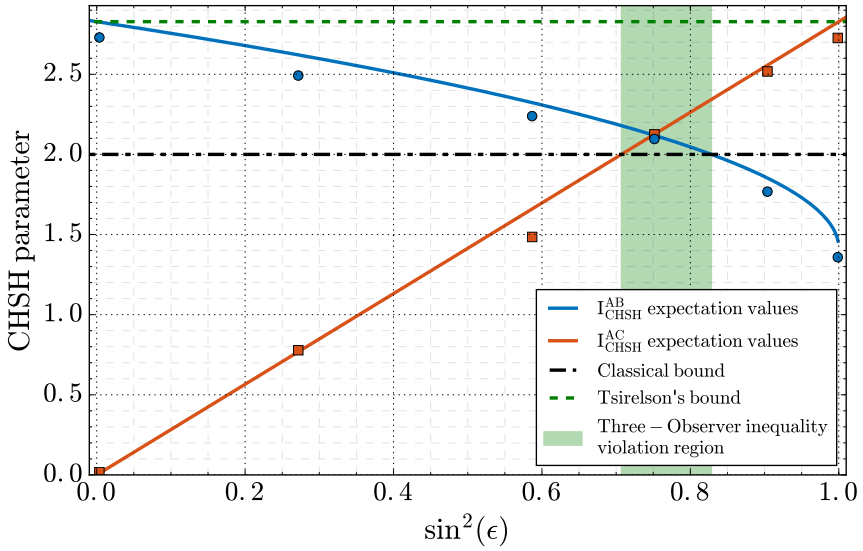

Figure 6.8.: Measurements of I^{AC}_{CHSH} (squares) and I^{AB}_{CHSH} (circles) for several values of ϵ. The red and green solid lines show the expected values of I^{AC}_{CHSH} and I^{AB}_{CHSH} (Eqs. 5.35 and 5.34), while the dash-dotted and dashed lines indicate classical and Tsirelson's bounds respectively. The green region highlights the values of ϵ in which double violation is expected. Poissonian errors are within the dimension of the points. In figure the correlation values at $\epsilon = 1.049$ are averaged with a weighted average and plotted as a single point.

Some of the experimental outcomes (those marked by * in the table) are plotted in figure 6.8. From the graph we see that the results show a good agreement with the theoretical model. For $\epsilon = 0$, there is no interaction between the polarization and the path degree of freedom, therefore *Charlie* is not performing any measurement. In this case, as expected, I^{AC}_{CHSH} is compatible with 0, while I^{AB}_{CHSH} is close to the Tsirelson's bound. By increasing ϵ, the quantity of information got by *Charlie* increases, as shown by the increase in his correlation I^{AC}_{CHSH} with *Alice*, while the state is more disturbed, determining a lowering in the correlation I^{AB}_{CHSH} between *Bob* and *Alice*.

6.4.2 *Double CHSH inequality violation*

To give a larger statistical evidence of the simultaneous double CHSH inequality violation several measurements have been taken in the region around $\epsilon = \pi/3$, where both I^{AB}_{CHSH} and I^{AC}_{CHSH} are expected to violate the classical bound (see bold entries in table 6.4.1). The measurements were performed at two different ϵ values in that region, $\epsilon = 1.049$ and $\epsilon = 1.053$. Figure 6.9 **(Top)** reports the results of 8 consecutive measurements with $\epsilon = 1.049 \pm 0.003$. In all trials, both I^{AC}_{CHSH} and I^{AB}_{CHSH} are above the classical bound, fluctuating around the mean values $I^{AC}_{CHSH} = 2.125 \pm 0.003$ and $I^{AB}_{CHSH} = 2.096 \pm 0.003$. Data are acquired at a mean coincidence rate of 700 counts per second, with an exposure time of 30 s for each measurement, therefore each trial takes about eight minutes to be measured. Therefore, these results show that the double violation is stable for a period longer than an hour, proving the reproducibility of the double violation and the stability of the setup.

A second series of trials, with $\epsilon = 1.053 \pm 0.003$ is shown in Figure 6.9 **(Bottom)**. Similarly to the previous case, both I^{AC}_{CHSH} and I^{AB}_{CHSH} are above the classical bound

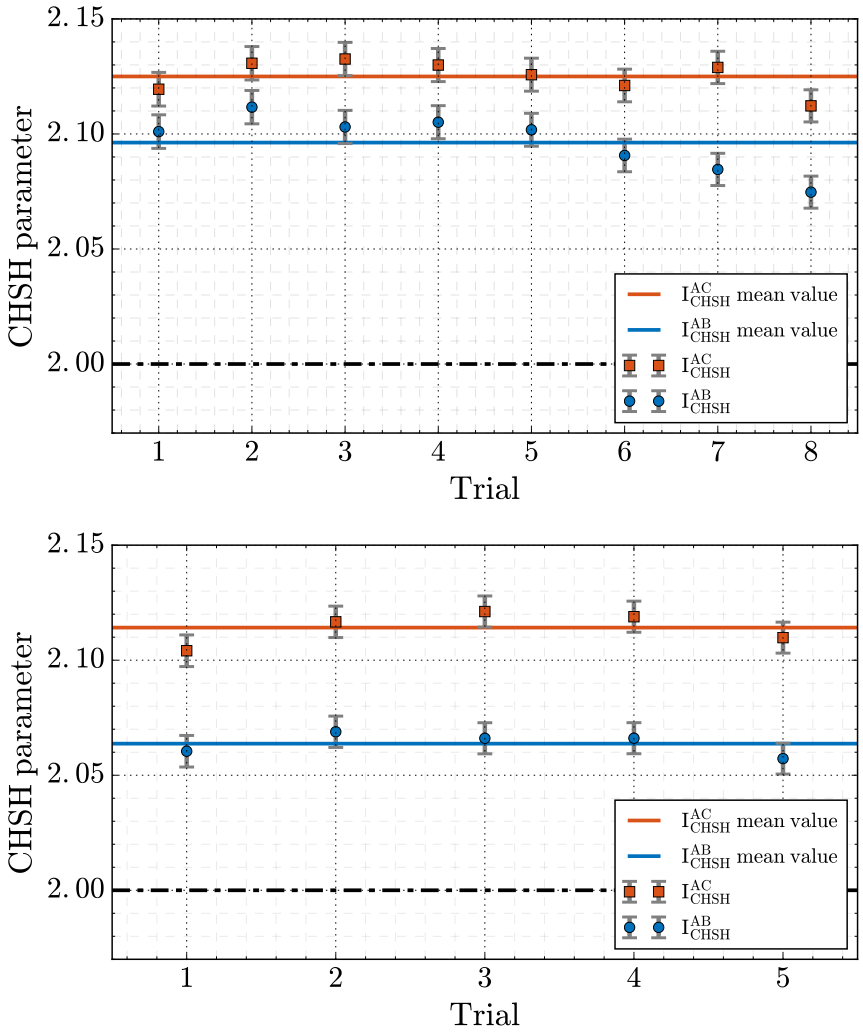

Figure 6.9.: Measurements of I^{AC}_{CHSH} (squares) and I^{AB}_{CHSH} (circles) in two consecutive series of trials. Red and blue solid lines indicate the mean value of I^{AC}_{CHSH} and I^{AB}_{CHSH} respectively. **(Top)** Eight consecutive trials were performed in an hour, with $\epsilon = 1.049 \pm 0.002$. Considering the poissonian error, the measurements show a violation of 10 standard deviations, fluctuating around mean values of $I^{AC}_{CHSH} = 2.125 \pm 0.003$ and $I^{AB}_{CHSH} = 2.096 \pm 0.003$. **(Bottom)** Another series of five consecutive trials were performed within a hour, with $\epsilon = 1.053 \pm 0.002$. Similarly to the previous case, all the measurements show a violation of 10 standard deviation, fluctuating around mean values of $I^{AC}_{CHSH} = 2.114 \pm 0.003$ and $I^{AB}_{CHSH} = 2.064 \pm 0.003$.

for the entire period of the acquisition, with $I^{AC}_{CHSH} = 2.114 \pm 0.003$ and $I^{AC}_{CHSH} = 2.064 \pm 0.003$.

7

CONCLUSIONS

We have shown experimentally that a double CHSH inequality violation between two different pairs of observers can be achieved by using a single two-qubit entangled state of two photons. We recall that the three observers choose randomly between the two possible measurements, with no agreement on the measurement strategy. Thanks to the stability of our setup (larger than 1 hour), we could perform several double violations increasing the statistical evidence of the experiment (section 6.4.2). The double violation was tested and repeated for different values of ϵ, the interaction strength of *Charlie*'s weak measurement. The experimental data well reproduce the theoretical model when ϵ is changed (section 6.4.1).

It is worth noticing that by slightly changing the measurement setting at *Charlie*'s side it is possible to obtain an optimal weak measurement [7]. Indeed, if the phases of the glass plate are set to $\phi = \phi_0$ and $\phi = \phi_0 + \pi$ the value of the A-C inequality can be varied as $I_{CHSH}^{(AC)} = 2\sqrt{2}[\cos\phi_0 - \cos(\phi_0 - \epsilon)])$, maximized to $I_{CHSH}^{(AC)} = 2\sqrt{2}\sin\epsilon$ for $\phi_0 = \epsilon - \pi/2$. The change in ϕ_0 does not change the value of $I_{CHSH}^{(AB)}$: this corresponds to a measurement that keeps the disturbance on the state fixed with a varying information gained on it.

The achievement of double violation and the realization of a simple weak measurement scheme have important applications for Quantum Random Number Generation QRNG, as demonstrated in [45], or for Quantum Key Distribution exploiting weak measurements [46]. In [45], for instance, it was shown that, by using sequences of weak measurements to violate a multi-user Bell inequality, it is possible to certify any amount of random bits from a pair of pure entangled qubits.

Appendices

A

QUANTUM INFORMATION THEORY

Information theory is the science that studies the transmission, processing, utilization, and extraction of information. Since its birth, dating back to the 1948 article "A Mathematical Theory of Communication" by Claude E. Shannon, information theory is the theoretical framework upon which large part of our technology is built. Information is strongly related to the physical system used to store it, as stated by Rolf Landauer in his famous sentence *"Information is physical"* [47].

In classical information theory, the information is carried by systems obeying the laws of classical physics. The state of a general system is described by a point in its phase space, while its evolution is described by the Hamiltonian of the system. There are two main ways of storing the information in a classical system: using an analog degree of freedom, such as the amplitude or the phase of an electromagnetic wave, or a digital one, by assigning different values to different, finite regions of the phase space. Nowadays, digital systems are dominant in general-purpose information transmission and processing, with analog ones playing a minor role. The key element of a digital system is the *bit* (*bi*nary digi*t*), which can assume the values 0 or 1. Each value is represented by a different region of the phase space and the separation between the two regions is such that a noise-induced bit switch is very unlikely.
At the beginning of the 20th century, however, classical physics has shown to be inadequate to describe systems at very small scale. For such systems, there is a fundamental limitation in the knowledge of the different measurable properties of a system, embodied by the *uncertainty principle*. Therefore, it is no longer possible to assign to a system a single point in the phase space, making classical physics inadequate to describe it. This led to the development of a new model for the description of physical systems: *quantum mechanics*. For this reason, the information stored in systems that cannot be described by classical physics can no longer be described using classical information theory, but requires the development of a new framework, *quantum information theory*.

In this chapter, quantum mechanics will be shortly introduced from an axiomatic point of view, I will then give a short introduction of quantum information.

A.1 QUANTUM MECHANICS

The fundamental difference between classical and quantum mechanics lies in the impossibility of knowing with arbitrary precision all the measurable properties of a physical system. Therefore, it is no longer possible to define a state by assigning a definite value to its measurable properties (e.g. position and momentum). This

requires the construction of a new theoretical framework for the description of physical systems. Among the different formulations of quantum mechanics, the axiomatic one introduced by Dirac and Von Neumann is the most widely used in quantum information. It is based on a series of postulates, listed here below [48, 49].

Postulate 1 ***States.*** *A state is the complete description of an physical system. The state of an isolated physical system can be described by a normalized vector $|\psi\rangle$, unique up to a phase factor, in a projective complex Hilbert space $\mathscr{H}$.*

Postulate 2 ***Composition.*** *If the state of a system A is in $\mathscr{H}_A$ and the state of a system B is in $\mathscr{H}_B$, the state of the composite system AB is in the tensor product $\mathscr{H}_A \otimes \mathscr{H}_B$. If system A is in the state $|\psi\rangle_A$ and system B is in $|\psi\rangle_B$, then the composite system state is in $|\psi\rangle_A \otimes |\psi\rangle_B$.*

Postulate 3 ***Dynamics.*** *The dynamics describes the evolution of a state over time. For any possible evolution of a closed physical system with state in $\mathscr{H}$ and for any fixed time interval $[t_0, t_1]$, there exists a unitary $U(t_0, t_1)$ describing it. A system in state $|\psi(t_0)\rangle$ evolves into $|\psi(t_1)\rangle = U|\psi(t_0)\rangle$. The unitary $U(t_0, t_1)$ is unique up to a phase factor and its form is determined by the Schrödinger equation*

$$\frac{d}{dt}|\psi(t)\rangle = -iH(t)|\psi(t)\rangle$$

where H is the Hamiltonian of the system.

Postulate 4 ***Observables.*** *An observable is a property of a physical system that in principle can be measured. All observables are represented by self-adjoint linear operators acting on $\mathscr{H}$. The possible values that an observables O can assume are the eigenvalues x of the correspondent operator. Since O is self-adjoint, it takes the form $O = \sum_x x\Pi_x$, where Π_x is the projector onto the subspace with eigenvalue x.*

Postulate 5 ***Measurements.*** *Measurement is the process of acquiring information about a measurable property of a system. If the state just prior to the measurement is $|\psi\rangle$, then the probability of observing outcome x is*

$$P_X(x) = \mathrm{Tr}\left[\Pi_x |\psi\rangle\langle\psi|\right]$$

If the outcome of the measurement is x, the state $|\phi_x\rangle$ of the system just after the measurement is

$$|\phi_x\rangle = \sqrt{\frac{1}{P_X(x)}}\Pi_x|\psi\rangle$$

A.2 THE DENSITY MATRIX FORMALISM

The formalism described in section A.1 is useful to describe systems that are in a state that is known exactly, (a *pure state*). It can happen, however, that a system is in a statistical ensemble of pure states. In this case, the system is said to be in a *mixed state*. The new formalism, while mathematically equivalent to the former, can be naturally applied to both pure and mixed states[4].

Consider a system that is in one of a number of states $|\psi_i\rangle$, with respective probability p_i. The state of the system is represented by the *density operator*

$$\rho = \sum_i p_i |\psi_i\rangle \langle\psi_i|$$

A pure state $|\phi\rangle$ is described by $\rho = |\phi\rangle \langle\phi|$. Density operators are characterized by $\rho \geqslant 0$ and $\mathrm{Tr}[\rho] = 1$.
Differently than in the classical case, however, it is not possible to uniquely define the states composing the mixture. For example, the equal mixture of $|0\rangle$ and $|1\rangle$, described by the density operator

$$\rho = \frac{1}{2}|0\rangle \langle 0| + \frac{1}{2}|1\rangle \langle 1| = \frac{\mathbb{I}}{2}$$

is not distinguishable from the equal mixture of $|+\rangle$ and $|-\rangle$

$$\rho = \frac{1}{2}|+\rangle \langle +| + \frac{1}{2}|-\rangle \langle -| = \frac{\mathbb{I}}{2}$$

The postulates of Section A.1 can be restated in terms of density operators [4].

Postulate 1 *The state of an isolated physical system is described by a density operator, which is a positive operator ρ with trace one, acting on a complex Hilbert space $\mathscr{H}$.*

Postulate 2 *If a system A is in the mixed state ρ_A and a system B is in ρ_B, the composite system state is $\rho_A \otimes \rho_B$.*

Postulate 3 *The evolution of a closed physical system in the interval $[t_0, t_1]$ is described by an unitary operator $U(t_0, t_1)$. A system in mixed state $\rho(t_0)$ evolves into $\rho(t_1) = U(t_0, t_1)\rho(t_0)U(t_0, t_1)^\dagger$. The Schrödinger equation for density operators is*

$$\frac{d}{dt}\rho(t) = -\frac{i}{\hbar}[H, \rho(t)]$$

with H the Hamiltonian of the system.

Postulate 5 *If the state before the measurement is ρ, then the probability of observing outcome x is*

$$P_X(x) = \mathrm{Tr}[\Pi_x \rho]$$

If the outcome of the measurement is x, the state ρ_x of the system just after the measurement is

$$\rho_x = \frac{1}{P_X(x)}\Pi_x \rho \Pi_x$$

A.2.1 *Subsystems and purification*

The density operator formalism is useful to study the behaviour of the subsystem A of a larger system AB. If the system AB is described by density operator ρ_{AB}, its subsystem A can be described using the *reduced density operator* ρ_A defined as

$$\rho_A \equiv \mathrm{Tr}_B[\rho_{AB}] \tag{A.1}$$

where Tr_B is the partial trace over system B.
Generally, the reduced density operator of an entangled system AB is a mixed state. Moreover, if the system AB is in one of the four Bell states, the reduced density matrix of each subsystem is $\rho_A = \frac{\mathbb{I}}{2}$, thus ruling out the possibility of using entangled states for faster than light communication [48].
On the other hand, given a density operator ρ_A on a system $\mathscr{H}_A$, it is always possible to find a system $\mathscr{H}_E$ such that $\rho_A = \mathrm{Tr}_A[\rho_{AE}]$ and the joint system is in a pure state $|\phi\rangle_{AE} \in \mathscr{H}_A \otimes \mathscr{H}_E$. This procedure is called *purification* [50].

A.2.2 *Generalized measurements*

The projective measurement described by Postulate 5 is not the most general kind of measurement that can be performed on a quantum system [50]. In general, it is possible to make the system $\mathscr{H}_A$ interact with another system $\mathscr{H}_B$, the *ancilla*, which is then measured with a projective measurement. The overall system is described by $\mathscr{H}_A \otimes \mathscr{H}_B$, and the interaction is represented by the unitary operator U. Before the measurement take place, the ancilla and the system are independent, so their state can be described by $\rho_A \otimes \rho_B$, and the ancilla can be prepared in a pure state $\rho_B = |\phi_B\rangle\langle\phi_B|$ (this is always possible by taking a large enough ancilla system because of purification). We can obtain information about the system by measuring the observable X on the ancilla. From Postulate 5, the probability of obtaining x from the measurement is

$$P_X(x) = \mathrm{Tr}_{AB}\left[(\mathbb{I} \otimes \Pi_x)\left(U\rho_A \otimes \rho_B U^\dagger\right)\right]$$

By taking the partial trace over system B, it is possible to write this procedure from the point of view of system A, obtaining

$$P_X(x) = \mathrm{Tr}_A\left[\rho_A \Lambda_x\right],$$

where ρ_A is the reduced density operator of system A and $\{\Lambda_x\}$ is a set of operators on $\mathscr{H}_A$ such that

- Λ_x is self-adjoint,
- Λ_x is non-negative,
- $\sum_x \Lambda_x = \mathbb{I}$.

A generalized measurement described by such set of operators is called *positive-operator valued measurement* (POVM). It can also be demonstrated that any group of operators meeting these requirements corresponds to a generalized measurement (Neumark/Naimark Theorem [48, 50]), therefore can be expressed using the formalism of Postulates 4 and 5 using a large enough ancilla system.

A.3 THE CIRCUIT MODEL

The mathematical framework at the basis of digital information processing is Boolean algebra, which can be used to describe all possible functions from n-bit into m-bit systems. This computational framework can be represented using the *circuit model* [4], which is based on *gates*, that implement logical functions $f : \{0,1\}^n \to \{0,1\}^m$, and *wires*, that connect different gates and provide the circuit with its inputs and

outputs. A general gate can be substituted by a network of simpler ones. It has been demonstrated, indeed, that all logical functions can be implemented by using just a finite set of 1-to-1 and 2-to-1 logical gates [4]. A similar information processing model can be introduced also in the quantum case. Similarly to the classical case, the basic computational quantum unit is called *quantum gate*. Postulate 3 restricts quantum gates to unitary operations from n-qubit into n-qubit systems. Quantum gates are linked together using *wires*, representing an ideal system that transmits a quantum state from one side to the other. The possibility of entanglement between different qubits, however, makes it impossible to assign a precise value to the state in each wire, requiring a collective description of the state at the different steps of the circuit. While the most general description of quantum circuits should require the use of the density matrix formalism and a more comprehensive model of quantum dynamics to take into account open system evolution (using complete positive trace-preserving linear transformation [51]), it is still possible to apply purification to reduce them to a system of pure-state qubits and unitary quantum gates [52]. It is therefore possible to study quantum circuits using the formalism introduced in Section A.1.

A.3.1 *Quantum wires*

The wire is the simplest component of a quantum circuit (this does not mean that it is simple to implement it physically, though). It is a system that transfers a qubit from one end to the other one and is used to connect gates or to provide input or output to the circuit. Qubit wires will be represented by a single straight line as in figure A.1.

Figure A.1.: Simple representation of a qubit wire.

A.3.2 *Quantum gates*

Quantum gates are unitary operations acting on quantum state-vectors [51]. In general, they act on n-qubit systems and can be represented, in matrix form, as a $2^n \times 2^n$ matrix. Among all possible quantum gates, however, just a small set of one- and two-qubit gates is necessary to approximate with arbitrary accuracy any possible unitary operation. This set is said to be *universal for quantum computation* [4].

Single-qubit gates

Single-qubit gates are represented by 2×2 unitary matrices in the computational basis. The circuit representation of single-qubit gates is shown in Figure A.2, with the letter identifying the gate (A stands for *arbitrary gate*).

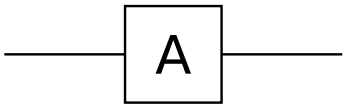

Figure A.2.: An arbitrary single-qubit gate.

An important set of single-qubit gates is represented by *Pauli gates*, whose matrix representation in the computational basis are

$$\sigma_x = \begin{pmatrix} 0 & 1 \\ 1 & 0 \end{pmatrix} \tag{A.2}$$

$$\sigma_y = \begin{pmatrix} 0 & -i \\ i & 0 \end{pmatrix} \tag{A.3}$$

$$\sigma_z = \begin{pmatrix} 1 & 0 \\ 0 & -1 \end{pmatrix} \tag{A.4}$$

Pauli matrices are strongly related to the Bloch sphere representation by the fact that the point in the sphere associated to a state $|\psi\rangle$ is the one whose coordinates are the expectation values of the Pauli operators $(\langle\psi|\sigma_x|\psi\rangle, \langle\psi|\sigma_y|\psi\rangle, \langle\psi|\sigma_z|\psi\rangle)$ [51]. In particular, the axes $\{X, Y, Z\}$ of the Bloch sphere correspond to the eigenvectors of the Pauli gates $\{\sigma_x, \sigma_y, \sigma_z\}$.
Another useful gate is the *Hadamard gate*, described by the matrix

$$H = \frac{1}{\sqrt{2}} \begin{pmatrix} 1 & 1 \\ 1 & -1 \end{pmatrix} \tag{A.5}$$

that transforms the computational basis $\{|0\rangle, |1\rangle\}$ into the diagonal one $\{|+\rangle, |-\rangle\}$ and vice-versa.
The *rotation gates*, that rotate the qubit about a corresponding axis of the Bloch sphere by an angle θ, are described by

$$R_x(\theta) = \begin{pmatrix} \cos\frac{\theta}{2} & -i\sin\frac{\theta}{2} \\ -i\sin\frac{\theta}{2} & \cos\frac{\theta}{2} \end{pmatrix} \tag{A.6}$$

$$R_y(\theta) = \begin{pmatrix} \cos\frac{\theta}{2} & -\sin\frac{\theta}{2} \\ \sin\frac{\theta}{2} & \cos\frac{\theta}{2} \end{pmatrix} \tag{A.7}$$

$$R_z(\theta) = \begin{pmatrix} e^{-i\frac{\theta}{2}} & 0 \\ 0 & e^{i\frac{\theta}{2}} \end{pmatrix} \tag{A.8}$$

The rotation about the z axis shifts the qubit phase of an angle θ and can be used to construct the *phase gate*

$$S = \begin{pmatrix} 1 & 0 \\ 0 & i \end{pmatrix}, \tag{A.9}$$

and the "$\frac{\pi}{8}$" *gate*

$$T = \begin{pmatrix} 1 & 0 \\ 0 & e^{i\frac{\pi}{4}} \end{pmatrix}. \tag{A.10}$$

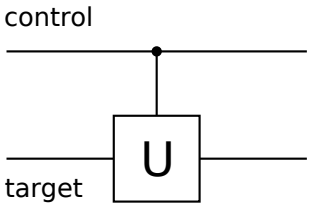

Figure A.3.: Controlled-U operation. The unitary U is applied to the target qubit only if the control qubit is in $|1\rangle$.

Two-qubit gates

The most important class of two-qubit gates is the one of *controlled operations*, shown in Figure A.3. They have two inputs, the *target* and the *control* bit, and perform the unitary operation U on the target qubit only if the control is in $|1\rangle$. An important controlled gate is the *CNOT gate*, with matrix

$$\mathrm{CNOT} = \begin{pmatrix} 1 & 0 & 0 & 0 \\ 0 & 1 & 0 & 0 \\ 0 & 0 & 0 & 1 \\ 0 & 0 & 1 & 0 \end{pmatrix} \tag{A.11}$$

in the two-qubit computational basis. The set formed by single-qubit gates and the CNOT gate is universal for quantum computation [4].
Another important controlled gate, that is used in our work, is the *controlled-phase-shift gate*, that implements a rotation around the z axis of the Bloch sphere of the target qubit conditioned on the value of the control qubit. It is described by the matrix

$$\mathrm{CP}(\epsilon) = \begin{pmatrix} 1 & 0 & 0 & 0 \\ 0 & 1 & 0 & 0 \\ 0 & 0 & e^{i\epsilon} & 0 \\ 0 & 0 & 0 & e^{-i\epsilon} \end{pmatrix} \tag{A.12}$$

A.3.3 *Measurement*

In general, the only way to get information about a physical system is through measurements. While the most general description of a measurement on a system is given by a POVM, the Neumark/Naimark theorem allows us to see it as a projective measurement on an ancilla subsystem. Moreover, projective measurements on an arbitrary basis are equivalent to a unitary transformation followed by a projective measurement on the computational basis. In the circuit model, a measurement in the computational basis is represented as in Figure A.4.

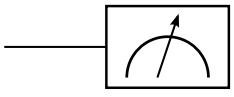

Figure A.4.: Projective measurement in the computational basis.

B

ELEMENTS OF CLASSIC OPTICS

Optics is the branch of physics that describes the phenomena associated to the propagation of light. Classical electrodynamics and the modern quantum theories provide an explanation for all the fundamental aspects of light propagation and interaction with matter. In this appendix we will focus on few aspects of optics, in particularly only on those that deal closely with our work. We will in particular face the following arguments:

- how to derive of electromagnetic wave equation from the Maxwell set of equations;
- we will discuss optical interference, one of the most characteristic traits of optics in general, that is a very powerful tool intensively exploited in a vast class of applications that require a high-precision measure (included this work);
- we will present the *gaussian beam* that is a particularly important solution of the wave equation because it is the beam produced by the common laser oscillators;
- finally we will introduce Lasers, the most important tool of modern experiments involving classical or quantum optics.

B.1 ELECTROMAGNETIC WAVES

Light is an electromagnetic field described by two related vectors fields that are real functions of position and time: the electric field $E(\mathbf{r}, t)$ and the magnetic field $B(\mathbf{r}, t)$. At the foundation of classic electrodynamic lies the Maxwell's equations that in vacuum and in the absence of sources read:

$$\nabla \cdot E(\mathbf{r}, t) = 0 \tag{B.1}$$

$$\nabla \cdot B(\mathbf{r}, t) = 0 \tag{B.2}$$

$$\nabla \times E(\mathbf{r}, t) = -\frac{\partial B(\mathbf{r}, t)}{\partial t} \tag{B.3}$$

$$\nabla \times B(\mathbf{r}, t) = \epsilon_0 \mu_0 \frac{\partial E(\mathbf{r}, t)}{\partial t} \tag{B.4}$$

Handling these equations one finds that the coupled electric and magnetic fields satisfy the wave equations:

$$\left(\frac{1}{c^2} \frac{\partial^2}{\partial t^2} - \nabla^2 \right) \mathbf{E} = 0 \tag{B.5}$$

$$\left(\frac{1}{c^2} \frac{\partial^2}{\partial t^2} - \nabla^2 \right) \mathbf{B} = 0 \tag{B.6}$$

where $c = \frac{1}{\sqrt{\epsilon_0 \mu_0}} = 3 \times 10^8 \frac{m}{s}$ is the speed of light in the vacuum. Since the common detectors are usually sensitive to the electric rather then the magnetic field, in the following we will discuss only the field $\mathbf{E}(\mathbf{r}, t)$. We also assume that the field is polarized along a fixed direction given by a unit real constant vector $\mathbf{u}$ such that $\mathbf{E}(\mathbf{r}, t) = u(\mathbf{r}, t)\mathbf{u}$ and we can use the scalar description of light waves given by the real classical wavefunction $u(\mathbf{r}, t)$ to simplify the treatment. Due to equation (B.5) the wave function satisfies the wave equation:

$$\left(\frac{1}{c^2} \frac{\partial^2}{\partial t^2} - \nabla^2 \right) u(\mathbf{r}, t) = 0 \tag{B.7}$$

This equation is linear and so the *principle of superposition* applies: given two or more solutions of the wave equation, also their sum is a solution of the same wave equation.

The wave equation takes a simpler form if the wave is monochromatic, i.e., its wavefunction has harmonic time dependence:

$$u(\mathbf{r}, t) = a(\mathbf{r}) \cos\left(\varphi(\mathbf{r}) + \omega t\right)$$

where $a(\mathbf{r})$ is a positive real function that describes wave amplitude, $\varphi(\mathbf{r})$ is a real function describing the *phase* of the field and ω is the angular frequency (related to the frequency ν by $\omega = 2\pi\nu$). In the classical treatment it is common to represent the real wavefunction $u(\mathbf{r}, t)$ of a monochromatic wave in terms of a complex function

$$U(\mathbf{r}, t) = a(\mathbf{r}) e^{i\varphi(\mathbf{r})} e^{i\omega t} \tag{B.8}$$

so that

$$u(\mathbf{r}, t) = \mathrm{Re}\left[U(\mathbf{r}, t)\right]$$

We can write also

$$U(\mathbf{r}, t) = U(\mathbf{r}) e^{i\omega t} \tag{B.9}$$

defining the *complex amplitude* $U(\mathbf{r}) \equiv a(\mathbf{r}) e^{i\varphi(\mathbf{r})}$, whose magnitude $|U(\mathbf{r})| = a(\mathbf{r})$ is the amplitude of the wave. Inserting (B.9) into the wave equation (B.7) we get the *Helmholtz equation*

$$\nabla^2 U(\mathbf{r}) + k^2 U(\mathbf{r}) = 0 \tag{B.10}$$

where

$$k \equiv \omega / c \tag{B.11}$$

is called the *wavenumber*.

The *optical intensity* of a classical monochromatic wave is defined as the square modulus of its complex wavefunction mediated over a whole period of its frequency

$$I(\mathbf{r}) = |U(\mathbf{r})|^2 \tag{B.12}$$

and for a monochromatic wave it does not vary with time.

The simplest example of solution for the Helmholtz equation (B.10) is the *plane wave*

$$U(\mathbf{r}) = A e^{-i\mathbf{k}\cdot\mathbf{r}}$$

where A is a complex constant and $\mathbf{k}$ is a real three-dimensional vector, called *wavevector*, that gives the direction of propagation. $\mathbf{k}$ magnitude depends on the wave frequency by equation B.11. This solution is called *plane wave* because the surfaces of constant phase, called *wavefronts*, describe parallel planes perpendicular to the wavevector $\mathbf{k}$ separated by the *wavelength*:

$$\lambda = \frac{2\pi}{k} = \frac{c}{\nu}$$

B.2 INTERFEROMETRY

Let's consider now two monochromatic EM waves described (using the same complex wave function description introduced in the previous section) by two functions $U_1(\mathbf{r})$ and $U_2(\mathbf{r})$. The optical intensity of the two wave function considered separately are clearly (eq. B.12) $I_{1,2} = |U_{1,2}(\mathbf{r})|^2$. The total optical field, for the superposition principle, will obviously be $U(\mathbf{r}) = U_1(\mathbf{r}) + U_2(\mathbf{r})$, and its intensity will read:

$$\begin{aligned} I(\mathbf{r}) &= |U(\mathbf{r})|^2 = |U_1(\mathbf{r}) + U_2(\mathbf{r})|^2 \\ &= |U_1(\mathbf{r})|^2 + |U_2(\mathbf{r})|^2 + U_1^*(\mathbf{r})U_2(\mathbf{r}) + U_1(\mathbf{r})U_2^*(\mathbf{r}) \end{aligned}$$

Expressing the field functions in term of phasors $\phi(\mathbf{r})$ as $U_i(\mathbf{r}) = \sqrt{I_i}e^{i\phi_i(\mathbf{r})}$, the intensity of the total field reads:

$$I = I_1 + I_2 + 2\sqrt{I_1 + I_2}\cos\phi(\mathbf{r}) \qquad \text{with} \qquad \phi = \phi_2 - \phi_1 \tag{B.13}$$

This is a fundamental relation in interferometry, that shows how the intensity of the sum of two optical fields depends both on the field intensity I_1 and I_2 and on the phase difference between the two fields ϕ. The last term in equation B.13 is due to the wave nature of the optic field, and modulates the total field intensity according to the phase difference ϕ. When the interference term is positive the interference is said to be *constructive*, while when the interference term is negative the interference is said to be *destructive*.

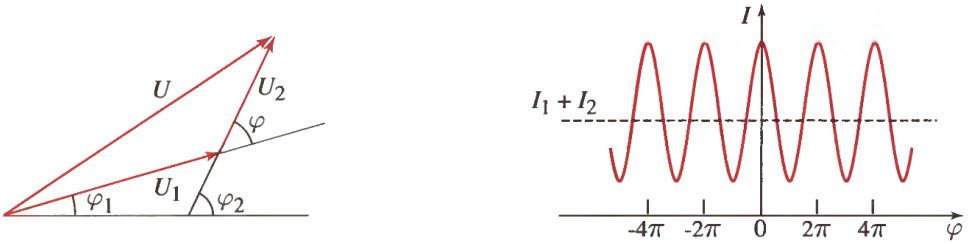

Figure B.1.: (**Left**) Phasor diagram for the superposition of two waves of intensities I_1 and I_2 and phase difference $\phi = \phi_2 - \phi_1$. **Right** dependence of the total intensity I on the phase difference ϕ. [35]

Let's consider now the case $I_0 = I_1 = I_2$. In this case $I = 2I_0(1 + \cos\phi) = 4I_0\cos^2(\phi/2)$, and we have:

$\phi = 0$ in this case we have that $I = 4I_0$, that is the condition of optimal constructive interference (the total intensity is four times greater than the intensity of the two initial fields);

$\phi = \pi$ in this case we have $I = 0$, the two waves erase each other, this is the condition of maximum destructive interference;

$\phi = \frac{\pi}{2}, \frac{3\pi}{2}$ in this case we have $I = I_1 + I_2$ the interference term vanish, and the total intensity is given by the sum of the two original fields.

The main idea of interferometry is to obtain information about the phase difference between two optical fields measuring the intensity of their interference. The phase difference between two optical beams propagating along two different paths is in general given by $\phi = 2\pi n_2 z_2/\lambda_0 - 2\pi n_1 z_1/\lambda_0$, where n_1 and n_2 are the refraction indexes of the medium encountered by the two beams, and z_1 and z_2 are the length of the two paths. From the equation it is clear that both path length and refraction index difference differences can introduce a phase difference. In general the product between n_i and z_i is an interesting quantity in optics an it is called *Optical Path Length* (OPL).

An *interferometer* is an optical instrument that splits a wave into two using a beam-splitter, delays them by unequal distances, redirects them using mirrors, recombines them using another (or the same) beamsplitter, and detects the intensity of their superposition. Depending on the specific configuration an interferometer can be used to measure small distance variation, refraction index variation, wavelength variation or can be used to manipulate the interference between two EW waves.

B.3 GAUSSIAN BEAMS

In the previous section, we introduced classical electrodynamics and the plane wave equation as the simplest solution to the Maxwell equations. Another simple solution to equation B.5 is the *spherical wave* described by the equation $U(\mathbf{r}) = \frac{A_0}{r} e^{-ikr}$. These two solutions represent the two opposed extreme of the wave collimation and localization. While the plane wave has a source that is spread all over the available space with plane wavefronts that propagates in a well defined direction, the spherical wave has a completely localized source with curved wavefronts that propagates in all the directions. Experimentally we are interested in a solution that combines both localization and collimation, i.e., that propagates along a fairly defined direction and that is space-confined.

A class of solution of this kind are the *paraxial waves*, that are solution to the wave equation with paraxial wavefronts, i.e., with wavefronts that make a small angle with the propagation direction. One way to construct a paraxial wave is to take a plane wave Ae^{-ikz} propagating in the z direction and modify its *complex envelope* A making it a slowly varying function of position, i.e., $A \to A(\mathbf{r})$, so the complex amplitude becomes:

$$U(\mathbf{r}) = A(\mathbf{r}) e^{-ikz} \tag{B.14}$$

The envelope must be approximately constant within a neighborhood of size $\lambda = 2\pi/k$ to have a wave that is locally like a plane wave with paraxial wavefront normals.

The complex amplitude (B.14) must satisfies the Helmholtz equation (B.10) and this implies that the envelope $A(\mathbf{r})$ respects the *paraxial Helmholtz equation* [35]:

$$\nabla_T^2 A(\mathbf{r}) - 2ik \frac{\partial A(\mathbf{r})}{\partial z} = 0 \tag{B.15}$$

where $\nabla_T^2 = \partial^2/\partial x^2 + \partial^2/\partial y^2$ is the transverse part of the Laplacian operator.

The simplest solution of equation (B.15) is given by the *paraboloidal wave*

$$A(\mathbf{r}) = \frac{A_1}{z} e^{-ik\frac{\rho^2}{2z}} \tag{B.16}$$

where

$$\rho^2 = x^2 + y^2$$

and A_1 is a complex constant. This wave is the paraxial approximation of the spherical wave if $\rho = \sqrt{x^2 + y^2} \ll z$.

The *Gaussian beam* is another solution of the paraxial Helmholtz equation obtained from (B.16) with a transformation of the z coordinate. Replacing z with $q(z) \equiv z + iz_0$, where z_0 is a real parameter called *Rayleigh range*, we get a shifted version of the paraboloidal wave in the form

$$A(\mathbf{r}) = \frac{A_0}{q(z)} e^{-ik\frac{\rho^2}{2q(z)}} \tag{B.17}$$

that is also a solution of (B.15).

We can define two real function $R(z)$ and $W(z)$ such that

$$\frac{1}{q(z)} = \frac{1}{R(z)} - i\frac{\lambda}{\pi W^2(z)}$$

and substitute (B.17) in (B.14) to obtain the *Gaussian beam complex amplitude*

$$U(\mathbf{r}) = \frac{A_0}{iz_0}\frac{W_0}{W(z)} e^{-\frac{\rho^2}{W^2(z)}} e^{-i\left[kz + k\frac{\rho^2}{2R(z)} - \zeta(z)\right]} \tag{B.18}$$

where

$$W(z) = W_0\sqrt{1 + \left(\frac{z}{z_0}\right)^2}$$

$$R(z) = z\left[1 + \left(\frac{z_0}{z}\right)^2\right]$$

$$\zeta(z) = \tan^{-1}\left(\frac{z}{z_0}\right)$$

and W_0 is related to the Rayleigh range z_0 by

$$\pi W_0^2 = \lambda z_0$$

The expression (B.18) is the most important result of this section. It shows that the *gaussian beam* is characterized by the two parameter A_0 and z_0 which are determined from the boundary conditions of the wave equation, while all the other parameters are related to the Rayleigh range z_0 and to the wavelength λ.

As stated at the beginning of this chapter *gaussian beams* play a fundamental role in optics because they describe the output of most lasers. Equation B.18 describes an EM field whose transverse amplitude profiles are given by a gaussian functions with waist $W(z)$ (the waist, $W(z)$, is the radius at which the field amplitude fall to $1/e$ of its axial value) dependent only on the relative position z along the beam propagation direction. From the EM transverse profile shape follows that also the EM intensity (irradiance) is described by a gaussian profile (this is the reason *gaussian beams* are so called).

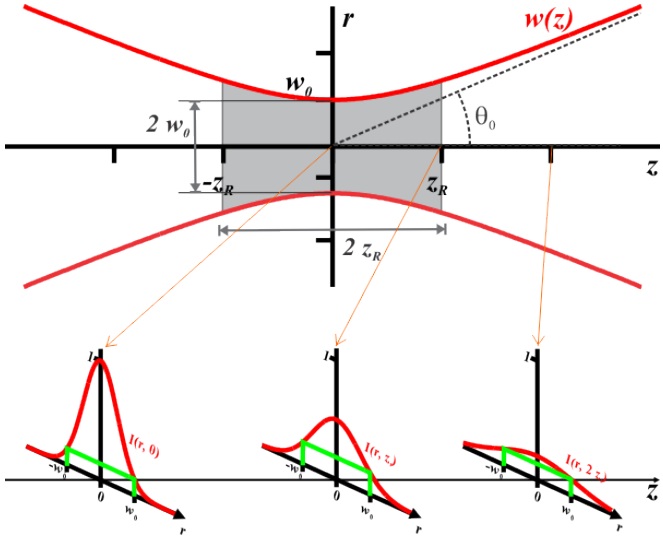

Figure B.2.: Gaussian beam example

B.4 LASERS

The laser is the fundamental tool of modern optics laboratories and, of course, of our experiment. The acronym laser stands for *Light Amplification by Stimulated Emission of Radiation* and it was invented in the 1960s. A laser is an optical system composed by two different parts: a gain medium (or optical amplifier) and something to provide optical feedback.

The gain medium is a material with properties that allow it to amplify light by way of stimulated emission. Light of a specific wavelength that passes through the gain medium is amplified.

The optical feedback is something that "folds back on itself" the optical field, allowing for the creation of a stable EM wave. The most common type of laser uses an optical cavity (a pair of mirrors on either end of the gain medium that trap the light) as optical feedback. We wont deal with here with the optical cavity characteristics and functioning.

In this section we present briefly the physical principles of laser operation, focusing mainly on the optical amplification process.

B.4.1 *Stimulated emission and Einstein's coefficient*

The quantum atomic theory predicts that light is emitted or absorbed whenever an electron in an atom makes a jump between two quantum levels, as shown in figure B.3. Due to conservation of energy, the angular frequency ω of the light must be around the value ω_0 fixed by

$$\hbar\omega_0 = E_2 - E_1$$

where E_2 and E_1 are respectively the energies of the upper and the lower level of the electron.

The radiative process by which an electron in a lower level is promoted to an upper level by absorbing the required energy from the incoming field is called *absorption*.

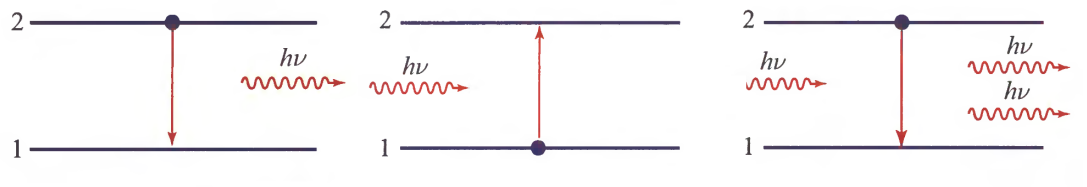

Figure B.3.: Mechanisms of atomic transition. (**Left**) Spontaneous emission. (**Center**) absorption. (**Right**) Stimulated emission. [35]

The process by which an electron in an upper level drops to a lower level is called *emission* and can be of two types: *spontaneous*, because the electron in the excited state has a natural tendency to de-excite and lose its excess energy, or *stimulated*, when the incoming field stimulates the downward emission.

It is fundamental to notice that the photons emitted by *stimulated emission* have exactly the same direction and phase of the incoming stimulating photon. The produced couple of photon is therefore perfectly coherent, and the optical fields turn out to be amplified.

The key idea is to prepare the system in a condition with a lot of excited atoms, so that when the EM field interacts with it, the EM field receives a substantial amplification. Photons produced by *spontaneous emission* don't contribute to the field amplification as they are produced with random direction in an incoherent way resulting useless for the amplification.

The rules that govern the three processes above mentioned are described by quantum electrodynamics, but can be found also following an intuitive two-level treatment proposed by Einstein in 1916 [53]. Suppose there are N_1 (N_2) atoms per unit volume occupying respectively the two energy states E_1 (E_2), with $E_1 < E_2$. The absorption rate is proportional to N_1 and to the density of photons $W(\nu)$ with the appropriate energy $\nu = \frac{E_2 - E_1}{h}$:

$$\left(\frac{dN_2}{dt}\right)_{ab} = B_{12} N_1 W(\nu)$$

Similarly, the stimulated emission rate will be:

$$\left(\frac{dN_2}{dt}\right)_{ab} = -B_{21} N_2 W(\nu)$$

Spontaneous emission rate will be dependent on N_2 but independent by $W(\nu)$:

$$\left(\frac{dN_2}{dt}\right)_{sp} = -A_{21} N_2$$

The three coefficients B_{12}, B_{21} and A_{21} are called Einstein coefficient.

At equilibrium the three processes balance each other and it is straightforward to obtain the relation:

$$W(\nu) = \frac{A_{21} N_2}{B_{12} N_1 - B_{21} N_2} \tag{B.19}$$

Clearly the three coefficients will depend on the specific atom considered but should be independent from the radiation. Supposing now that the system is at thermal equilibrium, the EM spectrum $W(\nu)$ will be the black body one:

$$W(\nu) = 8\pi h \nu^3 \left(\frac{n}{c}\right)^3 \cdot \frac{1}{e^{\beta h \nu} - 1} \tag{B.20}$$

where $\beta = \frac{1}{k_b T}$. The atom distribution over the available states will governed by the Boltzmann distribution:

$$N_1 = N_2 \frac{g_1}{g_2} e^{(\beta h\nu)} \tag{B.21}$$

where $\frac{g_1}{g_2}$ takes into account possible degeneracies of the energetic levels. Inserting equation B.21 into B.19 we find:

$$W(\nu) = A_{21} \cdot \frac{1}{B_{12} \frac{g_1}{g_2} e^{(\beta h\nu)} - B_{21}} \tag{B.22}$$

If we want equation B.22 to be in agreement with equation B.20 we must set:

$$g_1 B_{12} = g_2 B21$$

$$A_{21} = 8\pi h\nu^3 \left(\frac{n}{c}\right)^3 B_{21}$$

We are interested in the ratio between the spontaneous and stimulated emission rate at the equilibrium, from the above equations we obtain:

$$\frac{(dN_2/dt)_{st}}{(dN_2/dt)_{sp}} = \frac{1}{e^{\beta h\nu} - 1}$$

realizing that at ambient temperatures, the spontaneous emission is the predominant effect compared to stimulated emission.

B.4.2 *Population inversion*

To invert the equilibrium behaviour of the considered systems the *population inversion* is practised. Population inversion consist in pushing the system to a condition where there are more atoms in the excited state than in the ground state. This increase the stimulated emission rate and transforms the considered system into a *gain medium*.

When population inversion is achieved the amount of stimulated emission due to light that passes through is larger than the amount of absorption and spontaneous emission. Hence, the light is amplified (see figure B.4 for a schematic representation of the pumping process). By itself, this makes an optical amplifier. When an optical

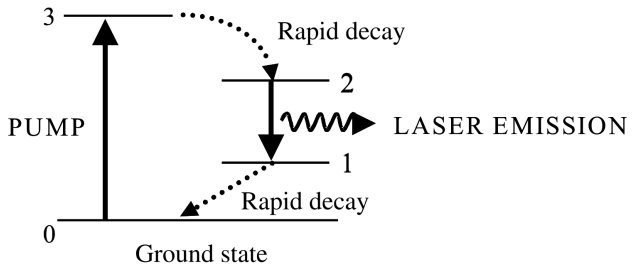

Figure B.4.: Example of a four-level pumping system used to achieve population inversion in the active medium. [54]

amplifier is placed inside a resonant optical cavity, one obtains a laser oscillator.

The presence of the cavity has a double effect on the radiation: it allows for amplification and it forces for a quantization of the EM field inside the cavity. Only the

EM frequencies allowed by the optical cavity geometry will be amplified. Hence by tuning the cavity geometry is possible to choose the laser beam shape and the laser beam frequency. See figure B.5 for a simple representation of a resonant optical cavity.

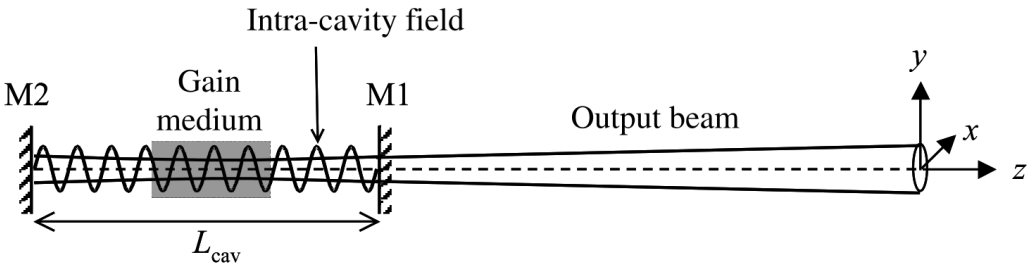

Figure B.5.: Sketch of a laser optical cavity. In figure the gain medium, the optical cavity ant the produced laser beam are visible. [54]

We have so far outlined the basic functioning principles of a laser, the minimum necessary for a generic comprehension of these instruments. We suggest to refer to [35] [54] for further information on the argument.

C

ELEMENTS OF QUANTUM OPTICS

As stated at the beginning of appendix A, since quantum information is built upon objects that obey the rules of quantum mechanics, to investigate such subject we need to employ quantum carriers. Clearly there are many different systems fulfilling this requirement (basically all the small-scale which can be systems described by quantum mechanics), each characterized by its peculiar physical laws, stability and manipulation techniques. One of the key requirement for an information carrier (being it quantum or not) is that it must propagate successfully through long distances without being significantly altered. Among all the possible choice the most suitable physical system (likewise for the classical information transmitting) is the electromagnetic field. Electromagnetic waves in fact can travel for long distances both in vacuum and in transparent mediums such as the air or the glass. Moreover, its low interaction rate with matter makes it very resistant to the noise induced by its coupling with the environment.

In the previous appendix B, we briefly introduced and described some aspects of classical electrodynamics. Classical electrodynamics provides in general an excellent description for all the electromagnetic phenomena whenever the relevant length scales and field strengths are large enough so that quantum mechanical effects are negligible. For small distances and low field strengths, such interactions are better described by quantum electrodynamics.

Electrodynamics itself played a crucial role in the development of quantum mechanics. At the beginning of the 20^{th} century in fact, some of the open questions in physics that pushed scientists to the development of quantum mechanics, had to deal with electromagnetism (black-body radiation, photoelectric effect).

With the development of quantum mechanics, physicist had to rebuild electromagnetism upon a new theoretical framework which required to translate the old description in terms of the classical observables to a new description in terms of operators. Such procedure is called *first quantization* [53]. The new developed theory proved to be very good for the description of non-relativistic quantum systems with a fixed number of particles, but it failed in the description of high energy relativistic systems, where the description in terms of operators must be substituted with a field description. A new procedure for the quantization of field theories, called *second quantization*, was then developed, and such framework lies at the basis of quantum electrodynamics.

The study of quantum electrodynamics, is far beyond the scope of this thesis. In this section will just give a very short introduction to quantum optics, limiting our self to some results needed to provide a photonic implementation of quantum information experiments.

C.1 QUANTIZATION OF THE ELECTROMAGNETIC FIELD

The quantization of electromagnetic field in the vacuum is obtained promoting the classical real field $E(\mathbf{r},t)$ and $B(\mathbf{r},t)$ to hermitian operators $\hat{E}(\mathbf{r},t)$ and $\hat{B}(\mathbf{r},t)$. Likewise we have done for classic optics, in this discussion we will focus only to the electric field.

The field operator $\hat{E}(\mathbf{r},t)$ can be separated into its positive and negative frequency parts:

$$\hat{E}(\mathbf{r},t) = \hat{E}^{(+)}(\mathbf{r},t) + \hat{E}^{(-)}(\mathbf{r},t) \tag{C.1}$$

To ensure that the operator $\hat{E}(\mathbf{r},t)$ is hermitian ($\hat{E}(\mathbf{r},t) = \hat{E}^{\dagger}(\mathbf{r},t)$), $\hat{E}^{(\pm)}(\mathbf{r},t)$ are set to be mutually adjoint:

$$\hat{E}^{(\pm)}(\mathbf{r},t) = \left(\hat{E}^{(\mp)}(\mathbf{r},t)\right)^{\dagger} \tag{C.2}$$

The positive frequency part of any general electromagnetic field $E(\mathbf{r},t)$ can be expanded in terms of an orthonormal set of mode functions $\{U_k(\mathbf{r})\}$ as:

$$E^{(+)}(\mathbf{r},t) = \sum_k A_k U_k(\mathbf{r}) e^{-i\omega_k t}$$
$$\text{with} \qquad \int_V U_k^*(\mathbf{r}) U_l(\mathbf{r}) d^3r = \delta_{kl}$$

where $\{A_k\}$ is the set of complex constants that represent the Fourier amplitudes of the field $E^{(+)}(\mathbf{r},t)$.

Similarly, the operator $\hat{E}(\mathbf{r},t)$, can be expanded in terms of a set of mode function, but this time the coefficients $\{A_k\}$ must be replaced by *quantum mechanical mode operators* ($\{\hat{a}_k\}$) that are normalized to have:

$$\hat{E}^{(+)}(\mathbf{r},t) = i\sum_k \sqrt{\frac{\hbar\omega_k}{2}}\hat{a}_k u_k(\mathbf{r}) e^{-i\omega_k t}$$

The operators $\{\hat{a}_k\}$ and their adjoints $\{\hat{a}_k^{\dagger}\}$ satisfy the *canonical commutation relations*:

$$\left[\hat{a}_k, \hat{a}_l^{\dagger}\right] = \delta_{kl} \tag{C.3}$$
$$\left[a_k, a_l\right] = \left[\hat{a}_k^{\dagger}, \hat{a}_l^{\dagger}\right] = 0 \tag{C.4}$$

These relations are the familiar algebraic relations used for the simple harmonic oscillator and so they define the amplitude operators for an infinite set of oscillators, one for each mode of the field. The Hamiltonian operator for the quantized electromagnetic field can be written in the form:

$$\hat{H} = \sum_k \hbar\omega_k \hat{a}_k^{\dagger}\hat{a}_k + constant \tag{C.5}$$

and so it is evident that the electromagnetic field in the vacuum is so equivalent in its dynamical properties to an infinite sequence of harmonic oscillators. The product

$$\hat{n}_k \equiv \hat{a}_k^{\dagger}\hat{a}_k \tag{C.6}$$

defines the *number operator* for the k-th mode. This operator has eigenvalues $n_k = 0, 1, 2, \ldots$ and eigenstates $|n_k\rangle$ and represents the *number of photons* in the k-th mode. The operators $\hat{a}_k$ and $\hat{a}_k^\dagger$ act in the Fock space, i.e. the infinite dimensional Hilbert space of "number representation" where a generic state with n_{k_1} photons in the mode k_1, n_{k_2} photons in the mode k_2 and so on has the form

$$|n_{k_1} n_{k_2} \cdots\rangle \equiv |n_{k_1}\rangle \otimes |n_{k_2}\rangle \otimes \cdots \tag{C.7}$$

The operators $\hat{a}_k^\dagger$ and $\hat{a}_k$ are called creation and annihilation operators because they respectively create and destroy one photon in the k-th mode, i.e.

$$\hat{a}_k^\dagger |\cdots n_k \cdots\rangle = \sqrt{n_k + 1}\, |\cdots n_k + 1 \cdots\rangle \tag{C.8}$$

$$\hat{a}_k |\cdots n_k \cdots\rangle = \sqrt{n_k}\, |\cdots n_k - 1 \cdots\rangle \tag{C.9}$$

The ground state of the electromagnetic field is the *vacuum state* where there are no photons

$$|\text{vac}\rangle \equiv |\{0_k\}\rangle \tag{C.10}$$

Applying each one of the annihilation operators to the vacuum state we obtain

$$\hat{a}_k |\text{vac}\rangle = 0 \tag{C.11}$$

because there are no photons to destroy. We can also generate the quantum state $|\{n_k\}\rangle$ that has $n = \sum_k n_k$ photons by applying the creation operators $\hat{a}_k^\dagger$ to the vacuum state,

$$|\{n_k\}\rangle = \prod_k \frac{\left(\hat{a}_k^\dagger\right)^{n_k}}{\sqrt{n_k!}} |\text{vac}\rangle \tag{C.12}$$

The state vectors $|\{n_k\}\rangle$ for all values of the integers $\{n_k\}$ form a complete orthonormal set and span the whole Fock space.

C.2 INFORMATION ENCODING USING PHOTONS

There exist many different way to encode the information into the degrees of freedom of the electromagnetic field. They are grouped into two different classes, called *continuous variables* and *discrete variables*.

Continuous variables encode the information in the quadratures of a single mode (j, λ) of the electromagnetic field (quadratures are, roughly speaking, the real and the imaginary part of the field operator). While continuous variables play an important role in quantum information, they are out of the scope of this thesis.

The other way to encode quantum information is using discrete variables. It consists of encoding the information into the degrees of freedom of a single photon. The most common encoding scheme implements a qubit using a single photon in two orthogonal modes of the electromagnetic field, a technique called *dual-rail encoding*. The orthogonal modes can be two orthogonal polarizations, two non-overlapping transverse modes or two non-overlapping temporal modes, giving, respectively, *polarization*, *path* or *time-bin* encoding. In this section, *polarization* and *path* encoding schemes, both employed in our work, will be rapidly reviewed.

Polarization encoding

Studying the set of equations B.1 one realizes that electromagnetic waves, travelling in homogeneous isotropic non-attenuating medium, are properly described as transverse waves, meaning that a plane wave's electric field vector **E** and magnetic field **B** are in directions perpendicular to the direction of wave propagation indicated by the wavevector **k**; **E** and **B** are also perpendicular to each other. The electric field

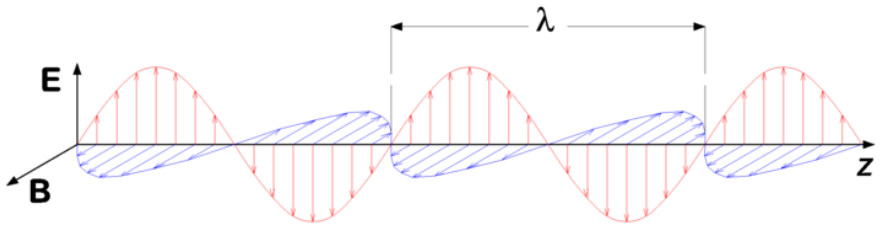

Figure C.1.: A "vertically polarized" electromagnetic wave of wavelength λ has its electric field vector **E** (red) oscillating in the vertical direction. The magnetic field **B** is always at right angles to it (blue), and both are perpendicular to the direction of propagation (**z**). [55]

associated to the electromagnetic wave shown in figure C.1 can be described by a function of the form $\mathbf{E} = \mathbf{e}E_0 e^{i(\mathbf{k}\cdot\mathbf{r}-\omega t+\phi_0)}$, where **e** indicate the direction of the electric field oscillation. Such electric field oscillation **e** is exactly the polarization of the EM wave. In the EM field quantization procedure such field property is inherited by photons (seen as minimum packet size of the electromagnetic field), and it is referred as photon polarization or spin. Polarization, being a two-dimensional mode space, is a perfect property to be used as a computational basis; we can therefore build a polarization encoding scheme where polarization represents a qubit in the two-dimensional complex Hilbert space of a single-mode field[1].

The quantization of the field introduces of a set of *quantum mechanical modes operators* $\left\{\hat{a}_H^\dagger, \hat{a}_H\right\}$ and $\left\{\hat{a}_V^\dagger, \hat{a}_V\right\}$ that act independently on the Fock space of photons with $|H\rangle$ and $|V\rangle$ polarization respectively. The computational basis states can be written as:

$$|0\rangle := \hat{a}_H^\dagger |0,0\rangle_{HV} = |1,0\rangle_{HV} = |H\rangle \tag{C.13}$$

$$|1\rangle := \hat{a}_V^\dagger |0,0\rangle_{HV} = |0,1\rangle_{HV} = |V\rangle \tag{C.14}$$

where $|n_H, n_V\rangle_{HV}$ is the Fock state representation of the polarization of a single-mode field.

Single-qubit gates are easy to implement in the polarization encoding by using wave-plates. Wave-plates are birefringent optical devices made of a birefringent material, characterized by a different refractive index for two orthogonal axes. The material used in most wave-plates is quartz, which is a positive uniaxial crystal ($n_e > n_o$) [35]. The axis characterized by the lower refraction index is called *fast axis* ($n_{slow} > n_{fast}$ because $v = c/n$), therefore quartz wave-plates have $n_{fast} = n_o$

1 The most frequently spatial mode used for polarization encoding is the TEM_{00} mode, which can be well approximated to a plane wave in the condition of not too strong focusing.

and $n_{slow} = n_e$. In the basis $\{|F\rangle, |S\rangle\}$ of the fast and slow axes, the unitary matrix representing the action of a wave-plate is:

$$\Lambda(\Gamma) = \begin{pmatrix} e^{i\frac{2\pi}{\lambda}n_{fast}d} & 0 \\ 0 & e^{i\frac{2\pi}{\lambda}n_{slow}d} \end{pmatrix} = e^{i\frac{2\pi}{\lambda}n_{fast}} \begin{pmatrix} 1 & 0 \\ 0 & e^{i\frac{2\pi}{\lambda}(n_{slow}-n_{fast})d} \end{pmatrix} \equiv \begin{pmatrix} 1 & 0 \\ 0 & e^{i\Gamma} \end{pmatrix} \tag{C.15}$$

where we dropped the overall phase factor $e^{i\frac{2\pi}{\lambda}n_{fast}}$ because the system is insensitive to it with, and where $\Gamma = \frac{2\pi}{\lambda}\,\Delta n\, d$, is the relative phase introduced by the plate.

The two most used common types of wave-plates are the *half wave-plate*, characterized by $\Delta n\ d = \frac{\lambda}{2} + m\lambda$ and $\Gamma = \pi + 2\pi m$, and the *quarter wave-plate*, with $\Delta\ nd = \frac{\lambda}{4} + m\lambda$ and $\Gamma = \frac{\pi}{2} + 2\pi m$. The value of m gives the order of the plate (*zero-order* plates have $m = 0$). The resulting scattering matrices are:

$$\Lambda_{HWP} = \begin{pmatrix} 1 & 0 \\ 0 & -1 \end{pmatrix} \qquad \text{and} \qquad \Lambda_{QWP} = \begin{pmatrix} 1 & 0 \\ 0 & i \end{pmatrix} \tag{C.16}$$

In general, wave-plates are mounted on rotator stages, so that the slow and fast axis form an angle ϵ with the computational basis axis, as shown in figure C.2.

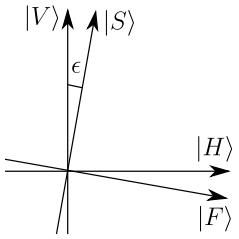

Figure C.2.: Relationship between the $\{|F\rangle, |S\rangle\}$ and the computational basis $\{|H\rangle, |V\rangle\}$. The laser beam is coming out of the page.

Since the rotation is described by

$$\begin{pmatrix} \hat{a}_F \\ \hat{a}_S \end{pmatrix} = \begin{pmatrix} \cos\epsilon & -\sin\epsilon \\ \sin\epsilon & \cos\epsilon \end{pmatrix} \begin{pmatrix} \hat{a}_H \\ \hat{a}_V \end{pmatrix} = R_y(2\epsilon) \begin{pmatrix} \hat{a}_H \\ \hat{a}_V \end{pmatrix} \tag{C.17}$$

the resulting rotated wave-plate scattering matrix is

$$\Lambda(\Gamma, \epsilon) = R_y^{-1}(2\epsilon)\Lambda(\Gamma)R_y(2\epsilon) = \begin{pmatrix} \cos^2\epsilon + e^{i\Gamma}\sin^2\epsilon & \cos\epsilon\sin\epsilon\left(1 - e^{i\Gamma}\right) \\ \cos\epsilon\sin\epsilon\left(1 - e^{i\Gamma}\right) & e^{i\Gamma}\cos^2\epsilon + \sin^2\epsilon \end{pmatrix} \tag{C.18}$$

Follows that the scattering matrix of the rotated half-wave plate and quarter-wave plate is given by:

$$\Lambda_{HWP}(\epsilon) = \begin{pmatrix} \cos^2\epsilon - \sin^2\epsilon & 2\cos\epsilon\sin\epsilon \\ 2\cos\epsilon\sin\epsilon & \sin^2\epsilon - \cos^2\epsilon \end{pmatrix} = \begin{pmatrix} \cos 2\epsilon & \sin 2\epsilon \\ \sin 2\epsilon & -\cos 2\epsilon \end{pmatrix} \tag{C.19}$$

$$\Lambda_{QWP}(\epsilon) = \begin{pmatrix} \cos^2\epsilon + i\sin^2\epsilon & \cos\epsilon\sin\epsilon\,(1-i) \\ \cos\epsilon\sin\epsilon\,(1-i) & \sin^2\epsilon + i\cos^2\epsilon \end{pmatrix} \tag{C.20}$$

Half- and quarter-wave plates can also be used to implement a generic R_z rotation (see A.8). This can be obtained by fixing the plate with *fast* and *slow* axes parallel to the computational basis, and then rotating the wave-plate along its vertical axis by an

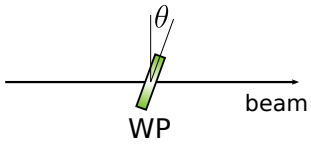

Figure C.3.: Wave plate used as phase shifter.

angle θ, as shown in figure C.3.
The corresponding scattering matrix of this system is

$$\Lambda_{HWP}(\theta) \simeq \begin{pmatrix} 1 & 0 \\ 0 & e^{i\frac{\pi}{\cos\theta}} \end{pmatrix} \tag{C.21}$$

for the half-wave plate and

$$\Lambda_{QWP}(\theta) \simeq \begin{pmatrix} 1 & 0 \\ 0 & e^{i\frac{\pi}{2\cos\theta}} \end{pmatrix} \tag{C.22}$$

for the quarter-wave plate.

Path encoding

In path encoding, the computational basis is composed by two non-overlapping spatial modes. The modes are usually described by the same mode function (usually TEM_{00}), with approximate wave-vectors $\mathbf{k}_1$ and $\mathbf{k}_2$ with the same wavelength but different directions. The *quantum mechanical modes operators* for such modes are $\hat{a}_{\mathbf{k}_1\sigma}$ and $\hat{a}_{\mathbf{k}_2\sigma}$, where σ is the polarization mode. The computational basis states of path encoding are

$$|0\rangle := \hat{a}^\dagger_{\mathbf{k}_1} |0,0\rangle_{\mathbf{k}_1\mathbf{k}_2} = |1,0\rangle_{\mathbf{k}_1\mathbf{k}_2} \tag{C.23}$$

$$|1\rangle := \hat{a}^\dagger_{\mathbf{k}_2} |0,0\rangle_{\mathbf{k}_1\mathbf{k}_2} = |0,1\rangle_{\mathbf{k}_1\mathbf{k}_2} \tag{C.24}$$

where $|n_{\mathbf{k}_1}, n_{\mathbf{k}_2}\rangle_{\mathbf{k}_1\mathbf{k}_2}$ is the Fock state representation of the two spatial modes, with the polarization degree of freedom neglected for simplicity.

Single-qubit operations in path encoding use beam-splitters and phase retarders. Beam-splitters are partially reflecting devices, used to mix two spatial modes creating interference effects. It is usually used with two incoming and two outgoing modes, as shown in figure C.4.
The mode transformation induced by the beam-splitter is

$$\begin{pmatrix} \hat{b}_{\mathbf{k}_1} \\ \hat{b}_{\mathbf{k}_2} \end{pmatrix} = \begin{pmatrix} t' & r \\ r' & t \end{pmatrix} \begin{pmatrix} \hat{a}_{\mathbf{k}_1} \\ \hat{a}_{\mathbf{k}_2} \end{pmatrix} \tag{C.25}$$

where input modes are marked with field operators $\hat{a}_j$ and output modes with $\hat{b}_j$, with j the approximate wave vector of the two spatial modes. Since the scattering matrix must be unitary, (r, t) and (r', t') must satisfy $|r'| = |r|$, $|t'| = |t|$, $|r|^2 + |t|^2 = 1$, $r^*t' + r't^* = 0$, and $r^*t' + r't'^* = 0$ [56]. The 50:50 beam-splitter has $r = r' = \frac{i}{\sqrt{2}}$ and $t = t' = \frac{1}{\sqrt{2}}$, therefore it is described by the scattering matrix

$$U_{BS} = \frac{1}{\sqrt{2}} \begin{pmatrix} 1 & i \\ i & 1 \end{pmatrix}. \tag{C.26}$$

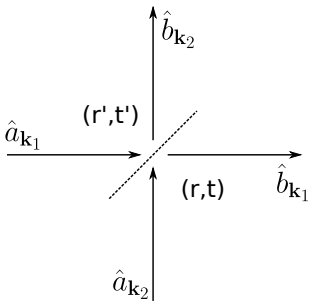

Figure C.4.: Quantum mechanical description of the beam-splitter. For simplicity, input modes are marked with $\hat{a}$ and output modes with $\hat{b}$.

The phase retarder simply consists of an element capable of introduce a different optical path length between the two spatial mode. The optical path difference between the two modes, however, must be shorter than the coherence length of the two modes, to keep the temporal overlap between the single-photon wave-packets in the two modes. The action of a phase retarder is described by the following scattering matrix:

$$U_{phase}(\phi) = \begin{pmatrix} 1 & 0 \\ 0 & e^{i\phi} \end{pmatrix}. \tag{C.27}$$

BIBLIOGRAPHY

[1] A. Einstein, B. Podolsky, and N. Rosen, *Can Quantum-Mechanical Description of Physical Reality Be Considered Complete?*, Phys. Rev. **47**, 777 (1935).

[2] N. Bohr, *Can Quantum-Mechanical Description of Physical Reality be Considered Complete?*, Phys. Rev. **48**, 696 (1935).

[3] J. S. Bell, *On the Einstein-Podolsky-Rosen Paradox* (1964).

[4] M. Nielsen and I. Chuang, *Quantum computation and quantum information*, Cambridge (2010), ISBN 978-1-107-00217-3.

[5] P. Kok and B. W. Lovett, *Introduction to Optical Quantum Information Processing*, Cambridge University Press, Cambridge (2010), ISBN 9781139193658.

[6] M. Le Bellac, *A Short Introduction to Quantum Information and Quantum Computation*, Cambridge University Press (2006), ISBN 0521860563.

[7] R. Silva, N. Gisin, Y. Guryanova, and S. Popescu, *Multiple Observers Can Share the Nonlocality of Half of an Entangled Pair by Using Optimal Weak Measurements*, Phys. Rev. Lett. **114**, 250401 (2015).

[8] P. A. M. Dirac, *The principles of quantum mechanics*, International series of monographs on physics (Oxford, England), Clarendon Press, 4th ed edition (1966).

[9] C. E. Shannon, *A mathematical theory of communication*, Bell Syst. Tech. J. **27**, 379 (1948).

[10] B. Hensen, H. Bernien, A. E. Dréau, A. Reiserer, N. Kalb, M. S. Blok, J. Ruitenberg, R. F. L. Vermeulen, R. N. Schouten, C. Abellán, W. Amaya, V. Pruneri, M. W. Mitchell, M. Markham, D. J. Twitchen, D. Elkouss, S. Wehner, T. H. Taminiau, and R. Hanson, *Loophole-free Bell inequality violation using electron spins separated by 1.3 kilometres*, Nature **526**, 682 (2015).

[11] L. K. Shalm, E. Meyer-Scott, B. G. Christensen, P. Bierhorst, M. A. Wayne, M. J. Stevens, T. Gerrits, S. Glancy, D. R. Hamel, M. S. Allman, K. J. Coakley, S. D. Dyer, C. Hodge, A. E. Lita, V. B. Verma, C. Lambrocco, E. Tortorici, A. L. Migdall, Y. Zhang, D. R. Kumor, W. H. Farr, F. Marsili, M. D. Shaw, J. A. Stern, C. Abellán, W. Amaya, V. Pruneri, T. Jennewein, M. W. Mitchell, P. G. Kwiat, J. C. Bienfang, R. P. Mirin, E. Knill, and S. W. Nam, *A strong loophole-free test of local realism*, [arXiv:1511.03189] (2015).

[12] M. Giustina, M. A. M. Versteegh, S. Wengerowsky, J. Handsteiner, A. Hochrainer, K. Phelan, F. Steinlechner, J. Kofler, J.-A. Larsson, C. Abellan, W. Amaya, V. Pruneri, M. W. Mitchell, J. Beyer, T. Gerrits, A. E. Lita, L. K. Shalm, S. W. Nam, T. Scheidl, R. Ursin, B. Wittmann, and A. Zeilinger, *A significant-loophole-free test of Bell's theorem with entangled photons*, [arXiv:1511.03190] (2015).

[13] N. Xu, J. Zhu, D. Lu, X. Zhou, X. Peng, and J. Du, *Quantum factorization of 143 on a dipolar-coupling nuclear magnetic resonance system*, Phys. Rev. Lett. **108** (2012).

[14] D. Dequal, G. Vallone, D. Bacco, S. Gaiarin, V. Luceri, G. Bianco, and P. Villoresi, *Experimental single-photon exchange along a space link of 7000 km*, Phys. Rev. A **93**, 10301 (2016).

[15] G. Vallone, D. Bacco, D. Dequal, S. Gaiarin, V. Luceri, G. Bianco, and P. Villoresi, *Experimental Satellite Quantum Communications*, Phys. Rev. Lett. **115**, 40502 (2015).

[16] G. Vallone, D. Dequal, M. Tomasin, F. Vedovato, M. Schiavon, V. Luceri, G. Bianco, and P. Villoresi, *Interference at the Single Photon Level Along Satellite-Ground Channels*, Phys. Rev. Lett. **116**, 253601 (2016).

[17] E. Schrödinger, *Discussion of Probability Relations between Separated Systems*, Math. Proc. Cambridge Phil. Soc. **31**, 555 (1935).

[18] M.-J. Hu, Z.-Y. Zhou, X.-M. Hu, C.-F. Li, G.-C. Guo, and Y.-S. Zhang, *Experimental Sharing of Nonlocality among Multiple Observers with One Entangled Pair via Optimal Weak Measurements*, [arXiv:1609.01863] (2016).

[19] D. Bohm, *Quantum theory*, Courier Corporation (1951).

[20] N. Brunner, D. Cavalcanti, S. Pironio, V. Scarani, and S. Wehner, *Bell nonlocality*, Rev. Mod. Phys. **86**, 419 (2014).

[21] J. F. Clauser, M. A. Horne, A. Shimony, and R. A. Holt, *Proposed Experiment to Test Local Hidden-Variable Theories*, Phys. Rev. Lett. **23**, 880 (1969).

[22] S. J. Freedman and J. F. Clauser, *Experimental Test of Local Hidden-Variable Theories*, Phys. Rev. Lett. **28**, 938 (1972).

[23] A. Aspect, J. Dalibard, and G. Roger, *Experimental test of Bell's inequalities using time- varying analyzers*, Phys. Rev. Lett. **49**, 1804 (1982).

[24] P. Busch, *"No Information Without Disturbance": Quantum Limitations of Measurement*, [arXiv:0706.3526] (2009).

[25] E. Schrödinger, *The Present Status of Quantum Mechanics*, Die Naturwissenschaftenturwissenschaften **23**, 1 (1935).

[26] Y. Aharonov, D. Z. Albert, and L. Vaidman, *How the result of a measurement of a component of the spin of a spin- 1/2 particle can turn out to be 100*, Phys. Rev. Lett. **60**, 1351 (1988).

[27] O. Oreshkov and T. A. Brun, *Weak measurements are universal*, Phys. Rev. Lett. **95**, 1 (2005).

[28] H. M. Wiseman and G. J. Milburn, *Quantum Measurement and Control*, Cambridge University Press (2010), ISBN 0521804426.

[29] M. G. A. Paris, *The modern tools of quantum mechanics: A tutorial on quantum states, measurements, and operations*, Eur. Phys. J. Spec. Top. **203**, 61 (2012).

[30] B. Tamir and E. Cohen, *Introduction to Weak Measurements and Weak Values*, Quanta **2**, 7 (2013).

[31] B. E. Y. Svensson, *Pedagogical Review of Quantum Measurement Theory with an Emphasis on Weak Measurements*, Quanta **2**, 18 (2013).

[32] L. Masanes, A. Acin, and N. Gisin, *General properties of nonsignaling theories*, Phys. Rev. A **73**, 12112 (2006).

[33] A. Christ, *Theory of ultrafast waveguided parametric down-conversion: from fundamentals to applications*, Ph.D. thesis, University of Paderborn (2013).

[34] J. D. Jackson, *Classical Electrodynamics Third Edition*, John Wiley Sons, INC. (1999), ISBN 047130932X.

[35] B. E. A. Saleh and M. C. Teich, *Fundamentals of Photonics , 2nd Edition*, Wiley 1200 (2007).

[36] R. W. Boyd and F. Jonsson, *Nonlinear Optics*, volume 5, Academic Press (2007), ISBN 0121216829, [arXiv:0102038].

[37] M. E. Peskin and D. V. Schroeder, *An Introduction To Quantum Field Theory*, volume 47, Westview Press (1995), ISBN 0201503972.

[38] R. S. Bennink, *Optimal collinear Gaussian beams for spontaneous parametric down-conversion*, Phys. Rev. A **81**, 053805 (2010).

[39] P. Kolenderski, W. Wasilewski, and K. Banaszek, *Modeling and optimization of photon pair sources based on spontaneous parametric down-conversion*, Phys. Rev. A **80**, 013811 (2009).

[40] A. Ling, A. Lamas-Linares, and C. Kurtsiefer, *Absolute emission rates of spontaneous parametric down-conversion into single transverse Gaussian modes*, Phys. Rev. A **77**, 043834 (2008).

[41] D. Ljunggren and M. Tengner, *Optimal focusing for maximal collection of entangled narrow-band photon pairs into single-mode fibers*, Phys. Rev. A **72**, 062301 (2005).

[42] M. Mitchell, *Parametric down-conversion from a wave-equation approach: Geometry and absolute brightness*, Phys. Rev. A **79**, 043835 (2009).

[43] A. Franzen, *ComponentLibrary* (2006), [Online; accessed 21-November-2016].

[44] C. Commons, *Attribution-NonCommercial 3.0 Unported*.

[45] F. J. Curchod, M. Johansson, R. Augusiak, M. J. Hoban, P. Wittek, and A. Acín, *Unbounded randomness certification using sequences of measurements*, [arXiv:1510.03394] (2015).

[46] J. E. Troupe and J. M. Farinholt, *A Contextuality Based Quantum Key Distribution Protocol*, [arXiv:1512.02256] (2015).

[47] R. Landauer, *Information is physical*, Phys. Today **44**, 23 (1976).

[48] J. Preskill, *Lecture Notes for Physics 219 : Quantum Computation* (2004).

[49] J. M. Renes, *Quantum information theory* (2015).

[50] M. G. A. Paris, *Lecture 02: Generalized measurements and the Naimark Theorem* (2009).

[51] G. Jaeger, *Quantum information: An overview*, Springer (2006), ISBN 0387357254, [arXiv:arXiv:1011.1669v3].

[52] J. Watrous, *An introduction to quantum information and quantum circuits*, ACM SIGACT News **42**, 52 (2011).

[53] L. Salasnich, *Quantum Physics of Light and Matter*, Springer (2014), ISBN 978-3-319-05178-9.

[54] M. Fox, *Quantum Optics*, Univ. Oxford **53**, 1689 (2013).

[55] P.wormer, [Own work, CC BY-SA 3.0].

[56] C. C. Gerry and P. L. Knight, *Introductory Quantum Optics*, Cambridge (2004), ISBN 9788578110796, [arXiv:arXiv:1011.1669v3].